A scanning electron micrograph (SEM) showing a series of interconnected, rounded, and textured structures, likely the PEDOT-coated microelectrodes, against a dark background.

Fabrication and Characterization of PEDOT coated Microelectrodes Array for Organ-on-Chip Application

Affan Kaysa Waafi

Master of Science Thesis

Fabrication and Characterization of PEDOT coated Microelectrodes Array for Organ-on-Chip Application

By

Affan Kaysa Waafi

in partial fulfilment of the requirements for the degree of

Master of Science
in Biomedical Engineering

at the Delft University of Technology,
to be defended publicly on
Monday January 29th, 2018 at 13:00.

Supervisor:	Prof. dr. Ronald Dekker	
Thesis committee:	Prof. dr. P.M. Sarro	TU Delft
	Prof. dr. R.A.M. Wolters	U Twente
	Dr. Vasiliki Giagka	TU Delft
	Nikolas Gaio. Msc	TU Delft

*This thesis is confidential and cannot be made public until December 31, 2021.
An electronic version of this thesis is available at <http://repository.tudelft.nl/>.*

Abstract

Organ-on-Chips (OOCs) are micro-fabricated devices that combine micro-engineering with *in-vitro* cell culturing. This combination results in an in-vitro model that mimics the minimal functional unit of a human organ. OOC devices are expected to provide accurate and predictive screening tools that will eventually reduce false negatives and false positives during drug research and development. By exploiting the accuracy of micro-fabrication techniques, multiple features such as micro-channels, micro-fluidics, micro-topologies, micro-pumps, etc., can be embedded in the device to replicate the biological conditions experienced by the cells in an *in vivo* human tissue. Moreover, it is possible to monitor the behavior and viability of the cells in the model through sensors embedded in the device.

The Cytostretch device, an OOC developed by TU Delft and Philips, consists of a stretchable membrane fabricated on a silicon chip and equipped with microelectrode arrays (MEA) and micro-grooves. This device provides a customizable platform for multiple organ models. The Cytostretch Silicon-based fabrication should guarantee a large-scale fabrication and a rapid commercialization. However, the design choices compromise the electrochemical performance of the Titanium Nitride MEA on the device. In order to solve this problem, this project focused on coating the Cytostretch MEA with PEDOT (Poly (3,4 – Ethylenedioxythiophene)). PEDOT is a conductive polymer, known to exhibit a superior electrochemical performance due to its high porosity. To the best of authors knowledge, this is the first time a PEDOT MEA is embedded in an Organ-on-Chip. Moreover this is the first work reported aiming to produce a stretchable PEDOT MEA at large-scale by following the “polymer-last approach”.

In this project three main issues were addressed and successfully solved. Firstly, the adhesion between the polymer layers composing the Cytostretch device was improved. Secondly, the process and the masks of the Cytostretch were optimized in order to coat the Titanium Nitride MEA with a noble metal (Platinum) in order to facilitate PEDOT deposition. Thirdly, the deposition of PEDOT on top of the Cytostretch electrodes was successfully performed by cyclic voltammetry deposition from an aqueous solution with NaPSS (Sodium-Poly (Styrene Sulfonate)) as the dopant material.

The performance of the novel stretchable PEDOT MEA was assessed with multiple characterization methods such as Electrochemical Impedance Spectroscopy, and Cyclic Voltammetry. Compared to the Titanium Nitride MEA, PEDOT electrodes exhibit an enhanced performance providing an outstanding 94% reduction of the electrochemical impedance at 1 kHz. The new electrodes showed an ohmic behavior over a wider range of frequency. Last but not the least, a significant increase of the total charge delivery capacity (CDC) was obtained during cyclic voltammetry tests. The results reported in this work demonstrate that the electrochemical performance of the Cytostretch can be drastically improved with PEDOT coating. The combination of robust microfabrication and the electrochemical deposition techniques presented in this work is an important step forwards toward the use of the Cytostretch device in pharmacological applications.

Acknowledgement

First of all, the past one and a half year in this project was full of fun, and also challenging moments. Therefore, I would like to thank Prof. Ronald Dekker that introduced me to the world of Organ-on-Chip, and also the wonder of micro-fabrication world. I would also like to thank Nikolas for the inspiring guidance both inside and outside the laboratory works. Their patience and wisdom had inspired me to keep learning, and to push myself to do my best. The most important thing that I learned from both of them is that I still have a lot of things I need to learn from them.

I am also thankful to all the lab colleagues, especially Marta, William, Cinzia, Juan and Manju for the enlightening discussion and their scientific advices. I would also like to thank all the EKL technicians and team for lending their technical support and expertise, despite the use of many non-standard materials and procedures in this research project. I would also like to thank Paul Dijkstra and the team in Philips Green house for the very helpful assistances in dicing and wire-bonding the device.

Special thanks to all the EKL master students; Hani, the first teammate I have, Shin and Arshaad for the healthy whiteboard discussions, Jin, Mary, Manvika, Raj, Cai, Shengtai, Sarat, Joost, Levar, Zhiqiao, Bart, Diane and Gandhi, for the never ending motivational supports in the lab, office, and lunch table. I am also thankful to meet many amazing friends in the biomedical engineering, and also in the badminton courts, whom with their encouragement, many challenging moments could be handled without hesitation.

I would also like to thank The Indonesian Endowment Fund for Education (LPDP), for providing me with the scholarship, with which I could take this one of the most amazing journey in my life. At last but not least, I would like to thank my families who always encourage me to spread my wings and never be afraid to fall.

Thank you.

Delft, January 28 2018

Affan Kaysa Waafi

Table of Content

ABSTRACT	V
ACKNOWLEDGEMENT	VII
TABLE OF CONTENT	IX
LIST OF FIGURES	XI
LIST OF TABLES	XV
CHAPTER. 1 INTRODUCTION	1
1.1 ORGAN-ON-CHIP DEVICE	1
1.2 CYTOSTRETCH	2
1.2.1 <i>Microelectrode Array (MEA)</i>	2
1.3 THESIS RESEARCH CONTRIBUTION: PEDOT POLYMER COATING ON THE CYTOSTRETCH MEA	3
1.3.1 <i>Thesis Outline</i>	3
CHAPTER. 2 MICROELECTRODES ARRAY AND PEDOT POLYMERS	5
2.1 MICROELECTRODE ARRAY	5
2.1.1 <i>Electrode to Electrolyte Interface</i>	6
2.1.2 <i>Microelectrode Materials</i>	8
2.2 MICROELECTRODES CHARACTERIZATION	8
2.2.1 <i>Electrochemical Cell and Instrumentation</i>	9
2.2.2 <i>Cyclic Voltammetry</i>	11
2.2.3 <i>Electrical Impedance Spectroscopy</i>	13
2.3 POLY (3,4 – ETHYLENEDIOXYTHIOPHENE)	14
2.4 ELECTROCHEMICAL DEPOSITION	15
2.4.1 <i>Electrochemical Cell Setup</i>	16
2.4.2 <i>Deposition Mode</i>	17
2.4.3 <i>Adhesion Layer</i>	19
2.4.4 <i>Dopant Materials</i>	19
2.4.5 <i>Solution Concentration</i>	21
2.4.6 <i>Bioactive Materials</i>	22
CHAPTER. 3 DEVICE FABRICATION	23
3.1 WAFER FABRICATION	23
3.1.1 <i>Platinum Coating</i>	24
3.1.2 <i>Adhesion between Polyimide and PDMS</i>	27
3.2 DEVICE PACKAGING AND RESULTS	29
CHAPTER. 4 ELECTROCHEMICAL DEPOSITION & PRELIMINARY CHARACTERIZATION	31
4.1 REFERENCE ELECTRODE CALIBRATION	32
4.2 TEST DEPOSITION	34
4.2.1 <i>Pt Electrodes Characterization</i>	34
4.2.2 <i>PEDOT:BF₄ Deposition</i>	35
4.2.3 <i>PEDOT:BF₄ Electrodes characterization</i>	36
4.3 REVISED FABRICATION	38
4.4 REVISED DEPOSITION	39

4. 4. 1	<i>Pt Electrodes Characterization</i>	39
4. 4. 2	<i>PEDOT:PSS Deposition and Characterization</i>	40
CHAPTER. 5	FINAL CHARACTERIZATION & ANALYSIS	47
5. 1	ELECTROCHEMICAL IMPEDANCE SPECTROSCOPY	47
5. 2	CYCLIC VOLTAMMETRY	49
5. 3	RAMAN SPECTROSCOPY	51
CHAPTER. 6	CONCLUSION	53
6. 1	RECOMMENDATION AND FUTURE WORK	54
APPENDIX		55
A.1.	FABRICATION RESULT	55
A.2.	FABRICATION FLOWCHART	63
A.3.	POLYIMIDE TO PDMS ADHESION	77
A.4.	NON-AQUEOUS REFERENCE ELECTRODE	79
A.5.	NON-AQUEOUS PEDOT DEPOSITION	83
A.6.	POSTER AND JOURNAL PAPER	85
REFERENCES		91

List of Figures

Figure 1.1. Overview of Cytostretch device with transparent flexible membrane covering the “dog bone” shaped hole (a). Flexible membrane of the cytostretch (b). Microgrooves, electrodes and wiring line on the membrane seen under optical microscope (c).	2
Figure 2.1. The use of the Cytostretch MEA in a cell culture of cardiac myocytes	5
Figure 2.2. The structure of double layer capacitance (Cdl) at the electrode-electrolyte (NaCl (aq)) interface based on BDM model. The double layer area, extends from the high charge concentration area near the metal surface to the diffuse area in the electrolyte.	6
Figure 2.3. The circuit model of electrode-electrolyte interface adapted from Randle’s model.....	8
Figure 2.4. The illustration of in-vitro electrical measurement / stimulation (a) and the schematic of two-electrode cell representation (b).	9
Figure 2.5. Several types of reference electrodes in electrochemistry measurement.	10
Figure 2.6. The schematic diagram of a potentiostat.....	11
Figure 2.7. (a) Potential sweep in LSV and the resulting I-V plot. (b) Potential sweep in CV and corresponding I-V plot.	12
Figure 2.8. (a) Resulting I-V plot of TiN electrode showing a capacitive characteristics. (b) I-V plot of PEDOT:PSS electrode showing several faradaic current peaks.	12
Figure 2.9. The structure of 3,4-ethylenedioxythiophene monomer (EDOT) (a), which combines into PEDOT polymer (b).....	15
Figure 2.10. The surface of the PEDOT film deposited potentiostatically at 1.2 V (a,b) shows a more rough topology, compared to the film deposited at 1.4 V (c,d). (e) The surface of PEDOT film deposited by cyclic voltammetry with different switching voltage.	18
Figure 2.11. The plot of Impedance of PEDOT film doped with different dopants, (a) PSS (b) pTS (c) PF6 (d) ClO4 (e) BF4.	20
Figure 2.12. The Impedance plot over time, from different coatings during the accelerated aging test (@ 1 kHz) (a). The half-life evaluation of PEDOT:BF ₄ (b) PEDOT:PSS (c) and CNT:PEDOT:PSS (d), showing the admittance over time.	21
Figure 3.1. The schematic cross-section from each fabrication step of the Cytostretch device.....	24
Figure 3.2. The SEM image of microelectrode coated with Pt showing cracks (a,b,c), and fully delaminated electrode showing the TiN surface (d). The illustration of buckling of the Pt coating, after the seeping of BHF etchant on the edge of Pt (e).	25
Figure 3.3. The SEM image of the new version of Pt coated microelectrode, as seen from the wafer top side (a), and the overlap between polyimide film with Pt coating (b). The schematic cross section of the modified Pt coating (c).....	26
Figure 3.4. The Pt coated MEA as seen under optical microscope (a). The SEM image of the full-sized (b), and small-sized (c) Pt coated microelectrode. The gap between Pt coating and the polyimide film on the smaller size Pt is filled with TiN (d). The schematic cross-section of microelectrode with the smaller-size Pt coating (e).	27
Figure 3.5. The delamination of polyimide film from PDMS after immersion in Acetone at 40°C for 5 minutes, as observed under optical microscope (a,b). The result of plasma etching treatment showing no delamination of the polyimide film after immersion in the same solvent for 20 minutes (c,d).	28

Figure 3.6. The final result of the Cytostretch device, as seen from the front side with PDMS membrane (a), and from the back side showing the MEA surface (b). The dices are positioned upside-down on the PCB, as seen from the back of the PCB (c), and the front-side (d).....	29
Figure 4.1. The sequence followed in this research, in order to investigate the feasibility and the optimization of the PEDOT deposition.	31
Figure 4.2. The miniaturized Ag/AgCl electrode.	32
Figure 4.3. The I-V plot from the CV measurement of Ferrocyanide:KCl solution, with different scan rates. Vertical dash line shows the average of formal redox potentials of Ferrocyanide, measured in this experiment.	33
Figure 4.4. The construction of the three electrode cell used in this experiment. The Cytostretch MEAs are connected by the copper interconnection line on the PCB, to the potentiostat as working electrodes (WE).	34
Figure 4.5. The Bode plots of EIS measurements from the Pt coated microelectrodes.	35
Figure 4.6. The I-V plot of LSV scan for determining PEDOT:BF ₄ deposition voltage (a), and the result of current measurement during the potentiostatic deposition (b).	36
Figure 4.7. The Bode plot of EIS measurement for PEDOT:BF ₄ coated MEA compared to the average result of Pt coating.....	36
Figure 4.8. PEDOT:BF ₄ coating deposited on the microelectrode surface (a), and side-deposition on the interconnection line (b). SEM image of side-deposition of PEDOT:BF ₄ coating on the interconnection line (c). The schematic cross-section of the side-deposition from area under the red line (d).	37
Figure 4.9. The result of contact angle measurement on PI surface, prior (a) and after (b) the oxygen plasma treatment. The lower images show the water drop on the PI surface as captured with the camera, prior (c) and after (d) the treatment.....	38
Figure 4.10. The Bode plots of EIS measurements from the new batch of TiN and Pt microelectrodes.....	39
Figure 4.11. The I-V plots of the deposition over different scan cycles (a), and the amount of charge delivered over time (b).	41
Figure 4.12. The Bode plots from EIS measurements of the deposited PEDOT compared to Pt coating prior to deposition.....	41
Figure 4.13. The I-V plots of the second deposition over different scan cycles (a), and the amount of charge delivered over time (b).....	42
Figure 4.14. The Bode plot of EIS measurement from the second PEDOT deposition.	42
Figure 4.15. The I-V plots of the third deposition over different scan cycles (a), and the amount of charge delivered over time (b).	43
Figure 4.16. The Bode plot of EIS measurement from the third PEDOT deposition.....	44
Figure 4.17. The plot of charge delivery from the second deposition shows the reduction of charge during deposition.	44
Figure 4.18. The results of PEDOT deposition on the Cytostretch MEA with the revised fabrication, showing no side-deposition (a,b). The result of the first deposition program, as seen under optical microscope (c), and SEM (d).....	45
Figure 5.1. The Bode plot of EIS measurement results from all three type of microelectrode in this project.	47
Figure 5.2. The circuit model of the PEDOT coated MEA, fitted from the measurement result.	48
Figure 5.3. The comparison of the measurement and fitting result, as shown in the Nyquist plot (a) and the more detailed plot in the high frequency region (b), and the Bode plot (c,d).....	49

Figure 5.4. The CV results from three types of the microelectrodes combined in one graph (a). The results of CV scan of the PEDOT (b), TiN (c), and Pt (d) electrodes. Note that each graph has different maximum y-axis value. Blue arrows indicate the position of faradaic arcs and peaks. ...	50
Figure 5.5. The results of Raman Spectroscopy of the PEDOT coated microelectrodes.	51
Figure A. 1. (a) The SEM image of the AlSi contact pad, after patterning in the step c. (b) A close-up image of the AlSi grainy structure, which was a result of the sputtering deposition.....	56
Figure A. 2. (a) The SEM image of Pt coating as seen from the wafer-front side, after the lift-off process in the step c. (b) Each dice has 12 microelectrodes, with 11 of them are Pt-coated.....	56
Figure A. 3. After the first polyimide deposition in step d, the extensions of the AlSi contact pads are covered, exposing only the connection sites to the wire-bonding and TiN.	57
Figure A. 4. (a) The SEM image of the first PI film surrounding the Pt coating, as seen from the front side of the wafer. (b) A close-up image of the Pt coated surrounded by PI film.....	57
Figure A. 5. The results of the step e, showing the TiN interconnection lines connected to the microelectrodes.	58
Figure A. 6. After step e, TiN lines are connected to the AlSi contact pad (a). The connection of TiN lines to the Pt (b).....	58
Figure A. 7. The connection sites between the TiN lines and AlSi contact pads.	59
Figure A. 8. After the second PI layers in the step f, the TiN lines and MEA are completely covered with PI insulation.....	59
Figure A. 9. (a) The MEA and TiN lines are covered with PI insulation after step f. (b) The connection sites of the TiN and AlSi after step f.....	60
Figure A. 10. After the PDMS deposition, curing, and patterning in the step g, the device surface is covered with PDMS, and then the contact pads area is exposed.....	60
Figure A. 11. The finished result of the membrane releasing in the step h showing the MEA surface at the PDMS membrane, as seen from the wafer backside.....	61
Figure A. 12. The resulting Pt coating surface, after step h (a). From the defected Pt coating (b), the surface quality of the microelectrode can be compared.	61
Figure A. 13. The relatively smooth surface of the TiN and Pt coating on the microelectrode.	62
Figure A. 14. The cross section of the test device before (top) and after (bottom) the membrane releasing.	77
Figure A. 15. The construction of Ag/AgCl reference electrode with a salt bridge.	79
Figure A. 16. The I-V plots from the CV measurements of the Pt pseudo-reference (a), and Ag/AgCl with + bridge (b) in a solution of Ferrocene:TBABF ₄ :ACN, for various scan rates. The dash lines show the average formal redox potential of Ferrocene, measured in this experiment.....	80
Figure A. 17. The I-V plot from the CV measurement of Ferrocyanide + KCl solution with Ag/AgCl + salt bridge reference system, with various scan rates. Vertical dash line shows the average of formal redox potentials of Ferrocyanide, measured in this experiment.	82
Figure A. 18. The I-V plot of LSV scan to determine the PEDOT:BF ₄ deposition voltage on the new batch of MEA (a), and the result of current measurement during the potentiostatic deposition (b).	83
Figure A. 19. The results of CV scan from two different microelectrodes, comparing the current response prior and after the deposition.	84

List of Tables

TABLE 2-1. List of reference electrodes commonly used in electrochemical measurement.	10
TABLE 2-2. The circuit models of electrode with the corresponding impedance characteristics.....	13
TABLE 2-3. The characteristics of dopant materials which are used in electrochemical deposition process	20
TABLE 4-1. The calibration results of miniaturized Ag/AgCl reference electrode in an aqueous solution of Ferrocyanide:KCl.	33
TABLE 4-2. The data of charge measurement and correction from each deposition.	45
TABLE 5-1. The parameter values of the circuit model of the PEDOT coated microelectrode.	48
TABLE 5-2. The CDC values of each microelectrode type.	51
TABLE A- 1. The result of immersion test of the test device in several organic solvents.....	78
TABLE A- 2. The calibration results of Pt wire pseudo-reference electrode on a solution of Ferrocene:TBABF ₄ in ACN.....	81
TABLE A- 3. The calibration results of Ag/AgCl + Salt Bridge electrode in a solution of Ferrocene:TBABF ₄ in ACN.....	81
TABLE A- 4. The calibration results of Ag/AgCl + Salt Bridge electrode in an aqueous solution of Ferrocyanide:KCl.	82

Chapter. 1 Introduction

1. 1 Organ-on-Chip Device

Organ-on-Chips (OOCs) are micro-fabricated devices that combine micro-engineering with *in-vitro* cell culturing. The combination of these two technologies results in a functional model of a living tissue/organ that can be used for biological and pharmacological experiments. One of the main goal of OOCs is to provide a highly accurate in vitro test tool for drug research and development (R&D) [1]. A more accurate *in-vitro* test can reduce the risk of false negatives and positives during in vitro toxicity tests and by doing so, cut the costs of drug R&D [1]. Moreover, these devices could be used for other applications such as efficacy tests and disease modeling [2], [3]. It is expected that in the future, human OOC models will replace animal tests, which in several cases cannot reliably predict the effects of a drug in humans due to the genetic differences between animals and humans. Furthermore, in combination with stem cells derived from human subject, such as induced pluripotent stem cells (iPSC), they might promote the development of personal medicines [2].

By exploiting high-precision micro-fabrication technology, various features can be added to the OOC device to accurately mimic the required biological environment [4]. A microfluidic channel is the most common feature that can be found in the previously developed OOC devices [5], [6]. This is used to stimulate the biological tissue cultured in the OOC device by means of fluid shear stress or chemical gradients. The microchannels in this kind of system can also be used to apply pneumatic pressure and induce strain or stress in the culture medium [7]. Micro-fabrication techniques can also be used to create micro patterns in order to form a specific topography or a porous membrane. The 'lung-on-chip' developed by Huh et al. [7] at the Wyss Institute, employs a porous flexible membrane as a support to grow epithelium culture on one surface of the membrane, and endothelium on the other surface. This membrane is suspended in the middle of microchannel, dividing the channel into two separate compartments. Air flow can be injected into the epithelium side of the channel, and culture medium on the other side, mimicking in this way the minimal functional unit of an alveolus. When the epithelium culture was stimulated with air flow an increase of surfactant production was observed, confirming the functionality of the lung model [7]. Other features that can also be embedded to the OOC device are microelectrodes, biosensors, micropumps, and many more.

Several attempts also have been taken to combine various OOC devices into a more complex representation of an organ or even a whole human body. With this highly complex organ system models, an investigation into the effect of certain drug on a body or a group of organs be carried out [8]. Maschmeyer et al. [9] combined the intestine, liver, skin, and kidney on chip to evaluate the viability and reproducibility of homeostasis in the multi-OOCs system. An investigation was also carried out by Skardal et al. [10] to combine three OOCs, the lung, heart, and liver-on-chip to study the response of multi organs to the drugs.

1. 2 Cytostretch

Cytostretch is an OOC platform developed by TU Delft and Philips (shown in Fig.1.1). This platform can be adapted in order to be used for various organ models [11]. This device is developed with Silicon-based microfabrication technology, and can be equipped with a flexible membrane, micro-grooves, and microelectrodes [11]. The stretchable membrane of Cytostretch can be inflated in order to apply strain to the cell culture and mimic the pulsatile condition of a beating heart. Micro-grooves in the membrane promotes cell alignment in the cell culture on top of the membrane. The microelectrode array (MEA) in the membrane can be used to electrically stimulate or monitor the cell culture. With the combination of these features, Cytostretch device can be used to promote the maturation of cardiac myocyte culture, as reported by Gaio et al. [11]

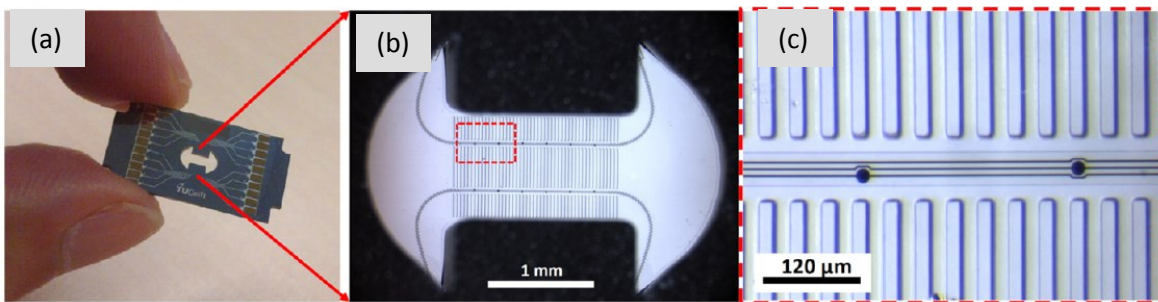


Figure 1.1. Overview of Cytostretch device with transparent flexible membrane covering the “dog bone” shaped hole (a). Flexible membrane of the cytostretch (b). Microgrooves, electrodes and wiring line on the membrane seen under optical microscope (c). [Pakazad et al. [12]]

In order to develop a fabrication sequence that is compatible with the silicon-based microfabrication, the so called “polymer last” approach is used. In this approach, all the functional and supporting structures are fabricated in the initial phase of the microfabrication process. Afterwards, polymer processing is performed to integrate the stretchable membrane, made from Poly-dimethylsiloxane (PDMS), and embed the device modules fabricated in the earlier phase. This means that the number of steps performed after the PDMS processing are reduced to the minimum, avoiding in this way the fabrication issues related to the low stiffness and the high thermal expansion and swelling of PDMS.

1. 2. 1 Microelectrode Array (MEA)

The Cytostretch device is equipped with Titanium Nitride (TiN) microelectrodes. Since this material is known to be inert in biological environments, it heavily relies on the double layer capacitance as the main mode of charge conduction [13]. Most of the use of TiN as microelectrodes relies on the fractal surface induced during sputter deposition of TiN [13], [14]. The fractal surface subsequently increases the surface area, which consequently increases the double layer capacitance of the electrode. The higher double layer capacitance allows more charge to be injected during stimulation, and at the same time lowers the electrochemical impedance [15].

However, the “polymer last” approach followed during the fabrication of the Cytostretch does not produce a microelectrode with a rough surface. This is due to the fact that the surface of TiN electrode is deposited on top of Silicon-dioxide (SiO_2), which produces a smooth surface area. This smooth surface significantly reduces the double layer capacitance of the microelectrode, resulting in a high electrochemical impedance [12]. In the past Gaio et al. [16] improved the impedance of

the Cytostretch device by covering the electrodes TiN electrodes with a Carbon Nanotube coating. Even though this work resulted in an improvement of the electrodes impedance from 2.2 M Ω down to 240 k Ω , the developed process was affecting the yield and the throughput of the Cytostretch device. Therefore, in this thesis, a new approach to improve the electrochemical performance of the Cytostretch MEA is investigated.

Poly (3,4 – ethylene dioxythiophene) (PEDOT) is a conductive polymer known to exhibit low electrochemical impedance due to its porous film surface. The stability and biocompatibility of PEDOT was previously proven in various studies, suggesting the suitability of PEDOT as microelectrode material for *in-vitro* and *in-vivo* applications [17]–[21]. In this work, the incorporation of PEDOT electrodes in the Cytostretch MEA is investigated, in order to improve its electrochemical performance.

1. 3 Thesis Research Contribution: PEDOT Polymer Coating on the Cytostretch MEA

The general goals of this thesis research is to improve the electrochemical performance of the Cytostretch MEA with PEDOT coating. Therefore, this research is focused on two main topics:

1. The integration of PEDOT coating into the fabrication of the Cytostretch MEA
2. To investigate the improvement of the electrochemical performances by the addition of PEDOT coating.

1. 3. 1 Thesis Outline

The remainder of the thesis is structured as follows: in Chapter 2, a literature review on PEDOT deposition, and the electrochemical characterization methods is presented. The mechanisms behind electrochemical charge transfer are also discussed. To incorporate PEDOT coating, the fabrication sequence of the MEA is divided into two main parts, the wafer-based Cytostretch MEA fabrication, and the PEDOT deposition on the MEA. Chapter 3 is mainly focused on the wafer-based fabrication sequence. In Chapter 4, the process to deposit PEDOT on the MEA is addressed. In this chapter the characterization of the MEA before and after the deposition are reported. A more detailed analysis of the performance of the PEDOT MEA is presented in Chapter 5. Finally, Chapter 6 presents the conclusions obtained from this project and the recommendations for the future development of the Cytostretch MEA.

Chapter. 2 Microelectrodes Array and PEDOT Polymers

2. 1 Microelectrode Array

The electrical activity of cells has been known for decades as a part of their response to external chemical and mechanical stimuli. This phenomenon happens in specific types of cells (e.g. neurons and muscle cells) also known as electrogenic cells. Their membranes contain certain ion channels that can be used to actively exchange ions with the extra-cellular matrix, generating a difference in ionic concentration [22], [23]. By doing so, the electrical potential of the intra-cellular matrix, is altered with respect to its surrounding. This combination of chemical and electrical phenomenon gives rise to the cellular electrical activity that can be measured as an electrical signal [22], [24], [25].

During in-vitro and in-vivo experiments, the stimulation and measurement of electrical signal are performed through electrodes, such as shown in Fig.2.1 [11], [12], [26]–[29]. These electrodes are employed as charge transfer interface between the electronics and a biological system such as a cell culture or an organ [6], [7]. From the recording of the electrical impulse produced by the cells, researchers can observe their behavior under certain conditions or stimuli. In other applications, MEAs are used to induce differentiation of stem cell into a certain cell lineage by means of electrical stimuli [7], [8].

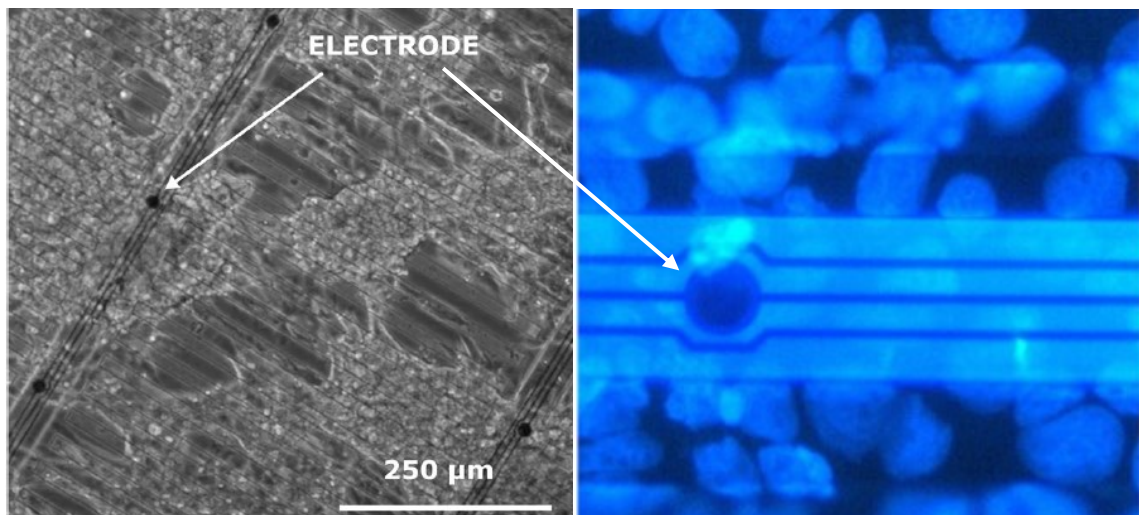


Figure 2.1. The use of the Cytostretch MEA in a cell culture of cardiac myocytes
(Gaio et al. 2016 & Pakazad et al. 2014 [11], [12])

In order to successfully monitor or stimulate the cells, the electrodes are designed to comply with the required mechanical properties, electrical performance, chemical stability, and biocompatibility.

2.1.1 Electrode to Electrolyte Interface

The charge transfer between the electrode surface and the cell culture medium, is affected by various electrical and chemical phenomena at the interface [30]–[34]. Therefore, the quality of the in-vitro MEAs can be described in term of its electro-chemical characteristics [27]. The impact of all electrical and chemical phenomena on the electrode-electrolyte interface to the flow of electric current in the system, are collectively termed as the electrochemical impedance.

Electrodes are in general made from metals or alloys. They conduct electricity by means of free electron movement driven by the electrical field [32], [35]. On the other hand, electrolyte solutions conduct electricity by means of ion movement in the solution and redox reactions between ions [35]–[37]. At the interface of these two phases of materials, charge transfer happens by redox reactions between the electrode surface with the ions in the solution, which is also known as faradaic charge transfer [35]. In parallel to charge transfer, a layer pair containing opposite charges forms immediately when a metal is immersed into the electrolyte solution, even without the application of an external voltage [32]–[34]. This layer formation is caused by the redistribution of charge carriers on the metal surface, which subsequently attracts ions with opposite polarity in the solution to the metal surface (Fig.2.2). Since each layer contains charges with an opposite polarity, this layer pair behaves as a parallel plate capacitor, also known as double-layer capacitance (C_{dl}).

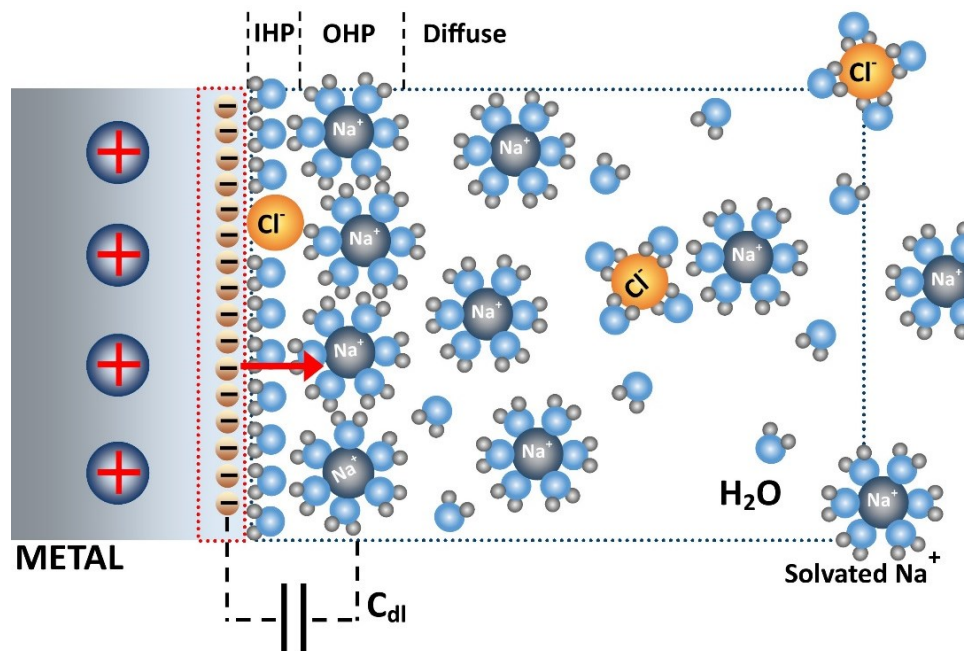


Figure 2.2. The structure of double layer capacitance (Cdl) at the electrode-electrolyte (NaCl (aq)) interface based on BDM model. The double layer area, extends from the high charge concentration area near the metal surface to the diffuse area in the electrolyte [30], [31], [34].

The structure of the double layer capacitance can be explained by using the water dipole model proposed by Bockris, Devanathan and Muller (BDM) [30], [31], [34]. In this model, C_{dl} is the sum of the ionic capacitance and the contribution of the water dipoles. The ionic capacitance can be

evaluated by using triple-layer model which combines the model previously proposed by Hemholtz, and Guoy-Chapman [34]. In this model, the ionic capacitance is distributed over three regions, namely the Inner Hemholtz Plane (IHP), the Outer Hemholtz Plane (OHP), and the diffuse region. At the surface of the electrode, a layer of strongly oriented water molecule is formed which corresponds to the IHP region. Due to the specific adsorption, some of the dehydrated ions (ions that are not surrounded by water molecules) are adsorbed along with the water layer. Next to the IHP is a less-oriented water molecules. Together with the solvated (hydrated) ions, this water layer forms a compact layer with high charge concentration, which is referred as the OHP region. The remainder of the charges are distributed in the diffuse region extending toward the rest of the solution.

The combination of charge transfer and double layer formation at the electrode-electrolyte interface produces a potential difference at the electrochemical cell that is known as the half-cell potential (E_{hc}) [34], [38]. The term “half-cell” refers to the fact that the potential difference is always measured between two electrodes. The value of this potential corresponds to the type of reaction (oxidation or reduction), electrode material, involved reactants, and environment condition [38].

From an electronics point of view, it is important to understand the impact of each electrochemical component to the electrical performance of the complete system. For instance, the double layer capacitance, as the name implies, behaves as a capacitor (C_{dl}) in the electrode-electrolyte system [33], [34], [39]. A linear resistance component (R_f) is generally used as the most simple equivalent for faradaic charge transfer impedance (Z_f), but in some cases it might need to be represented with a more complex model [34], [38]–[40]. An electrode that only utilizes faradaic charge transfer as the main current conduction mechanism is categorized as an Ideal Non-Polarizable Electrode (NPE), while an electrode that does not allow faradaic reactions at surface is called an Ideal Polarizable Electrode (IPE). In reality, most of the electrodes allow both faradaic and capacitive current conduction, thus they fall in between IPE and NPE categories.

The faradaic reaction at the electrode-electrolyte interface can also happen as a multi-stage reaction where the product of the first reaction becomes the fuel for the second stage reaction and so on. In a multi-stage reaction, a charge transfer reaction is often preceded by a non-charge transfer reaction, such as chemical adsorption [34], [41], [42]. In such a case, the difference in the reaction rates at the different stages will produce what is called an “adsorption pseudo-capacitance” component (C_{ps}) [41]. This phenomenon is distinctly characterized by the variation of capacitance with the varying potential at the electrode-electrolyte interface.

An electrochemical Impedance Spectroscopy is often employed with the goal to create an electronic circuit model that best represents the electrode-electrolyte system. Several models have been developed to represent the electrochemical phenomena at the electrode-electrolyte interface [40], [42], [43]. Typically, Randle’s model is used to explain the relation between the components of the impedance. In this model the electrochemical impedance can be represented as a parallel circuit with a faradaic branch and a non-faradaic (or double layer capacitive branch) as shown in Fig.2.3. In addition, R_s represents the total ohmic impedance of the interconnections and solution resistance. For the simplification of impedance analysis, the half-cell potential is often omitted from the electrode-electrolyte model.

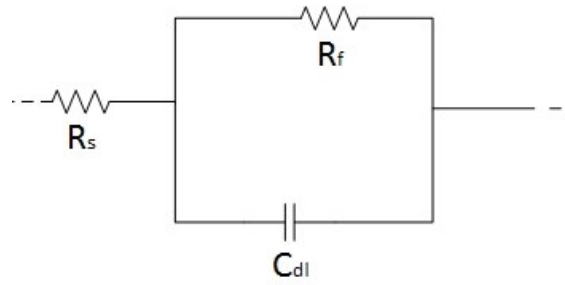


Figure 2.3. The circuit model of electrode-electrolyte interface adapted from Randle's model.

2. 1. 2 Microelectrode Materials

In order to get higher spatial resolution, up to single cell measurements, researchers often use MEAs with a surface area of $2000 \mu\text{m}^2$ or less for each electrode [27], [44]. However, the small dimension of the electrode results in a high electrochemical impedance, which proportionally raises the thermal noise of the recorded signal [39]. Therefore, previous studies investigated several approaches, including the use of novel material to lower the impedance of microelectrode.

Noble metals, such as Platinum, Gold, and Silver, are the mostly used materials for in-vitro microelectrodes. Platinum, in particular, is often used for the reversibility of the faradaic reactions at its surface. In fact, most of the faradaic reaction at the Pt surface involve a multi-step reaction with intermediate adsorption/desorption steps which effectively slow down the reaction rate [34], [45], [46]. Therefore, during a small potential disturbance the rate of the faradaic reaction can be negligible.

Inert materials such as Titanium Nitride, or Glassy carbon have also been introduced recently [13], [14], [47], [48]. TiN is mostly used for stimulation electrode due to the fractal surface obtained by tuning the parameters of the sputter deposition [13]. The fractal surface area significantly increase the charge injection capacity of the TiN electrode.

Recently, conductive polymers were used as surface coating for microelectrodes because of their tendency to form a film with a high surface area [49]–[51]. Moreover, conductive polymers are superior to conventional conductive material in terms of mechanical flexibility and chemical stability [52]. Certainly, compared to metals, CPs have a lower conductivity [50]. However, the large surface area of CP coating contributes to the low electrochemical impedance of the resulting MEA [50], [53].

2. 2 Microelectrodes Characterization

The use of MEAs for in-vitro assays can be divided into two main purposes: the recording of biological electrical activity or delivery of electrical stimulation to the cell culture or tissue [26], [27]. A stimulation MEA, is often characterized by the amount of charge that can be injected safely without causing irreversible reactions on the electrode surface or the surrounding medium. This parameter is referred as charge delivery capacity (CDC) [13], [27], [54], [55]. While, for a recording MEA the electrochemical impedance of the electrodes is more important [21], [27], [56], [57]. An increase in the impedance results in the increase of the thermal noise, which can be detrimental to the quality of the recorded signal. However, the relatively small area of the microelectrode makes

it difficult to lower the impedance as the impedance is inversely proportional to the area of the electrode [54]. In addition to its functionality, the MEAs must be biocompatible as well as chemically stable in the saline, in-vitro environment [27], [52].

In-vitro electrical recording or stimulation can be seen as an electrochemical cell, where the cell culture and its medium serve as the electrolyte solution [27], [58]. In this electrochemical cell, the MEA serves as the working electrode on top of which the charge transfer process is observed. This is coupled with a return electrode that can be built-in or added externally to complete the electrical circuit of the stimulation, or a reference electrode in the case of measurement, such as shown in Fig.2.4.

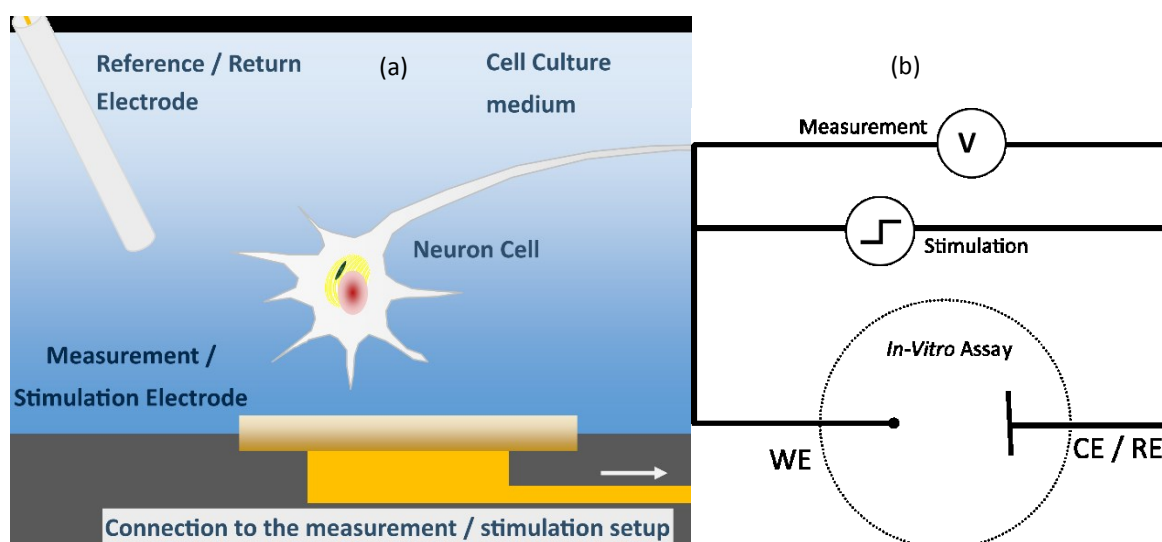


Figure 2.4. The illustration of in-vitro electrical measurement / stimulation (a) and the schematic of two-electrode cell representation (b).

2. 2. 1 Electrochemical Cell and Instrumentation

The characterization measurement is often done in a three-electrode cell setup. In this setup, the electrical current flows from the working electrode (WE) to the counter electrode (CE) [38]. A reference electrode (RE) is added to provide a constant voltage reading to which a potential measurement on the WE can be referenced. Ideally, a reference electrode is a NPE in order to prevent polarization and the resulting deviation of electrode potentials during charge conduction. In reality, a reference electrode contains a redox couple (e.g. Ag & Ag⁺) in equilibrium with the surrounding electrolyte, which gives a constant potential when a small current is applied. The primary standard reference electrode is the Standard Hydrogen Electrode (SHE), which is accepted by convention as the standard 0 V in electrochemistry [38]. However, due to the impracticality of the SHE, secondary reference electrodes are typically used, such as Ag/AgCl or Saturated Calomel Electrode (SCE). Tab.1 gives the standard values of half-cell potentials for several reference electrodes that are commonly used in the electrochemical measurements. The reference electrode can also be used in combination with a potentiostat to compensate the voltage drop at the electrode surface due to the solution resistance [38]. Fig.4 illustrates the construction and use of reference electrodes in the electrolyte solution.

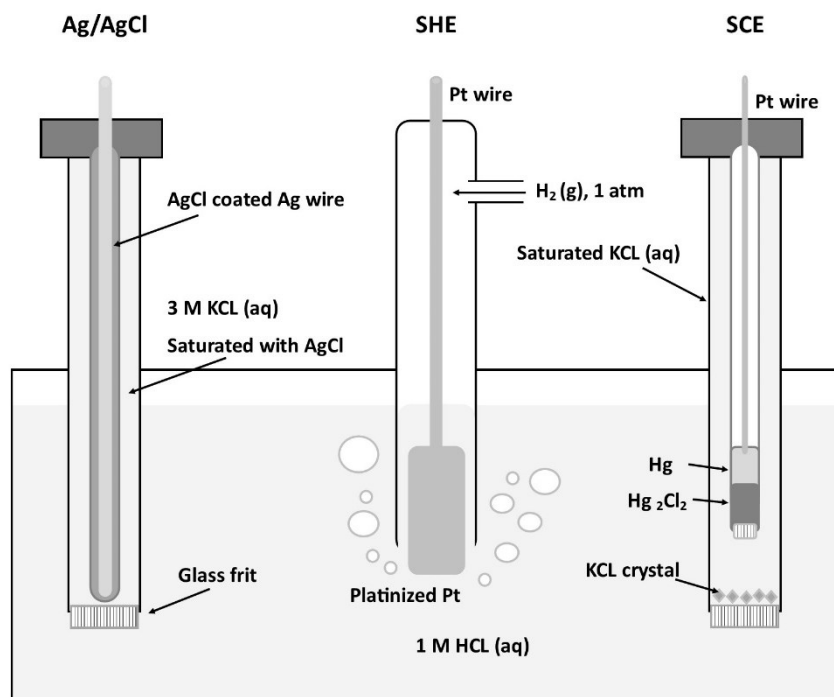


Figure 2.5. Several types of reference electrodes in electrochemistry measurement. (Adapted from [38], [59])

TABLE 2-1. List of reference electrodes commonly used in electrochemical measurement [38], [59], [60].

Electrode Name	Redox Reaction	E_{hc} (V .vs SHE)
SHE	$Pt H_2 \leftrightarrow 2H^+ + 2e^-$	0.0000
Ag/AgCl	$Ag Ag + Cl^- \leftrightarrow AgCl + e^-$	0.2223
Ag/AgBr	$Ag Ag + Br^- \leftrightarrow AgBr + e^-$	0.0711
SCE	$Hg 2Hg + 2Cl^- \leftrightarrow Hg_2Cl_2 + 2e^-$	0.2412

A potentiostat is designed to accurately produce a potential difference between WE and RE. The potential difference is set up by adjusting the current from the WE to the CE until the desired potential value is reached [38]. The schematic diagram of the potentiostat is shown in the Fig.2.6. In this diagram, a three-electrode cell is shown. The potential difference ΔV is measured, and compared to the set-point V_i to adjust the controlled current I_c through the CE. The potential V_s is measured on the variable resistor R_s to get an accurate measurement of the current. The value of R_s can also be adjusted to increase the measurement resolution. The large input impedance at the RE port prevents the electrical current flow to the RE, thus keeping the reference potential constant. Since, the potential at the CE is not controlled, an electrode with a very large size is often used as the CE to effectively reduce the impedance, and avoid the contribution of the CE from affecting the measurement result.

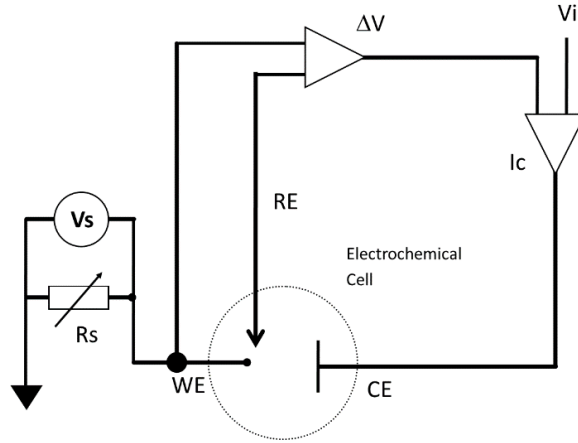


Figure 2.6. The schematic diagram of a potentiostat

2. 2. 2 Cyclic Voltammetry

The voltammetry measurement was originally used to analyze redox reactions in electrochemistry experiments [38], [61]. In this measurement, the voltage of the working electrode (with respect to the reference) is swept over a certain range to get the response current. As the voltage approaches the oxidation or reduction potential of the molecule in the solution, the current will increase or decrease dramatically due to the faradaic charge transfer [38], [61]. The measurement in which the voltage is swept in one direction over a certain voltage range is called linear sweep voltammetry (LSV). When the voltage sweep is done repeatedly in two directions, it is called cyclic voltammetry (CV).

The result of voltammetry is often presented as a current vs voltage (I-V) plot. From this plot, the reversibility of the reaction can be observed by comparing the increase or decrease of the current peaks from each CV cycle. Examples of the voltage signals used in the voltammetry, and the corresponding measurement results are shown in Fig.2.7. If the reaction in the electrode-electrolyte is known to be reversible within the observed voltage range, the decrease or increase of the current peak during a repeated CV can be attributed to the physical change at the electrode surface.

From, the CV measurement, the charge delivery capacity (CDC) of the MEA can be determined [54], [62]. This parameter represents the amount of charge that can be stored on the electrode surface in a certain voltage range. This voltage range is often attributed to a specific faradaic reaction. The most commonly used voltage range is the “water window” which correspond to the oxidation and reduction of water molecules (-0.6 to 0.9 V vs SCE, on a Pt electrode) [63]. The CDC value also shows the stability of the electrode over time during continuous cycling, by looking at the trend of the CDC values from each cycle. The value of CDC (in C/cm²) from each cycle can be calculated using:

$$CDC = \frac{1}{vA} \int_{E_c}^{E_a} |i| dE \quad (1)$$

In the above formula, i is the measured current (A), v is the scan rate (V/s), and A is the geometrical area of electrode (cm²). E_a and E_c are the peak anodic and cathodic potential respectively [54].

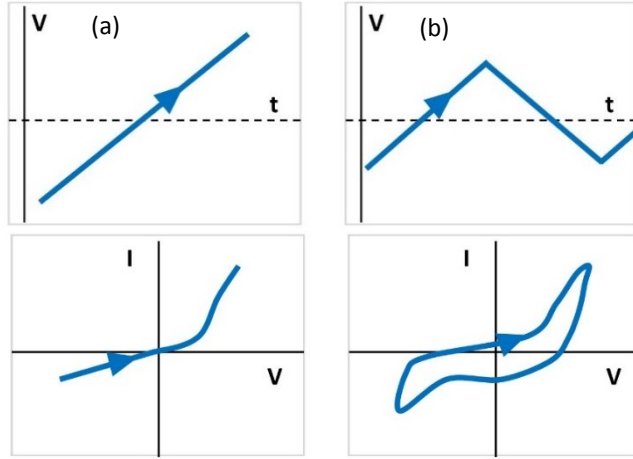


Figure 2.7. (a) Potential sweep in LSV and the resulting I-V plot.
(b) Potential sweep in CV and corresponding I-V plot.

Since the parameters v and A are constant, the decrease of CDC values over repeated scans can be attributed to the increase of electrochemical impedance which lowers the response current. The increase of impedance can then be investigated to identify the degradation of the electrode surface [62]. Usually, continuous CV measurements are done in combination with accelerated aging to observe the stability of the electrode over extended period. In some cases, the CDC value can also increase over repeated scans, which corresponds to a decrease of the impedance. This is possibly caused by the failure of the interconnection insulation, which subsequently increases the total electroactive area. Therefore, CV measurements can also be used for evaluation of the delamination between layers, as investigated by Nichols et al. [64]

From the resulting I-V plot, it is relatively easy to identify the main mode of electrode conduction. An electrode with a large double layer capacitance shows a large hysteresis between forward and reverse scans due to the capacitive current [65]. In the case of an electrode with faradaic charge transfer, the I-V plot is characterized by several current peaks at the oxidation or reduction potential of the electrode material or the ions in the solution [66], as shown in Fig.2.8.

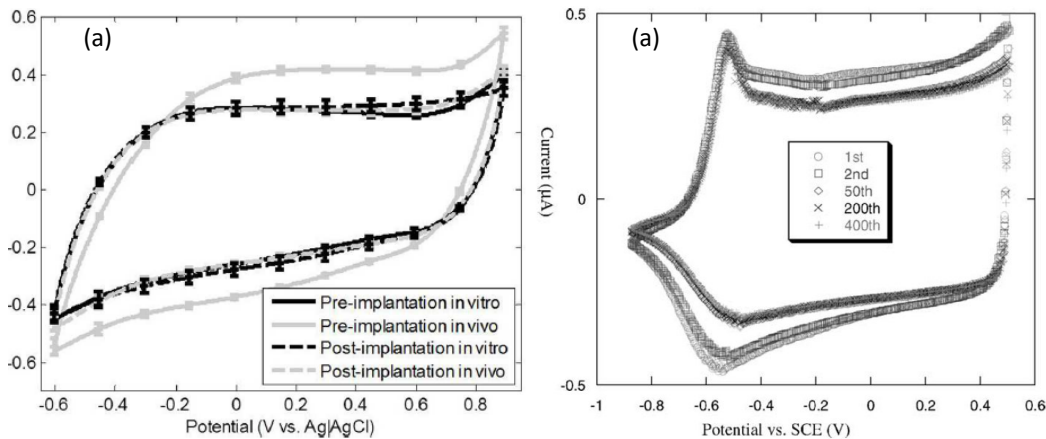
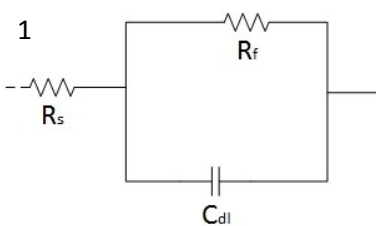
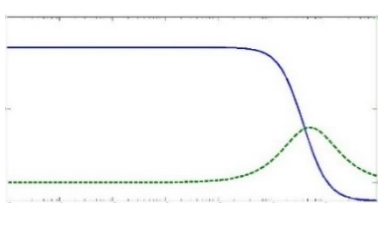
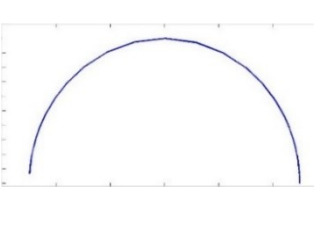
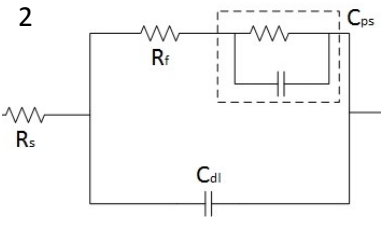
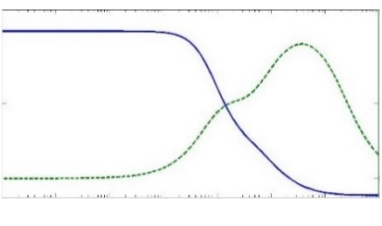
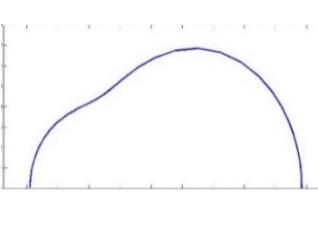
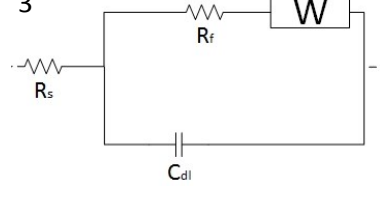
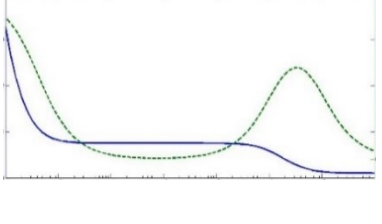
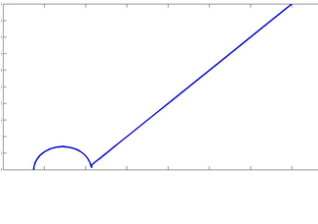


Figure 2.8. (a) Resulting I-V plot of TiN electrode showing a capacitive characteristics (Meijs et al., 2015 [63]). (b) I-V plot of PEDOT:PSS electrode showing several faradaic current peaks (Cui and Martin, 2003 [64]).

2. 2. 3 Electrical Impedance Spectroscopy

In impedance spectroscopy, a single-frequency AC voltage signal is applied to the electrodes and the resulting current response is measured [38], [67]. The measurement is then repeated for a number of frequencies on the range that needs to be investigated. From the measured current, the impedance can be derived. Since AC signal is used, phase shift can be observed on the measured current, which gives the information about the capacitance and also the non-linear characteristics of the MEA system. The result is often presented as a Bode diagram and also Nyquist plot. The combination of the Nyquist plot and Bode diagram can be used to determine the best circuit model to represent the MEA system. The variation of circuit models and the corresponding impedance measurement results are shown in the Tab. 2.

TABLE 2-2. The circuit models of electrode with the corresponding impedance characteristics. (Adapted from Cesiulis et al. 2016 [65])

Circuit model	Bode diagram (Blue line = Z , Green dash = $-\phi$)	Nyquist Plot ($-Z''$ vs Z')
<p>1</p> 		
<p>2</p> 		
<p>3</p> 		

In Tab.2, circuit model 1 shows the characteristics of the standard electrode model. It consists of a faradaic resistance and a double layer capacitance in parallel, connected to a series resistance that represent the resistance of the interconnection lines. In model 2, the pseudo-capacitance (C_{ps}) is added to the faradaic branch with an equivalent circuit as derived by Taylor and Gileadi [34], [42]. The third circuit model shows the characteristics of electrode with a Warburg-impedance (W) component. Warburg impedance is related to the ions diffusion in the solution [42], [43]. Every electrode can exhibits a characteristic that represents one of these types or its combinations depending on the material, the electrolyte solution and the measurement conditions.

Warburg impedance can be characterized by the formula derived in Eqn.2 [68]. In this equation, R is the impedance at the very low frequencies. The parameters L and D , are the diffusion length and diffusion constant respectively.

$$Z(\omega) = \frac{R \times \cotanh ([i\tau\omega]^\alpha)}{(i\tau\omega)^\alpha} \quad (2)$$

$$\tau = \frac{L^2}{D} \quad (2.1)$$

From the Bode phase plot, the charge conduction mode of the electrode can also be inferred. A phase of 0° , which represents ohmic behavior, can be related to the faradaic charge transfer at the interface. On the other hand, a -90° phase represents a capacitive charge conduction, which corresponds to the double layer capacitance phenomena. An inert material with high surface area such as fractal Titanium Nitride is known to exhibit a capacitive behavior over large frequency ranges, due to the lack of a faradaic reaction at the electrode surface [13]. As for materials with faradaic conductivity such as conductive polymers (e.g. PEDOT), they generally show a broad range of ohmic characteristics [69], [70].

In several cases, capacitance can also be represented with a constant phase element. This component is used to account for the non-perfect surface (rough, porous, etc) which produce a capacitance with an arbitrary constant phase value. The characteristics is formulated in Eqn.3 based on the results derived in [71]. In this formula, C is the complex capacitance. If the value of α is equal to 1, then the CPE behaves as an ideal capacitor with a phase of -90° .

$$Z = \frac{1}{[C(i\omega)^\alpha]} \quad (3)$$

In general, there is no standard for frequency range that should be covered in the EIS scan for microelectrode. However, the measurement result for an in-vitro MEAs is typically reported as the value of impedance at 1 kHz frequency, in addition to the Bode diagram and Nyquist plot [27]. This frequency range often corresponds to the spectrum range of neuron action potential.

2. 3 Poly (3,4 – Ethylenedioxythiophene)

The most widely used conductive polymer materials in the bioelectricity field are Polypyrrole (PPy), Polyaniline (PAni), Polythiophene (PTh) and Poly (3,4-ethylenedioxythiophene) (PEDOT) [72], [73]. Among these materials, PEDOT is considered as the most promising conductive polymers for biomedical purposes [27], [29], [50], [72]–[74]. PEDOT is best known for its low electrochemical impedance, biocompatibility and long-term stability in the biological environment [19], [20].

The conductivity of PEDOT, like also in other conductive polymers, is related to the conjugated π bond in its polymer chain backbone structure [75], [76], as shown in Fig.2.9. In case of PEDOT polymer, the conductive state corresponds to the oxidized state of the PEDOT backbone. To maintain this conductive-ionized state, counter charges are required otherwise the polymer chain will revert back to its low-conductive neutral state [75], [76]. The counter charges are provided with the addition of a dopant material in the polymer film. For the PEDOT polymer, mostly anion dopants are used, due to the PEDOT stability as hole-conductor (p-doped) material [77]. By adding a dopant, other characteristics of the resulting polymer, such as its surface porosity, and stability, change as

well. In addition to the dopant, the deposition process can also affect the final properties of the conducting polymers [70].

Several efforts have been done to characterize PEDOT for *in-vitro* MEAs, in particular to investigate its biocompatibility [78]–[80]. The biocompatibility of electrodes is important for a device that interacts with living cells. In addition to the biocompatibility, the possibility to add bioactive molecules during synthesis can simultaneously change the electrical and the biological performance of the electrodes. The bioactivity properties are vital during stem cell differentiation, especially in cases where both biological and electrical stimuli are needed. The stability of PEDOT in the biological environment has also been reported. Schander et al. reported the long term stability of PEDOT coated MEAs by immersing a MEA into phosphate buffered saline (PBS) solution at body temperature [20]. The stability of coating was proven for 7 weeks continuous current stimulation, and up to 10 months in case of idle condition without any stimulation.

In terms of electrical performance, PEDOT has several advantages compared to metals. Aside of its low electrochemical impedance, PEDOT film tends to have larger charge injection capacity (CIC). CIC is defined as the amount of charge required to polarize the surface of electrode to the potential level of water electrolysis (0.9 to – 0.6 V on Platinum electrode) [63]. Venkatraman et al. [69] showed that PEDOT coated MEA have a larger charge injection limit and lower impedance, compared to bare Platinum-Iridium (PtIr) electrodes. The large CIC of PEDOT films is speculated to be caused by its rough and highly porous surface. This characteristic implies that more pulses can be delivered through the MEA surface without causing irreversible reaction of the polymer film or surrounding electrolyte.

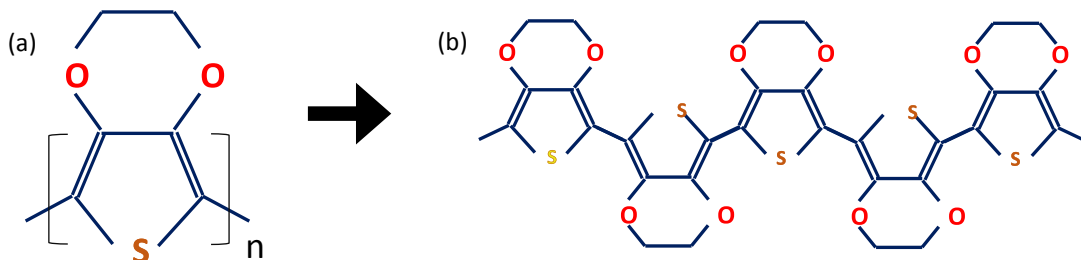


Figure 2.9. The structure of 3,4-ethylenedioxythiophene monomer (EDOT) (a), which combines into PEDOT polymer (b).

The drawbacks of PEDOT polymer compared to conventional metal-based electrode is the relatively lower bulk conductivity, which makes them unsuitable for interconnection lines. In addition, there is a temperature limitation in which PEDOT can be processed, that needs to be considered when developing the fabrication process. As reported by Kiebooms et al., the irreversible degradation of PEDOT:PSS film starts at the temperature above 150°C [81], [82].

2. 4 Electrochemical Deposition

There are various methods that can be used to deposit the PEDOT polymer. Currently, five deposition techniques have been developed, namely oxidative molecular layer deposition (oMLD), vapor phase polymerization (VPP), chemical vapor deposition (CVD), electrochemical deposition (ECD) and chemical oxidative polymerization (COP) [83]–[89]. Three of them, oMLD, VPP and CVD,

deposit PEDOT from the vapor phase of its monomer, resulting in higher conductivity due to a more orderly structure of the resulting PEDOT film [83], [86], [89]. Furthermore, the low solubility of the EDOT monomer in the water makes the vapor deposition process a promising alternative, especially for large scale fabrication. However, these deposition techniques require complex equipment and post-deposition processing to pattern the PEDOT film into the desired structures. The other two deposition methods, ECD and COP use a more simple process to deposit PEDOT from a solution.

In the chemical oxidative polymerization process, PEDOT and the dopant materials are chemically synthesized in solution. Due to the low solubility of EDOT, Poly (Styrene Sulfonate) is commonly added to the solution as dopant as well as a surfactant. The EDOT monomers are then oxidized into PEDOT by adding an oxidizing agent (e.g. $\text{Na}_2\text{S}_2\text{O}_8$, FeCl_3) to the solution [90]. Afterwards, a spin or spray coating process can be used to deposit the already prepared solution of PEDOT with the dopant, to the substrate [88], [91]. The advantage of this method is the compatibility with the lithography patterning process [91]. However, with this deposition method the resulting PEDOT film tends to have a more disordered structure which results in a considerably lower conductivity.

The electrochemical deposition process is the most common method for depositing PEDOT for MEA applications [18], [70], [92], [93]. The electrochemical deposition process allows the tuning of multiple process parameters in order to obtain the desired film characteristics, including its biocompatibility. It is also a relatively simple process since it combines deposition, doping and the patterning simultaneously. Moreover, using the ECD process, it is possible to perform the deposition as final step of the fabrication. In this way, it is relatively easy to incorporate PEDOT coatings on currently available MEAs. However, with the current technology available for ECD, the deposition must be done individually for each electrode. Due to this, up-scaling the process to a large-batch production is not yet feasible.

Electrochemical deposition is also proven to be very versatile. This method is also used in various biomedical applications, outside its major role for microelectrode coating. Several studies suggest that PEDOT can be used for controlled drug delivery by incorporating drug substance either in the electrolyte solution or on the electrode substrate before the ECD [87], [94]. A study by Sebaa et al. showed another example of the use of PEDOT coating, deposited with ECD for corrosion prevention in the biomedical implant [95].

In the following sections, the deposition parameters that need to be optimized and the relation of each parameter to the deposition result, will be discussed.

2. 4. 1 Electrochemical Cell Setup

In the ECD, a three electrodes setup is often used. It consists of a working electrode where the PEDOT film will be deposited, a counter electrode which provides the balancing charge, and a reference electrode [92], [96]. In this setup, the reference electrode does not pass any current, therefore the net potential on its surface can be assumed to be constant (value depends on the electrode type). The reference electrode is used to provide an accurate measurement of the voltage on the working electrode [60]. The three electrodes are immersed in the solution, which contains the EDOT monomer and dopant material. When a positive potential from an outside source is applied to the working electrode, EDOT monomers will be attracted to its surface.

On the surface, simultaneous oxidation and polymerization of EDOT monomers occur, resulting in the formation of oligomers [92]. It will then undergo further reaction with neighboring oligomers to form longer chains of PEDOT polymers. At a certain length of polymer chain, the threshold of solubility will force the precipitation of the PEDOT film onto the electrode surface. This chain of reactions continue until charge equilibrium is reached or all the ions in the solution have reacted. During these oxidation-polymerization reactions, some of the dopant molecules will be trapped in between layers of polymer chains, forming the charge-transfer complex with the PEDOT chain, maintaining its conductivity.

2. 4. 2 Deposition Mode

One of the parameters which affects the physical and electrical characteristic of the finished layer is the mode of electro-polymerization. In general, to polymerize EDOT monomers on the working electrode, positive charge must be supplied to the electrode surface. This can be in form of positive potential or current, passing through the working electrode towards the counter electrode. In literature, there are 4 known modes of deposition for ECD, namely *potentiostatic*, *galvanostatic*, *coulostatic*, and *cyclic voltammetry* deposition [70], [92], [97].

In the potentiostatic mode, constant voltage is applied between the working and the counter electrodes. This is the most simple and commonly used deposition mode. Previous results suggest that potentiostatic mode is slightly superior to the other deposition modes in terms of impedance bandwidth of the resulting PEDOT film [70], [98]. Moreover, the kinetics and mechanism of this deposition mode has been extensively discussed in the literature, resulting in a better understanding and finer control of the deposition process [92], [99]. On the other hand, in the galvanostatic mode, a constant current is passed from working electrode to the direction of counter electrode. In the coulostatic mode, a specified amount of charge is discharged from the working electrode in a short pulse within specified period. Finally, in the cyclic voltammetry mode, the potential between the working and counter electrodes is cycled repeatedly within a certain range.

For deposition using the potentiostatic mode, the value of the oxidation potential of the EDOT monomer in aqueous solution, is around 0.8 V (vs Ag/AgCl) [100]. However, the exact value can differ for each electrode and the solution composition, which can be determined with the linear-sweep voltammetry method [101], [102]. During the deposition, an electrical voltage above the oxidation value is needed to start the polymerization reaction on the electrode surface. The deposition rate can be interpreted from the current measured in the working electrode. A higher current means a faster charge transfer on the surface of the electrode, which corresponds to the amount of polymerized PEDOT. Over time, the measured current will also increase due to the decrease of impedance, caused by the PEDOT film forming on the electrode. In general, a higher voltage will lead to a faster deposition rate. Cysewska et al. [98] showed that increasing the deposition potential up to 1.4 V results in a more compact film and higher conductivity of PEDOT:ClO₄. However it is also reported in the same work that a lower deposition voltage results in a higher surface area due to a more porous film structure. In the case of a MEA, both the conductivity and surface area contribute to the total impedance of the system. The larger surface area is beneficial for stimulating electrodes due to the increase of charge injection capacity. Therefore the deposition potential has to be optimized depending on the structure, function, and dimension of each microelectrode. A contrasting result was reported by Niu et al. [97], where PEDOT film was deposited electrochemically using the cyclic voltammetry method. The lower peak

potential shows a more compact film which is suggested to be the result of slower deposition process. Vice versa, the higher peak potential shows more fractal and rough surface. However it should be noted that these contradicting results might also be the result of the different deposition modes used. The SEM images from the resulting film on these studies are shown in Fig.2.10

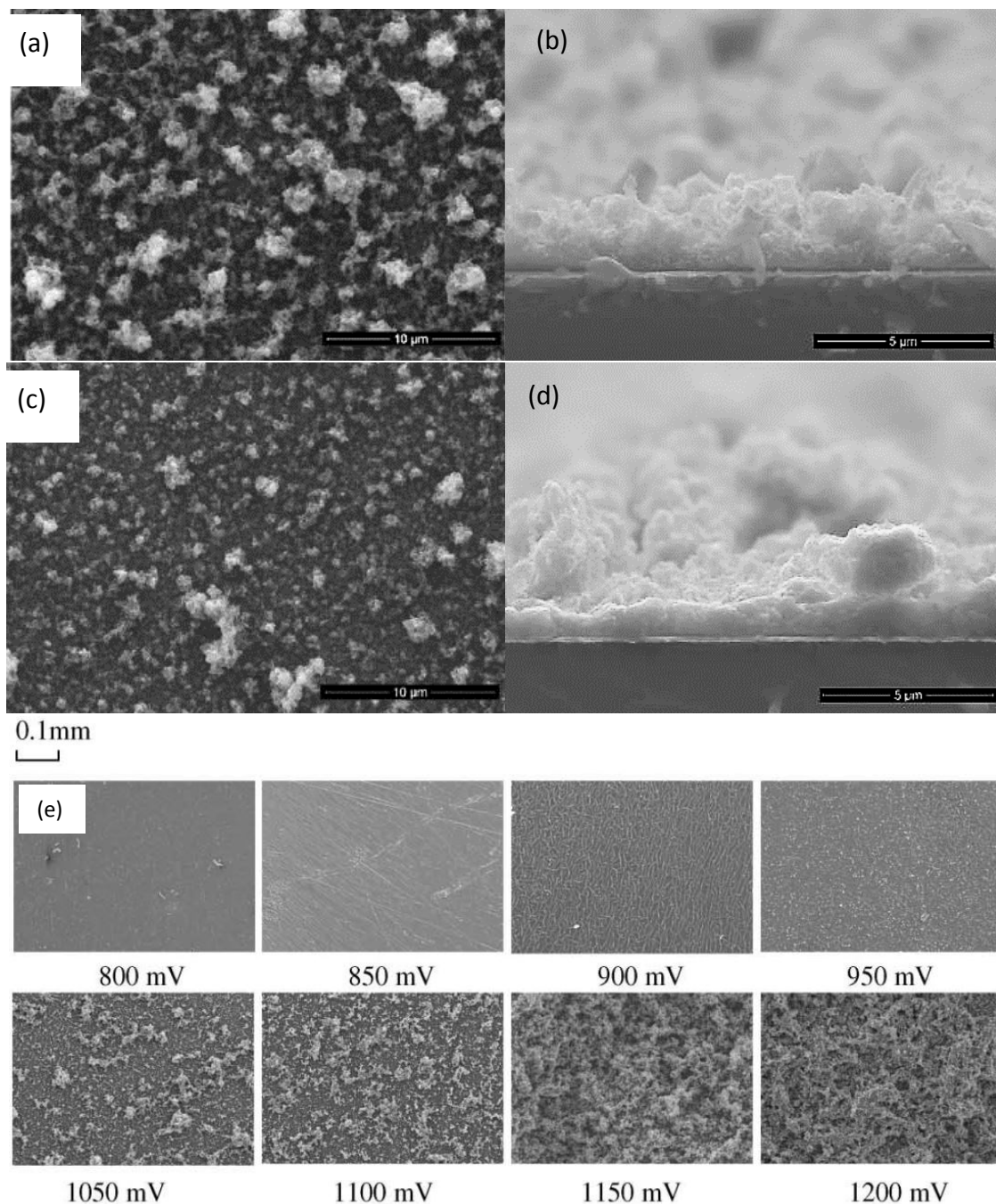


Figure 2.10. (Top) The surface of the PEDOT film deposited potentiostatically at 1.2 V (a,b) shows a more rough topology, compared to the film deposited at 1.4 V (c,d). (Cysewska et al. 2015 [98]). (e) The surface of PEDOT film deposited by cyclic voltammetry with different switching voltage. (Niu et al. 2001 [97])

A more detailed potentiostatic deposition procedure was proposed by Randriamahazaka et al [92]. It consists of a two steps deposition process. In the first step, a potential of 0,8 V (vs. Ag/AgCl) is applied to completely polarize the working electrode surface before initiating oxidation of the monomers. On the second step the potential is stepped up to the constant oxidation potential value (> 0.8 V) to start the polymerization. The first step will eventually confine the abrupt transient current at the beginning of the potential stepping, due to the double layer charging. Since the first step will not result in any deposition, the transient current will not affect the quality of the film. This way, the main deposition process in the second step will have less transient current, and the deposition rate can be stabilized.

In general, the resulting film thickness is related to the total charge passing through the electrode surface during electrodeposition. The film thickness (in cm) can be approximated from Eqn.4;

$$\tau = \frac{q \cdot (m+px)}{F \cdot \rho \cdot (2+p)} \quad (4)$$

Where q is the deposition charge density (C/cm^2), m and x are the molecular weight of the EDOT monomer and dopant respectively (g/mol), p is the doping level, F is the Faraday constant (C/mol) and ρ is the CP density (g/cm^3) [70]. Due to the varying density of the resulting film, the above equation is only used to make an approximation of the total thickness of the finished layer.

2. 4. 3 Adhesion Layer

The electrochemical deposition of PEDOT, requires the use of noble metals or other inert conductive material as an adhesion promoter on the electrode surface [103]. It is suggested that the adhesion between polymeric film and inert metal relies on the mutual hydrophobicity between the two materials [104]. The most widely used metals are Gold (Au), Platinum (Pt), Iridium (Ir) or its alloys. Having noble metals as the electrode surface during ECD also results in less corrosion due to the acidic environment of the deposition solution. Apart from noble metals, glassy carbon can also be used as an adhesion layer for PEDOT. A result by Kayinamura et al. [104] suggests that PEDOT deposited on glassy carbon exhibits a lower impedance with near-ohmic characteristics over broad range of frequencies, compared to PEDOT on platinum or gold substrates. Another result published by Xiliang Luo and Xinyan Tracy Cui [105], shows a possibility to coat PEDOT on Magnesium for non-electronic application, which proves that PEDOT can also be deposited electrochemically on more reactive materials.

2. 4. 4 Dopant Materials

In previous works, various dopants materials have been used to improve the PEDOT electrode performance [70], [93], [106], [107]. The dopant materials can also affect the surface morphology of the electrode which in turn changes the electrical performance. The most widely used material is Poly (styrenesulfonate), simply known as PSS, which also acts as surfactant to increase the solubility of EDOT monomer in the water [108]. The use of PEDOT:PSS has been reported in several experiments for in-vitro measurement [20], [79], [106]. The use of dopant material other than PSS usually is done in combination with an organic solvent such as acetonitrile or a surfactant such as Sodium Dodecyl Sulfate (SDS) [109], [110].

Other variations of dopants include Carbon Nanotubes (CNT), Tetrafluoroborate (BF_4), Sulphate (SO_4), para-Toluene Sulfonate (pTS), and perchlorate (ClO_4). Among these materials,

tetrafluoroborate (BF_4) shows a superior performance as dopant material [70], [93], [111]. Compared to the commonly used PSS dopant, BF_4 is a much smaller salt molecule which can produce a more dense polymeric film. Several findings suggest that ClO_4 is superior to BF_4 in term of conductivity, but BF_4 has the advantage of proven biocompatibility and stability [93], [112]. The electrochemical impedance spectroscopy measurement reported in [70], shows that PEDOT: BF_4 has a lower impedance over a wide range of frequencies compared to ClO_4 , PSS, pTS, and PF_6 , as shown in Fig.2.11. In the result reported in [93], the electrochemical impedance of PEDOT: BF_4 coating was reported as being lower than that of CNT:PEDOT:PSS. To give a comparison between the different dopant materials, the characteristics for each dopant are presented in Tab.2-3.

The dopant composition can also alter the stability of the polymer coating. Mandal et al. [93] reported on the accelerated ageing of PEDOT: BF_4 , PEDOT:PSS, and CNT:PEDOT:PSS coatings, showing that PEDOT: BF_4 film exhibits the longest half-life compared to the other coating composition, as shown in Fig.2.12.

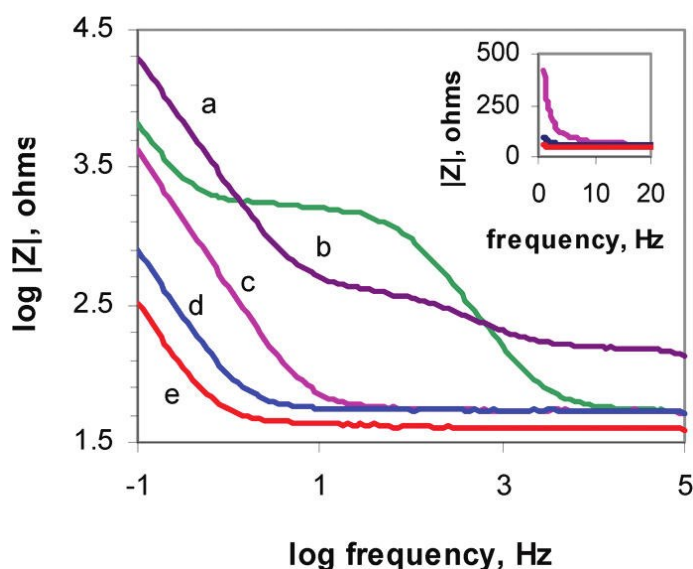


Figure 2.11. The plot of Impedance of PEDOT film doped with different dopants, (a) PSS (b) pTS (c) PF_6 (d) ClO_4 (e) BF_4 . (Reprinted from Kayinamura et al. 2010 [30])

TABLE 2-3. The characteristics of dopant materials which are used in electrochemical deposition process

DOPANT MATERIALS	CHARACTERISTICS	REFERENCES
Poly(styrene sulfonate) PSS	Big molecule (polymer), less dense PEDOT film. Acts as surfactant to increase the solubility of EDOT in water. Known to be biocompatible. Low chemical stability.	[18], [20], [69], [70], [79], [106], [113]
Para-Toluene Sulfonate pTS	Big molecule. Lower impedance than PSS doped PEDOT but higher than the more simple salt molecule dopant. Common use in biomedical application.	[70], [114], [115]

Perchlorate ClO₄	Small molecules, compact PEDOT film with high porosity and low impedance. Its biocompatibility is still underreported. [70], [112], [116]
Hexafluoro-phosphate PF₆	Small molecules, compact PEDOT film with high porosity, lower impedance than PEDOT:PSS. [70], [97], [112]
Tetrafluoro-borate BF₄	Small molecules, compact PEDOT film with high porosity, lower impedance than PEDOT:PSS. [21], [70], [93], [111], [112] Biocompatible and stable in the long term <i>in-vitro</i> and <i>in-vivo</i> application.
Carbon Nanotube CNT	Large variation of molecule type and sizes. The structure of resulting film follows the type of CNT. [19], [107] Inherent high conductivity, inert and chemical stability. Its <i>in-vitro</i> use is still uncommon and underreported.

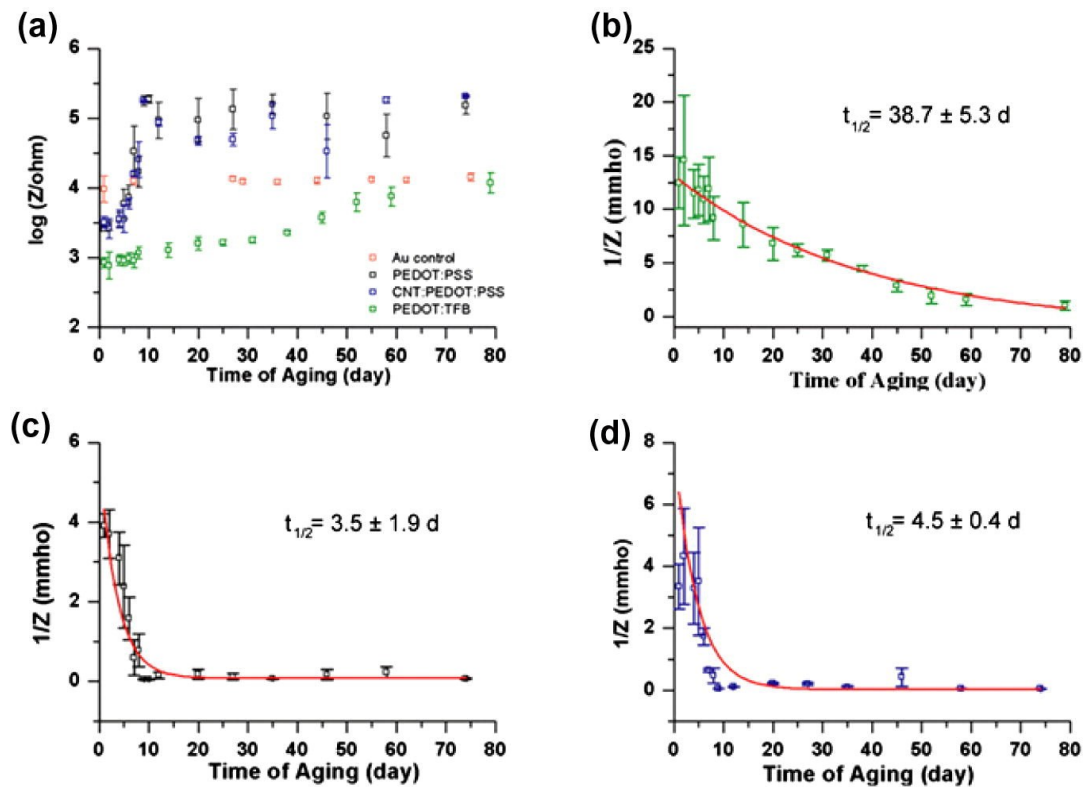


Figure 2.12. The Impedance plot over time, from different coatings during the accelerated aging test (@ 1 kHz) (a). The half-life evaluation of PEDOT:BF₄ (b) PEDOT:PSS (c) and CNT:PEDOT:PSS (d), showing the admittance over time. (Mandal et al. 2014 [93])

2. 4. 5 Solution Concentration

In order to mix the monomer and dopant into a solution, several solvents have been used. Deionized (DI) water is the most common solvent in PEDOT ECD because of its ease of handling. However, due to the ability of water molecules to form an electron donor (OH⁻ radicals), it can also

get involved in the polymerization reaction at the electrode surface, creating a disorder in the polymeric chain. To replace DI water, acetonitrile is commonly used as solvent. Randriamahazaka et al. [92] used acetonitrile to improve the long-term stability of the resulting PEDOT film. The solubility of EDOT monomer is also increased in Acetonitrile compared to DI water [92].

The concentration of monomer and dopant in the electrodeposition solution determine both the rate of deposition and the properties of the resulting layers. It may seem counter-intuitive, but increasing the solution concentration does not necessarily improve the electrochemical characteristics of PEDOT film. Higher monomer or dopant concentrations will increase the polymerization rate, which may result in a more disordered cluster of polymer chains. This disorder can then introduce a less dense layer in the latter phase of polymerization, with non-conductive defects or voids in between [70]. Kayinamura et al. [70] suggested that monomer concentration should be less than 0.0125 M but not less than 0.00625 M, to provide sufficient amount of monomer in the solution while maintaining control over the deposition rate. In the same work, the increase of the dopant material concentration also produced the same negative effect as the monomer concentration. However, the above work did not include a wide range of solution concentrations, while there are several evidences of the successful deposition with a higher solution concentration [92], [97]. The mostly used value of solution concentration in the literature is 0.01 M for the EDOT monomer and 0.1 M for the dopant materials [21], [70], [92], [93].

An example of a successful electrodeposition process by Mandal et al. [93], was done by using a solution of EDOT and tetrabutylammonium tetrafluoroborate (TBABF₄) in acetonitrile. The use of BF₄ dopant reported in this experiment, showed a stable low impedance in an accelerated ageing test up to 75 days equivalent. To coat the microelectrode with PEDOT:BF₄ the probe was first coated with a thin layer of Au by electrochemical deposition. The conductive polymer deposition was done from a solution containing 10 mM EDOT monomer, and 0.1 M TBABF₄ in acetonitrile. The deposition process was performed by applying a constant potential of 1.3 V for 60 seconds, and the resulting thickness was around 1.5 µm. As already discussed in Section 2.4.2, the thickness of the film is dependent of the amount of charge delivered. Thus, this deposition sequence may result in different thickness for different microelectrode size, due to the difference in current density.

2. 4. 6 Bioactive Materials

The incorporation of bioactive molecules can alter the polymeric film characteristic towards the cell culture or initiate specific reactions from the cell on the electrode surface. As shown by Xiao et al. in their experiment, the addition of Adenosine Tri-Phosphate (ATP) to the electrolyte solution induced cell adherence to the electrode surface [101]. This can be an advantage for recording electrodes which require a close proximity to the target cells to get a signal with good quality [102]. The addition of bioactive materials can be done by mixing them into the electrochemical solution. In the polymerization process, this material is attracted and trapped in the polymer film along with the dopant. In the case of certain biomolecules which cannot be combined with ECD, ion exchange mechanisms can be used after the main electrochemical deposition process to incorporate them in the PEDOT film [78], [102], [117].

Chapter. 3 Device Fabrication

The fabrication process of the device for this project can be divided into two parts: (i) the fabrication of the MEA and (ii) the electrochemical deposition of PEDOT coatings on the electrodes of the MEA. The end goal of the first part is to fabricate and package a Cytostrecth device with platinum coated microelectrodes. In order to do this, the wafer-scale microfabrication process previously presented by Pakazad et al. [12] and Gaio et al. [11] was modified and optimized in order to cover the TiN electrodes of the Cytostretch with a layer of Pt coating. Meanwhile, the second part consists of a post processing step in which PEDOT is deposited on top of the platinum electrodes by electrochemical polymerization.

This chapter focuses on the first step of the fabrication, presenting the fabrication of the Cytostretch chip and the optimization performed in order to coat the electrodes with Pt. Meanwhile in Chapter 4, the electrochemical deposition process of PEDOT is presented.

3. 1 Wafer Fabrication

The wafer-scale fabrication is illustrated in the Fig.3.1. The Cytostretch devices in this experiment are fabricated on 4 inch silicon wafers (Fig.3.1-a). The process starts with the deposition of 2 and 6 μm of Silicon-dioxide (SiO_2) by plasma-enhanced chemical vapor deposition (PECVD) on the front and backside of the wafer, respectively (Fig.3.1-b). The SiO_2 layer on the back is patterned by dry-etching to define the membrane area. The process continues by sputtering a 1.5 μm -thick aluminum-silicon (AlSi) layer on the frontside of the wafer. The AlSi is then patterned by dry-etching to define the contact pads. Next, a 100 nm-thick platinum layer is evaporated on the wafer and patterned by lift off to form the electrodes of the MEA (Fig.3.1-c). In the next step, the interconnection lines extending from the contact pads to the MEA are fabricated. For this, an 800 nm-thick photosensitive polyimide (Fujifilm LTC 9305) layer is deposited by spin coating, patterned and cured at 350° C for 1 hour, in the low pressure N_2 atmosphere (Fig.3.1-d). Subsequently, a layer of 200 nm of TiN is sputtered in the front side of the wafer, and patterned by dry etching (Fig.3.1-e). A second layer of 800 nm-thick polyimide is deposited and patterned to provide electrical insulation of the metal lines (Fig.3.1-f). Subsequently, a PDMS layer is deposited by spin coating on the front side of the wafer at a spin speed of 6000 rpm for 60 s and cured for 30 min at 90 °C, results in a layer thickness of 10- μm . The contact pads are then open by patterning the PDMS layer by means of reactive ion etching using an Al layer as hard mask (Fig.3.1-g). Finally, the membrane is released by removing the Si and the SiO_2 layers underneath the membrane using deep reactive ion etching (DRIE) and buffered hydrofluoric acid (BHF), respectively (Fig.3.1-h). The detailed results from each step of the fabrication sequence, explained in the Appendix A.1.

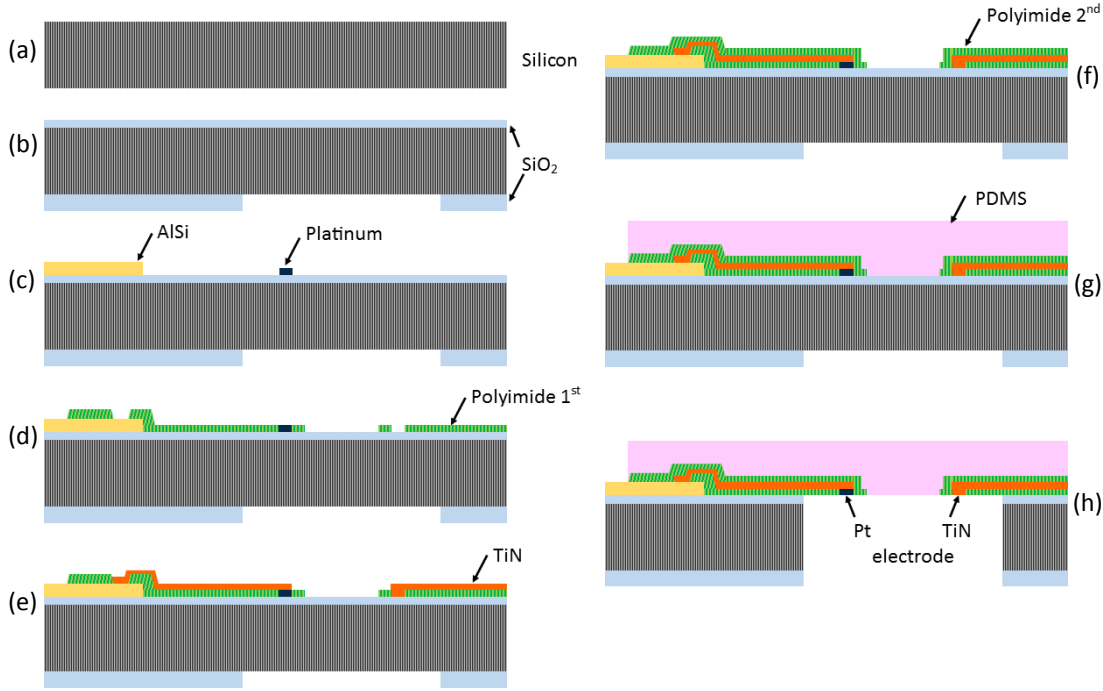


Figure 3.1. The schematic cross-section from each fabrication step of the Cytostretch device.

3. 1. 1 Platinum Coating

During the fabrication process a problem with the adhesion of the platinum coating was encountered. During the wet etching in step (h), the 80 nm platinum coating detached from almost every microelectrode, showing a poor adhesion between the Pt layer (deposited in step (c)) and the TiN layer (deposited in step (e)). In order to reduce this problem, a 10 nm –thick layer of titanium (Ti) was added in between the Pt and the TiN. Ti is a material that is commonly used as an adhesion layer for both Pt and TiN. With the addition of this titanium layer, the platinum coating was expected to be strongly bonded with the adjacent TiN surface.

However, the addition of the Ti did not solved the problem, in fact during the fabrication of one wafer, 92 % of the electrodes lost their Pt coating as shown in Fig.3.2. From the SEM observation, it was hypothesized that the adhesion problem was concurrent with the crack on the platinum coating. Additionally, most of the cracks looked like converging toward the middle of the microelectrode, resembling the result of mechanical buckling. From this observation, the cracking of the platinum coating was hypothesized to be due to the pressure from the surrounding polyimide and PDMS films. The pressure most likely appeared as a result of the water absorption, which subsequently caused swelling of the polymer during the wet etching process. However, at the same time there were no crack observed on the TiN layer, nor on the device that were fabricated with only TiN microelectrodes. This indicated that the TiN layer is strong enough to resist the pressure from the surrounding polymer film. Therefore, a proper mechanical bonding between the Pt and TiN layer should be able to resolve this problem.

The lack of mechanical integrity between the Pt coating and the TiN layer, regardless the addition of adhesion layer, might be the result of the BHF etchant seeping through a gap between the edge of the Pt and the surrounding polyimide during the wet etching process (step (h)). The seeping of

the BHF etchant might also initiate and then spread from eventual defects on the Pt surface due to non-uniform deposition. This etchant then etched away a small portion of Ti layer at the beginning of the wet etching step. At this point, the adhesion of Pt toward the TiN layer was gradually reduced, and at the same time, the pressure from surrounding polyimide film buckled the Pt layer and created cracks. From this crack, the etchant can easily seep through, and etch the remaining Ti layer.

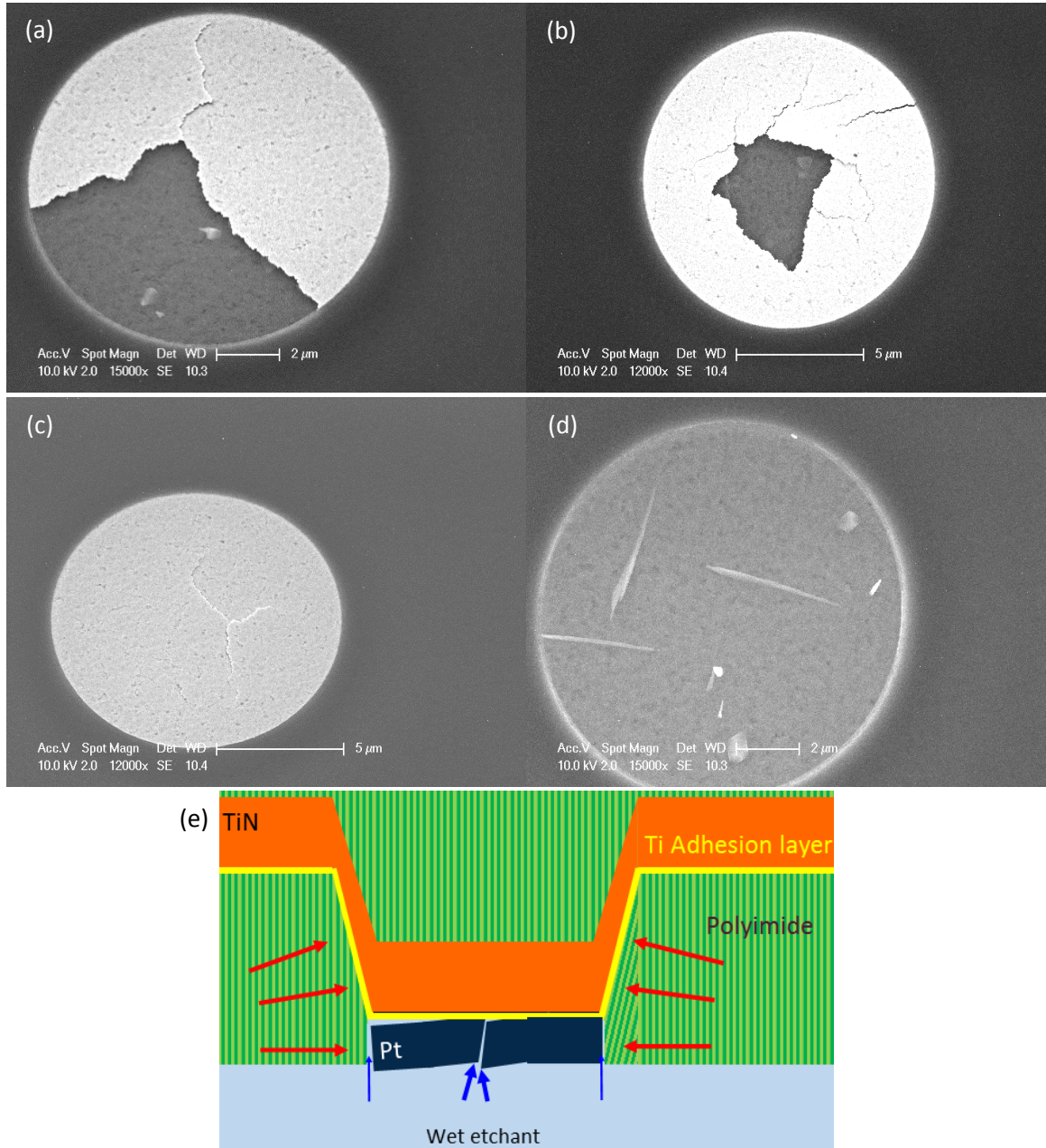


Figure 3.2. The SEM image of microelectrode coated with Pt showing cracks (a,b,c), and fully delaminated electrode showing the TiN surface (d). The illustration of buckling of the Pt coating, after the seeping of BHF etchant on the edge of Pt (e).

To solve this problem, a thicker platinum layer was used, in combination with a dimension adjustment of the first PI layer at the step (d) (in Fig.3.1), which subsequently created an overlap between the edge of the Pt and the PI film. The thickness of Pt coating was increased from 80 nm

to 100 nm. The additional thickness is expected to increase the conformality of the platinum layer and reduce the chance of defects in the coating surface. At the same time it also increases the distance between the titanium adhesion layers to the BHF during wet etching. By overlapping the polyimide film, the titanium adhesion layer was expected to be completely isolated from the BHF etchant leak, as shown in the Fig.3.3-b.

In this revised fabrication sequence, a new set of lithography mask was used. In this mask set, the diameter of the circular microelectrode was increased from 12 to 30 μm . The expansion of the microelectrode size might also contributed to the adhesion by increasing the area of the Ti adhesion layer accordingly. This combination of multiple approaches was proven to be successful. The final result of Pt coating and the corresponding cross section are shown in the Fig.3.3.

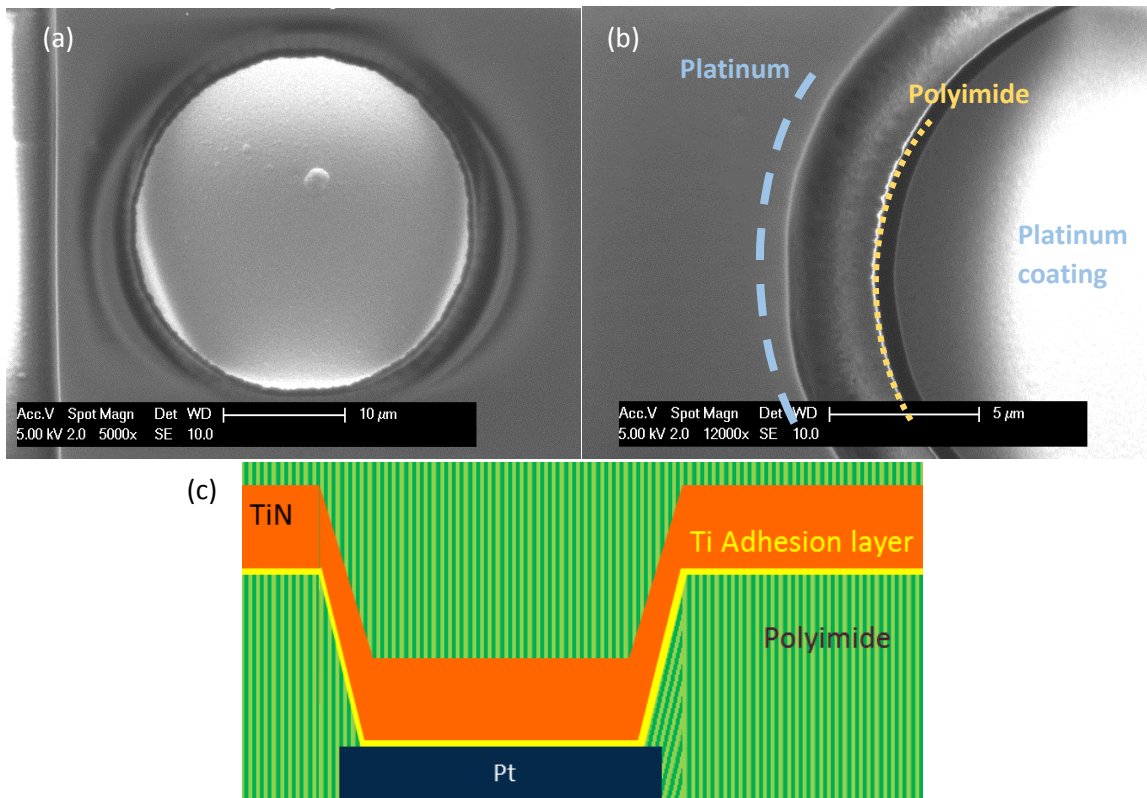


Figure 3.3. The SEM image of the new version of Pt coated microelectrode, as seen from the wafer top side (a), and the overlap between polyimide film with Pt coating (b). The schematic cross section of the modified Pt coating (c).

In order to investigate the effect of the size of the microelectrode to the adhesion of the Pt coating, the masks were designed in such a way that some of the Pt disks were smaller than the electrodes, as shown in the Fig.3.4. As can be seen in the Fig.3.4, it turned out that the size difference did not affect the adhesion between the Pt coatings with TiN layer. From the SEM images in Fig.3.4-c,d, it can be observed that in the case of the smaller Pt coating, the adhesion layer is fully isolated by the surrounding TiN layer during wet etching. After this change, 100% of the Pt coatings was not delaminated from the microelectrode surface, nor were any apparent cracks observed at the end of the process. The final flowchart of the fabrication processes is attached in the Appendix A.2.

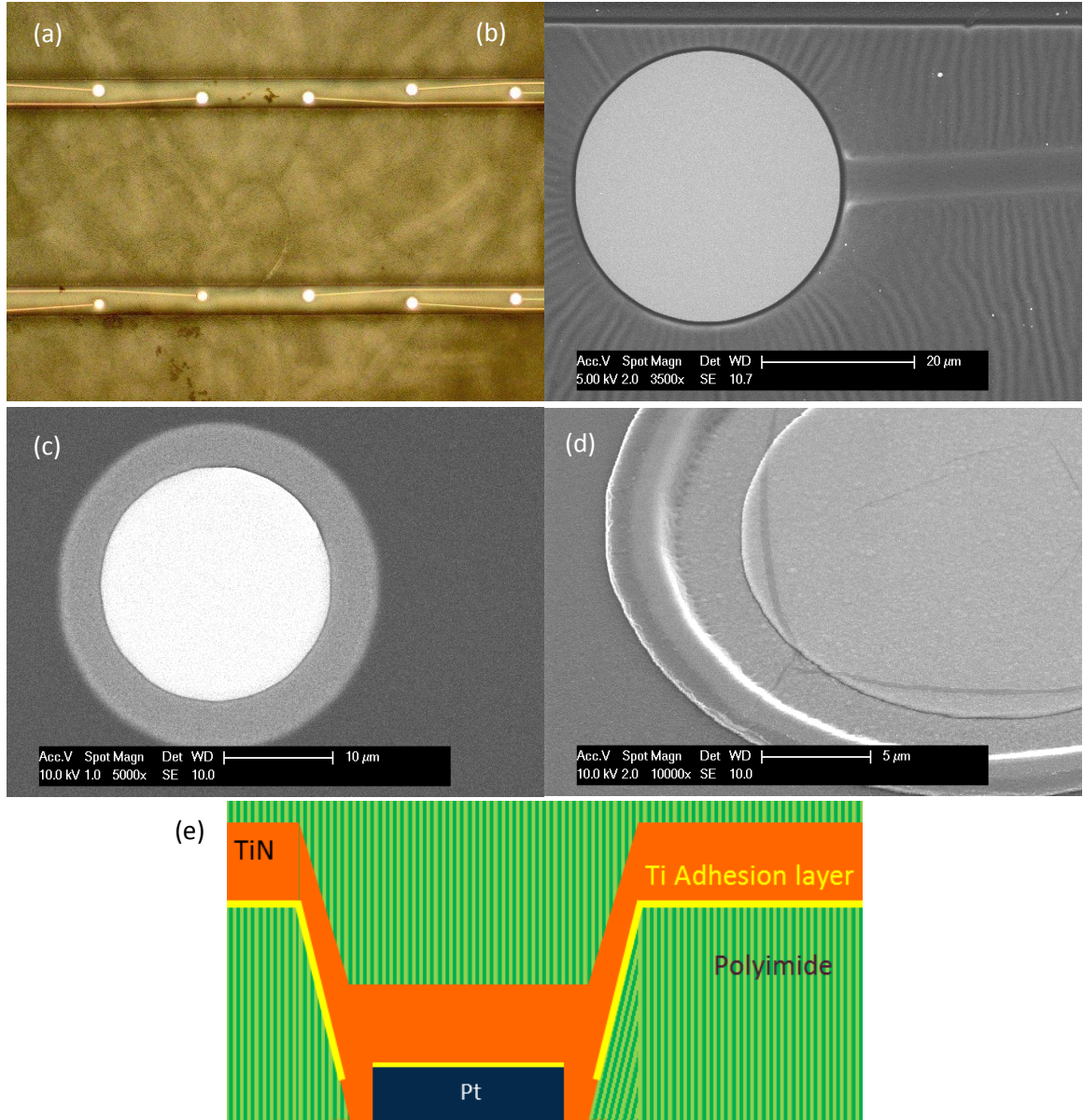


Figure 3.4. The Pt coated MEA as seen under optical microscope (a). The SEM image of the full-sized (b), and small-sized (c) Pt coated microelectrode. The gap between Pt coating and the polyimide film on the smaller size Pt is filled with TiN (d). The schematic cross-section of microelectrode with the smaller-size Pt coating (e).

3. 1. 2 Adhesion between Polyimide and PDMS

An additional adhesion issue between polyimide (deposited in step (f), Fig.3.1) and PDMS layer (deposited in step (g)) was identified. This was noticeable after the immersion of the device in the Acetone solvent that was used to remove the resist after the wet etching in step (h), which caused the delamination of the polyimide film from the PDMS membrane (Fig.3.5). This adhesion issue might result in delamination of the PI structures during the application of strain to the membrane. In order to solve this problem, plasma etching treatment was tested to improve the adhesion between the two layers.

Plasma etching treatment is done by bombarding the surface of the material with argon plasma. The bombardment performed for a short time increases the surface roughness of the polyimide film. The rough surface is hypothesized to create a physical interlock on the interface between the polyimide film and the PDMS membrane [118].

To test the plasma etching treatment, a batch of test device was fabricated with implementing this treatment. The fabrication of the test devices roughly followed the same steps as the full device except for the omission of the electrodes and the interconnection structures. The treatment was done after the curing of the polyimide film prior to the deposition of the PDMS layer. Test devices with and without plasma etching treatment were fabricated in order to compare and assess the effectivity of the treatment.

The adhesion of the Polyimide to PDMS membrane was evaluated by immersing the test device in several organic solvents (Acetone, N-Methyl Pyrrolidone, TMAOH). The results of immersion test in the acetone are shown in the Fig.3.5. The detailed test procedure and the results of immersion in the different solvents are explained in the Appendix A.3. From the results of the immersion test, it can be concluded that the plasma etching treatment can significantly improve the adhesion between polyimide and PDMS layers. Therefore, plasma etching treatment was included in the fabrication of the Cytostretch device.

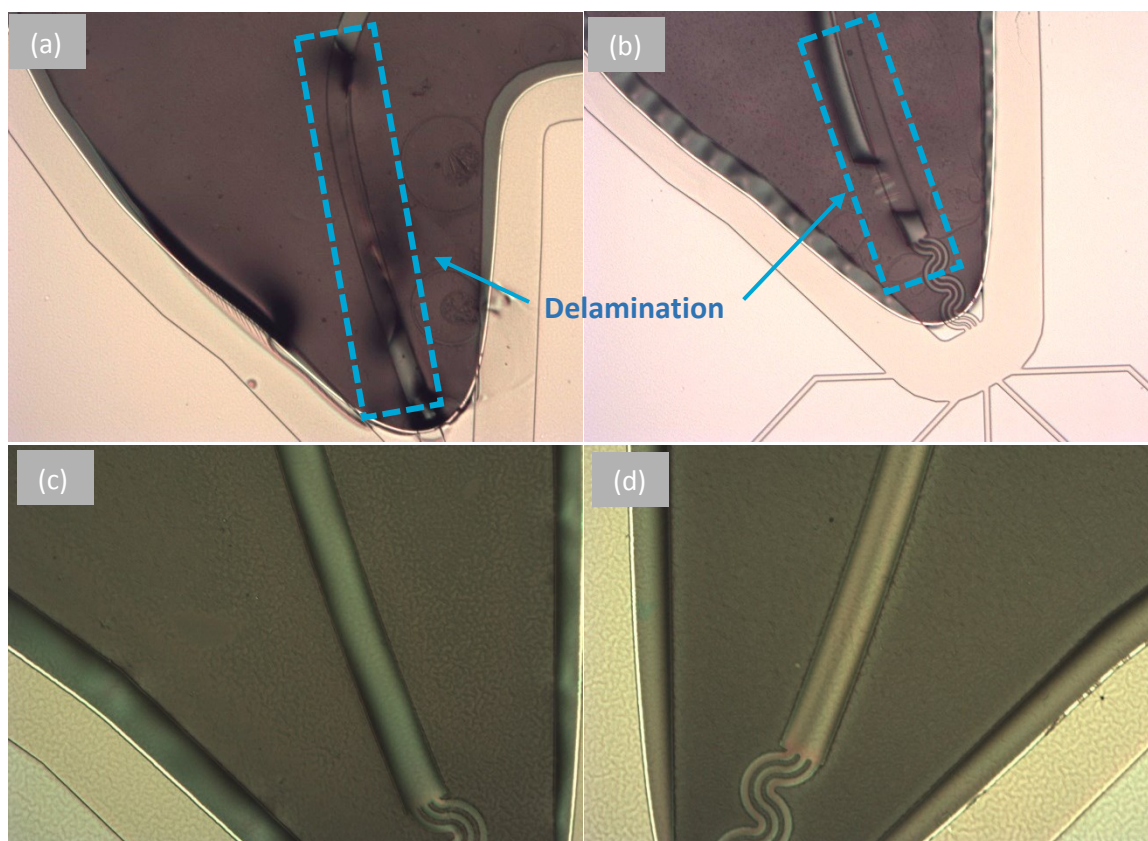


Figure 3.5. The delamination of polyimide film from PDMS after immersion in Acetone at 40°C for 5 minutes, as observed under optical microscope (a,b). The result of plasma etching treatment showing no delamination of the polyimide film after immersion in the same solvent for 20 minutes (c,d).

3. 2 Device Packaging and Results

The final results of the device fabrication is shown in the Fig.3.6-a,b. The wafer is diced and the devices are wire-bonded onto a printed circuit board (PCB), in order to be used on the electrochemical experiment phase. Glass tubes were fixed on the PCB with epoxy glue (cured at 75° C for 90 minutes). The glass tube is used to contain the electrolyte solution during deposition and characterization. The final packaging, and the construction of the electrochemical cells are shown in the Fig.3.6-c to f.

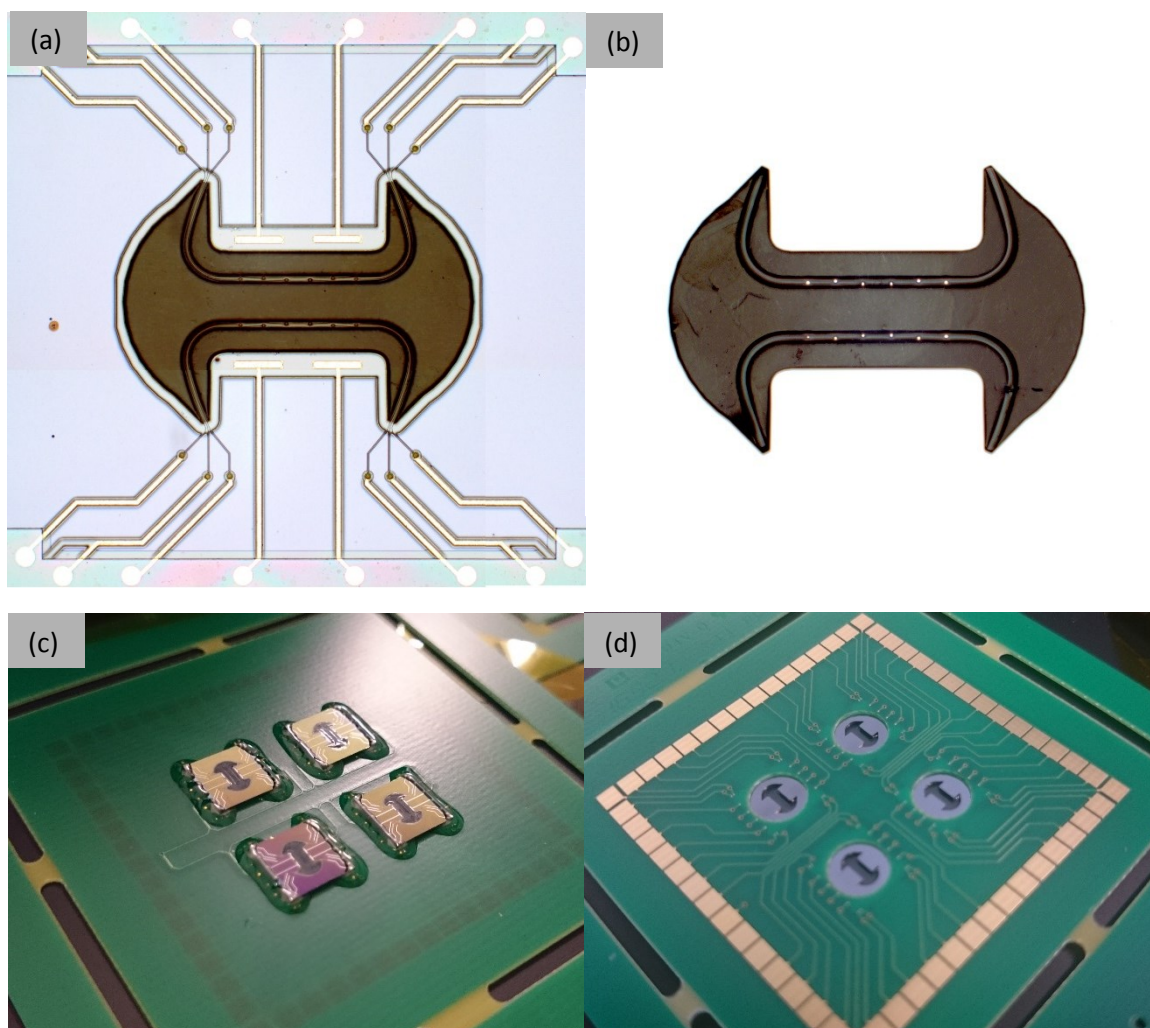


Figure 3.6. The final result of the Cytostretch device, as seen from the front side with PDMS membrane (a), and from the back side showing the MEA surface (b). The dices are positioned upside-down on the PCB, as seen from the back of the PCB (c), and the front-side (d).

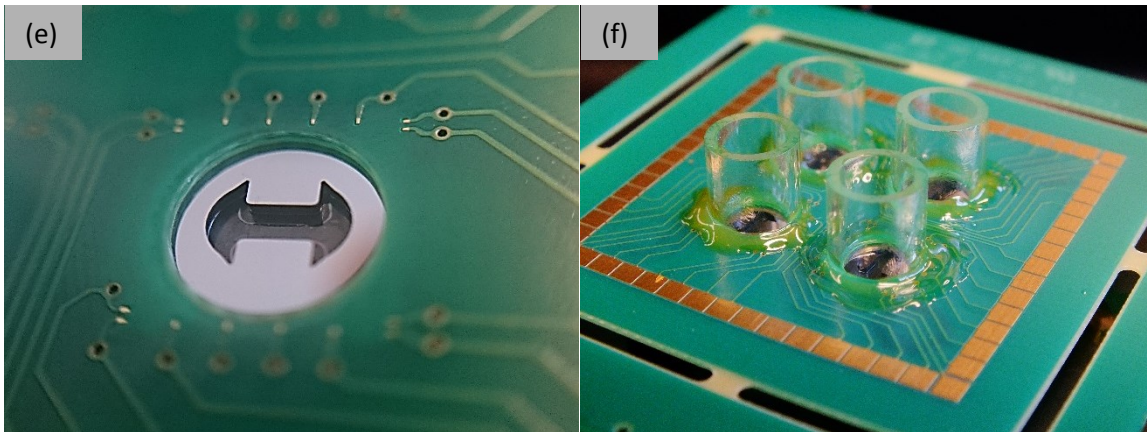


Figure 3.6. (cont.) Close-up image of the dice on the PCB which shows the structure on the flexibe membrane (e). The glass tube is fixed on top of every dice (f).

Chapter. 4 Electrochemical Deposition & Preliminary Characterization

In this chapter, the electrochemical deposition and characterization of PEDOT electrodes for the Cytostretch device are presented. To ensure the reproducibility of the process and the result, two different reference electrodes were used in this work. The calibration of the employed reference electrodes is presented in the Section 4.1 and Appendix A.4. A test-deposition was performed to evaluate the feasibility of the process (Section 4.2). The test deposition was also aimed to identify the critical deposition parameters that need to be adjusted in this preliminary attempt. During this step an adhesion issue in the Cytostretch fabrication process was identified. Consequently the fabrication process of the device was improved in order to address this problem. Afterwards, the deposition of PEDOT on the Cytostretch electrodes was repeated and subsequently optimized. The new version of the device with PEDOT electrodes was characterized as reported in Section 4.3. Figure 4.1 summarize the content of this chapter, visualizing the process followed in order to obtain the optimal PEDOT electrodes.

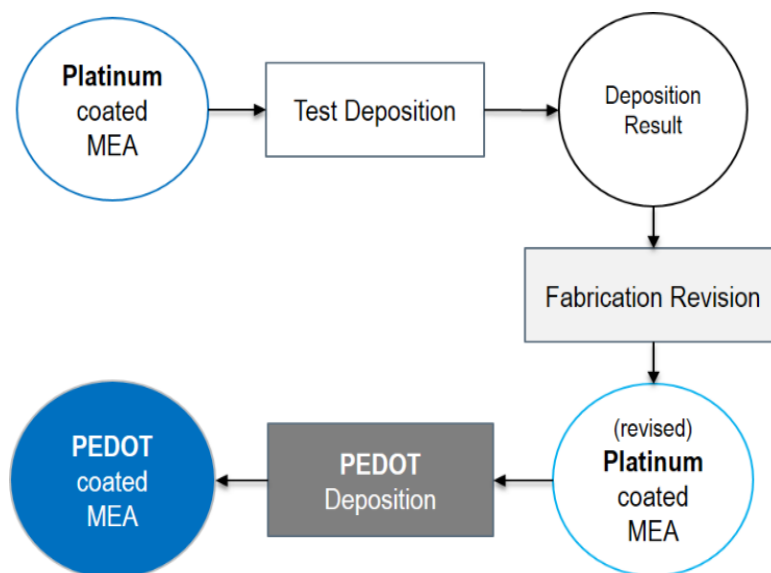


Figure 4.1. The sequence followed in this research, in order to investigate the feasibility and the optimization of the PEDOT deposition.

4. 1 Reference Electrode Calibration

The reference electrodes used in this project for the electrochemical deposition of PEDOT were calibrated in order to ensure their functionality. From this calibration, the value and the stability of electrode potentials can be assessed. In this work PEDOT was deposited in both an aqueous and a non-aqueous solution. Consequently, two different kinds of reference electrodes were employed: an aqueous Ag/AgCl reference electrode and a non-aqueous reference electrode. The calibration of the aqueous reference electrodes is reported in Sections 4.1.1, while the calibration of the Non-aqueous reference electrodes is reported in Appendix A.4.

The reference electrode that was used in the aqueous electrochemical experiment, in this research is the leak-less miniaturized Ag/AgCl electrodes ($\varnothing = 2\text{ mm}$), manufactured by eDAQ (Fig.4.2). To ensure the functionality of this reference electrode, a calibration was performed with cyclic voltammetry in an aqueous solution of **0.004 M Ferrocyanide** ($\text{K}_4\text{Fe}(\text{CN})_6$) with a supporting electrolyte of **0.125 M KCl**. The cyclic voltammetry is performed to obtain the formal redox potential of ferrocyanide, which then can be compared to the absolute value of the formal potentials reported in the literature. The calibration procedure was developed based on the procedure presented by Pavlishchuk and Addison [119]. The CV measurement was done with a Pt strip and a Pt coil as working and counter electrode, respectively. The measurements were performed at different scan rates in order to assess the variations of half-cell potentials over the different scan rates. The results of cyclic voltammetry over different scan rates are shown in the Fig.4.3, and the redox potential values are listed in the Tab.4-1.



Figure 4.2. The miniaturized Ag/AgCl electrode.

In Tab.4-1, E_o and E_r are the oxidation and reduction peaks respectively, in each scan cycle. E_{ro} is the measured formal potential of the Ferrocyanide, which is defined as the average of reduction and oxidation potentials. The v and ΔE are the scan rates and the difference of oxidation-reduction peaks from each scan. The half-cell potential E_{hc} , is calculated from the difference of the measured formal potentials to the reported absolute value (439.2 mV Vs SHE) [120], [121]. The value of half-cell potential shows the voltage bias of the reference electrode during the measurement, in respect to the Standard Hydrogen Electrode (SHE).

From the measurement results, it can be concluded that the Ag/AgCl reference electrode was providing a stable half-cell potential of 209.9 mV (vs. SHE). This value is slightly different from the

reported half-cell potential of the same type of references (222.3 mV, in Section 2.2.1), but the difference is insignificant (12.4 ± 1.05 mV). Moreover, the variation of potentials from each scan was negligible proving the functionality of the reference electrode.

A similar calibration process was repeated for the miniaturized Ag/AgCl with a salt bridge, proving its functionality and stability in a non-aqueous medium. The complete set of results of the calibration of this reference electrodes is reported in Appendix A.4.

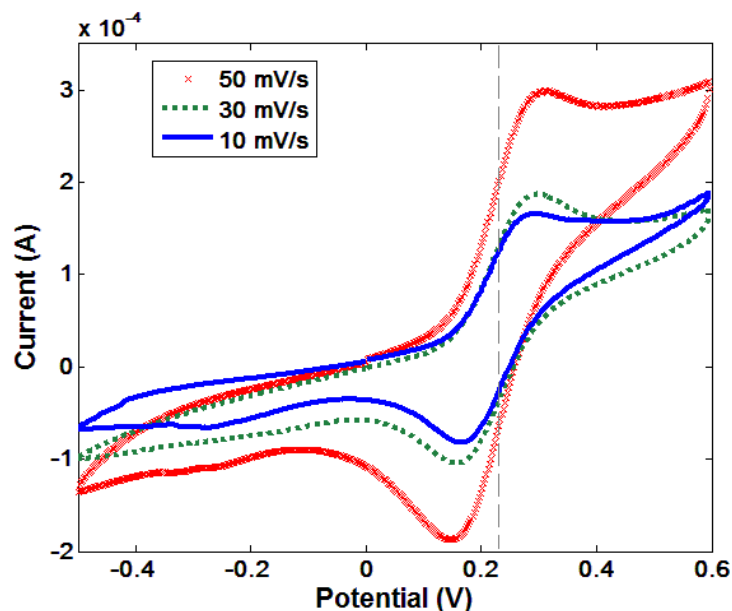


Figure 4.3. The I-V plot from the CV measurement of Ferrocyanide:KCl solution, with different scan rates. Vertical dash line shows the average of formal redox potentials of Ferrocyanide, measured in this experiment.

TABLE 4-1. The calibration results of miniaturized Ag/AgCl reference electrode in an aqueous solution of Ferrocyanide + KCl.

ν (mV/s)	E_o (mV)	E_r (mV)	E_{ro} (mV)	ΔE	E_{hc} (mV)
10	292.6	164.9	228.8	127.7	210.5
	293.5	164.2	228.9	129.3	210.3
	295.4	163.7	229.5	131.7	209.7
30	298.6	157.0	227.8	141.6	211.4
	301.2	155.8	228.5	145.3	210.7
	302.6	155.3	228.9	147.3	210.3
50	313.6	148.9	231.3	164.7	208.0
	314.4	147.3	230.9	167.1	208.4
	314.2	144.5	229.3	169.7	209.9
Average =			229.3 ± 1.05		209.9 ± 1.05

4. 2 Test Deposition

In order to investigate the deposition of the PEDOT coating, a test deposition was performed to demonstrate the feasibility of the process. The result of this preliminary deposition was expected to give an insight into the approach needed for optimizing of the deposition. In this section the preliminary characterization of the MEA before the deposition will be presented. Next, the discussion of the deposition process and results will be presented and discussed.

4. 2. 1 Pt Electrodes Characterization

The electrochemical performance of the Pt electrodes was characterized before benign coated with PEDOT. EIS was performed with a three electrodes cell setup in combination with Metrohm Autolab Potentiostat/Galvanostat. Fig.4.4 shows the setup of the Cytostretch device for the electrochemical cell.

The measurement was performed in a Phosphate-Buffered Saline (PBS) solution (produced by Sigma Aldrich), with an Ag/AgCl reference electrode and a Pt strip as the counter electrode, with a considerably larger surface area (ca. 16 mm²). The magnitude of the signal in the EIS was 50 mV rms with 0 V bias, with a frequency range of 0.01 Hz to 10 kHz. All the electrochemical measurements in this experiment were performed in a faraday cage to block electromagnetic noise.

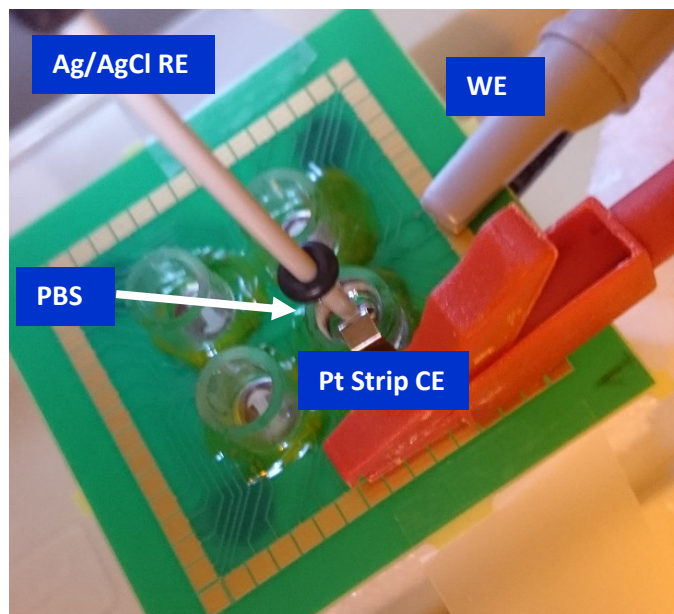


Figure 4.4. The construction of the three electrode cell used in this experiment. The Cytostretch MEAs are connected by the copper interconnection line on the PCB, to the potentiostat as working electrodes (WE).

The bode plots of EIS measurement of the Pt MEA are shown in the Fig.4.5. In the figure, the results shown are the average of 5 microelectrodes. From the measurement results, the average impedance of the Pt MEA at 1 kHz is 110.6 k Ω . This result gives an estimation of the performance of the fabricated Pt electrodes and proves the electrical connection of the Pt coating with the rest of the interconnection line.

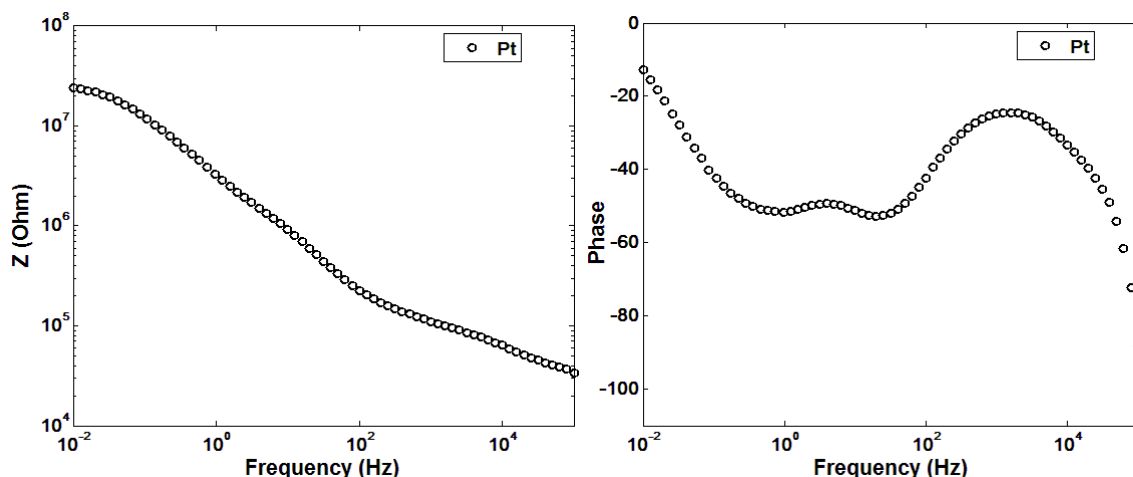


Figure 4.5. The Bode plots of EIS measurements from the Pt coated microelectrodes.

4. 2. 2 PEDOT:BF₄ Deposition

In this experiment Acetonitrile (ACN) solvent was used to dissolve the monomers and dopant materials. The most commonly used solution concentration for EDOT monomers in aqueous solution is 0.01 M [20], [70], [88]. This value is related to the limited solubility of EDOT in the water. With an organic solvent, a higher concentration can be used to increase the deposition rate. In this test deposition, the solution of **0.05 M EDOT** monomers, with **0.1 M TBABF₄** dopant in **ACN** was used. This value is higher than the average value that is used in most literature, thus the deposition rate is also expected to be faster. Moreover, this parameter can be adjusted later depending on the result of this test deposition.

The oxidation potential was investigated by performing linear sweep voltammetry (LSV) from 0.6 to 1.6 V vs. Ag/AgCl. From the LSV scan, it can be observed that a significant increase of current through the working electrode, starts at above 1.2 V. Therefore, ideally the deposition could be done above this potential threshold. To prove this, a two-step potentiostatic deposition sequence was tested. In the first step, a polarization voltage of 0.7 V was applied for 15 seconds, and in the second step oxidation voltage of 1.3V for 35 seconds. The relatively short duration of this deposition was chosen to avoid the possible adhesion problem between polymer layers (PI & PDMS) due to the ACN solvent. As already explained in Section 2.3, by dividing the potential step into two step (from 0 to 0.7 V and 0.7 to 1.3 V, instead of 0 to 1.3 V), the transient current in the beginning of the potential step can be minimized. A polarization potential of 0.7 V was chosen since this value is well below the oxidation voltage of EDOT monomers. The result of the LSV scan, and the current measurement during potentiostatic deposition are shown in Fig.4.6.

From the measured current (Fig.4.6 (a)), it can be observed that the current during the polarization step is decaying toward 0 A, and that the deposition rate was relatively constant. The average deposition current during the oxidation step was 485 nA, and the amount of charge delivered was 17.5 mC. After the deposition process was completed, the remaining solution was drained from the cell and the MEA, and the electrochemical cells were rinsed with DI water. A vacuum oven was used to dry the device completely before performing follow-up measurement.

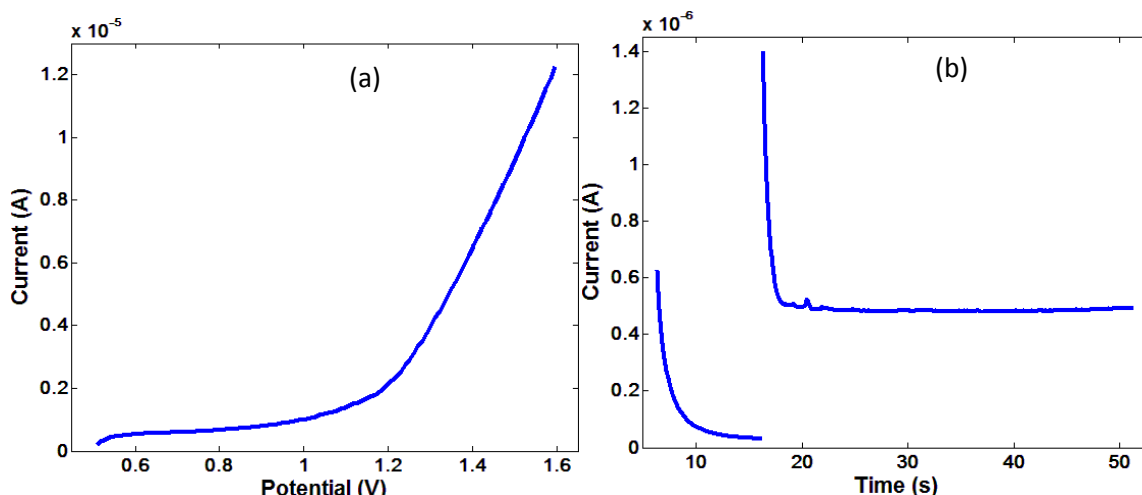


Figure 4.6. The I-V plot of LSV scan for determining PEDOT:BF₄ deposition voltage (a), and the result of current measurement during the potentiostatic deposition (b).

4. 2. 3 PEDOT:BF₄ Electrodes characterization

The electrochemical characterization of the PEDOT:BF₄ electrodes was performed to investigate the change of electrochemical characteristics. The results of EIS measurement of the deposited electrode are shown in the Fig.4.7.

The value of impedance at 1 kHz is 74.9 kΩ: 32.3 % lower than the average impedance prior to deposition. The phase plot also shows the change of the electrochemical characteristics, toward a more ohmic behavior over a broad range of medium frequencies, and capacitive characteristics on the low and high frequencies ranges. This result proves the feasibility of the deposition, and the improvement of impedance by PEDOT:BF₄ coating.

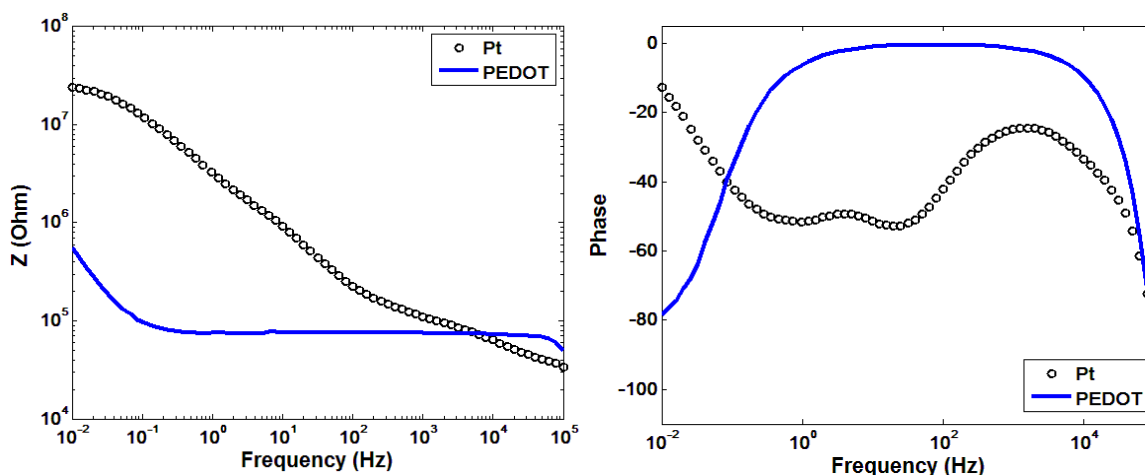


Figure 4.7. The Bode plot of EIS measurement for PEDOT:BF₄ coated MEA compared to the average result of Pt coating.

From this measurement, it is observed that the value of impedance at 1 kHz is 74.9 k Ω : 32.3 % lower than the average impedance prior to deposition. The phase plot also shows the change of the electrochemical characteristics, toward a more ohmic behavior over a broad range of medium frequencies, and capacitive characteristics on the low and high frequencies ranges. This result proves the feasibility of the deposition, and the improvement of impedance by PEDOT:BF₄ coating.

However, as observed under optical microscope and SEM (Fig.4.8), there were multiple side-depositions in areas that were not supposed to be coated with PEDOT:BF₄. These side-depositions indicate the possible delamination of polyimide insulation which resulted in the PEDOT:BF₄ deposited on the interconnection lines. The side-deposition also reduced the validity of the measurement, since the characterization might also include the contribution of the side-deposition areas.

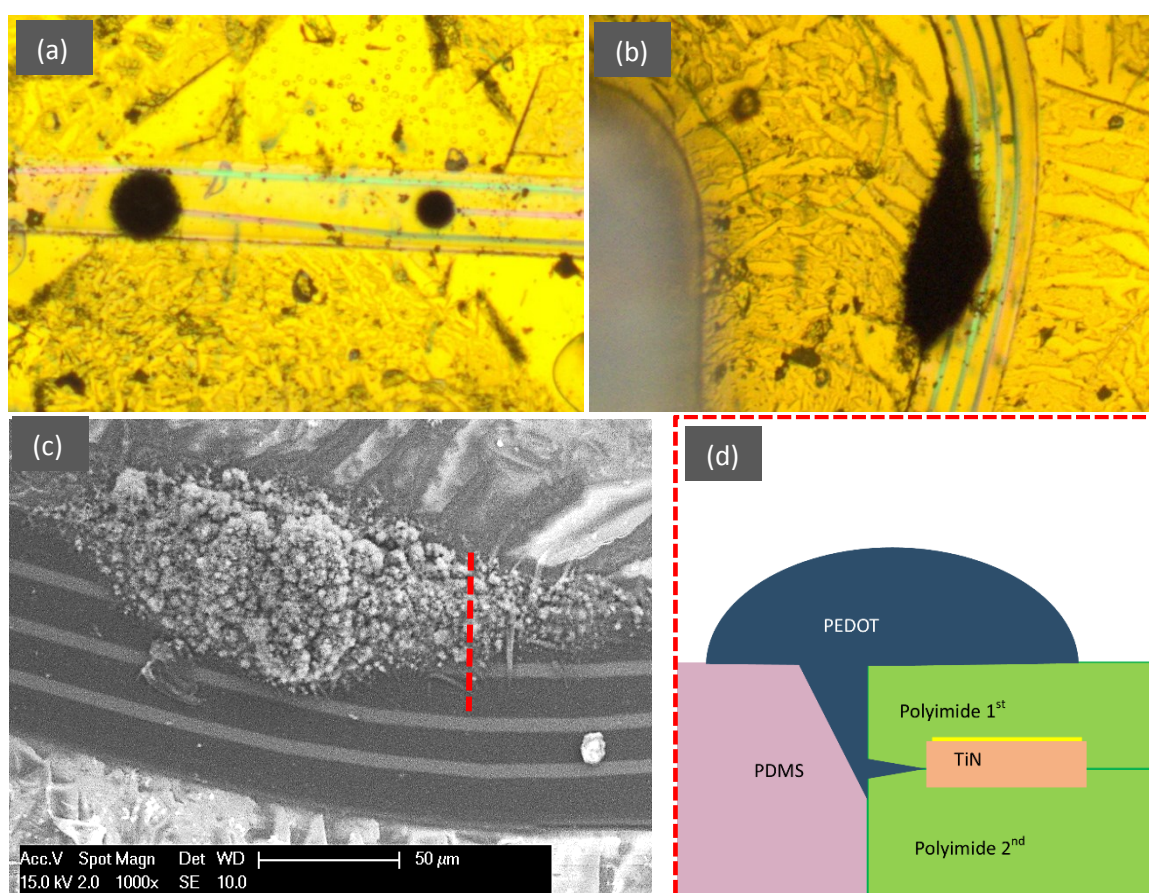


Figure 4.8. PEDOT:BF₄ coating deposited on the microelectrode surface (a), and side-deposition on the interconnection line (b). SEM image of side-deposition of PEDOT:BF₄ coating on the interconnection line (c). The schematic cross-section of the side-deposition from area under the red line (d).

The possible cause of the delamination could be due to the organic solvent in the experiment, or the inherent lack of adhesion between two layers of polyimide thus created leakage. To investigate the cause and overcome this problem, another batch of Cytostretch devices was fabricated. An additional oxygen plasma treatment of the polyimide was added to improve the adhesion between polyimide layers. The modified fabrication sequence is presented in Section 4.3.

In addition to the adhesion problem, the use of aqueous reference electrode in this experiment was also problematic, since the reference potential might be corrupted by the undetermined liquid junction. Therefore a set of non-aqueous reference electrodes was employed in the following tests and depositions.

4. 3 Revised Fabrication

The occurrence of side-deposition proved that the adhesion between the two layers of polyimide insulation was not sufficient. To address this problem, the fabrication process of the Cytostretch device was modified in order to improve the adhesion between the two polyimide layers insulating the TiN metal lines. Therefore an oxygen plasma treatment was performed in the TEPLA Plasma 300 (Power: 600 Watt, Time: 60 s, O₂: 250 ml/min) to solve this issue. This treatment was done after the dry etching of the TiN layer at the step (e) in Fig.3.1.

This oxygen plasma treatment is supposed to alter the wettability of the polyamide, making the polymeric surface hydrophilic. Nakamura et al. suggested that the increase of hydrophilicity of the treated surface is mainly induced by the increase of hydrophilic groups (C-O bond) on the polyamide surface [122]. With the increase in hydrophilicity of the first polyimide film, it is suggested that the chemical and mechanical bonding between polyimide layers can be improved [122].

In order to prove the efficacy of the treatment, the hydrophilicity of the polyimide surface before and after the oxygen plasma treatment was compared with the contact angle measurement (shown in Fig.4.9).

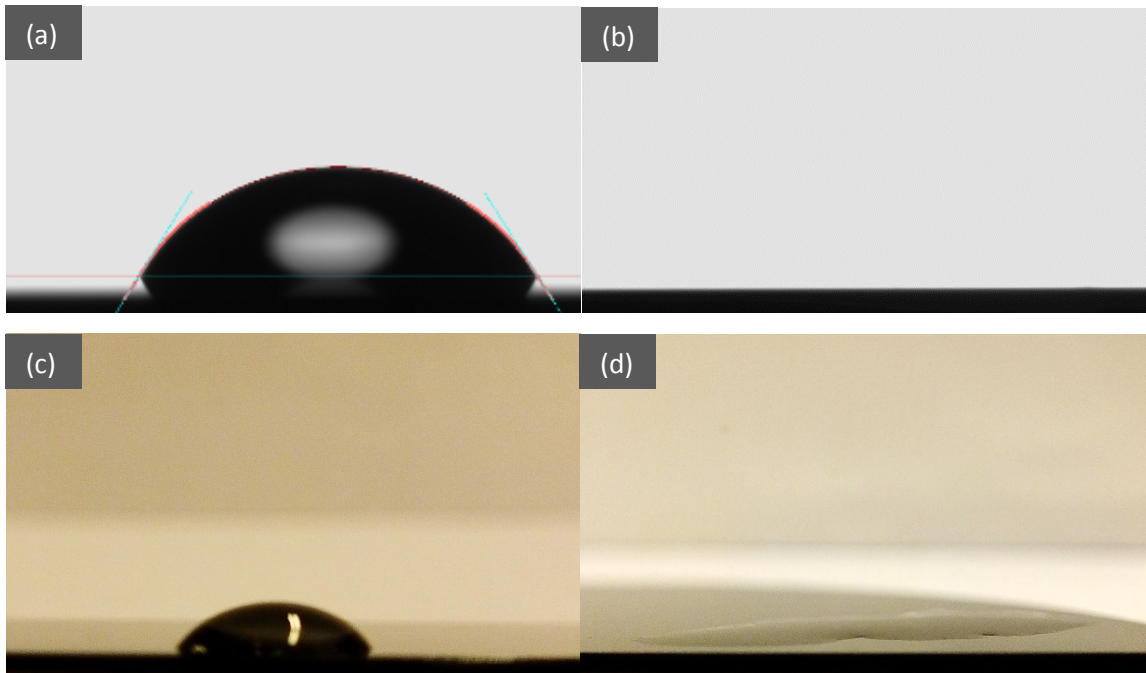


Figure 4.9. The result of contact angle measurement on PI surface, prior (a) and after (b) the oxygen plasma treatment. The lower images show the water drop on the PI surface as captured with the camera, prior (c) and after (d) the treatment.

From the measurement results, it can be observed that the hydrophilicity of polyimide surface is increased after the oxygen plasma treatment. The average result of the contact angle from the

pristine polyimide film is 57.6°, while after the treatment contact angle can not be measured at all due to the very low contact angle. This measurement result, confirms the increase in hydrophilic characteristics of the PI surface. Previous investigation results by Nakamura et al. [122] showed a strong relation between the adhesion and the hydrophilicity of the PI film surface. The improvement in adhesion was further tested by performing PEDOT deposition on the MEA fabricated with the modified process as presented in Section 4.4.

4. 4 Revised Deposition

A new set of samples was fabricated implementing the adhesion treatment presented in the previous section. In the following sections, the result of the preliminary characterization of the new batch, and the deposition sequence will be discussed.

4. 4. 1 Pt Electrodes Characterization

To characterize the new batch of Pt coated MEA, a series of measurements (EIS) was performed with the same setup and range of the previous batch. The results of the EIS measurements of the TiN and platinum coated MEA in the second batch are shown in the Fig.4.10. The results shown in the figures are the average of 5 measurement results.

The impedance of the Pt coated electrodes increased, compared to the previous batch. The impedance value at 1 KHz increased from 110.6 kΩ in the first batch to 874 kΩ in the second batch. Unlike the first batch, the Pt microelectrodes of the second batch exhibit an ohmic characteristic at low frequencies.

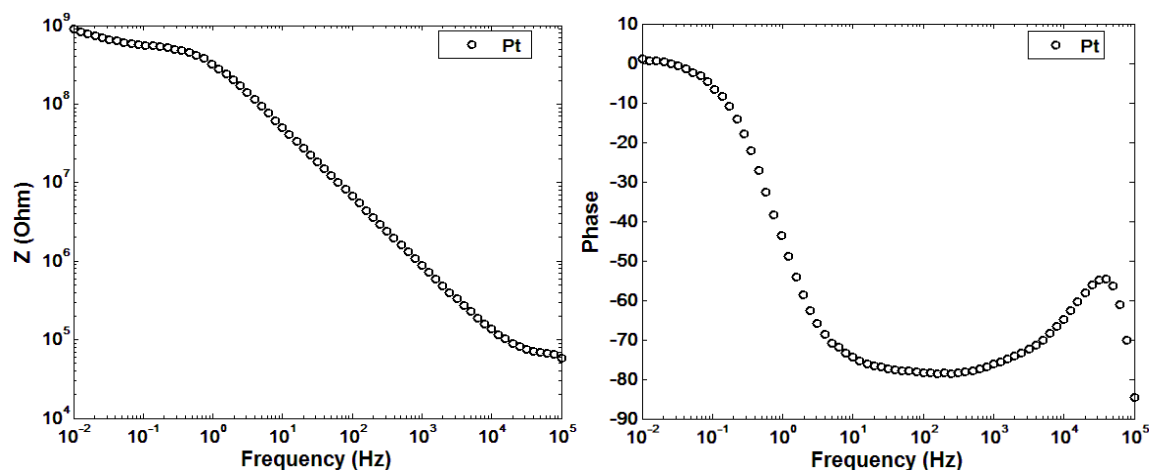


Figure 4.10. The Bode plots of EIS measurements from the new batch of Pt coated microelectrodes.

From the results of the preliminary characterization, it can be inferred that the adhesion problem in the previous batch was not due to the use of Acetonitrile solvent. Instead, it was caused by insufficient adhesion between the two layers of polyimide, which allows the EDOT solution to creep into the leakage site and causing side-deposition. The electrochemical deposition presented in the Section 4.4.2 further confirm this hypothesis.

4. 4. 2 PEDOT:PSS Deposition and Characterization

In order to deposit PEDOT, a mixture of **0.015 M EDOT** monomers, with **0.1 M NaPSS** (Sodium Poly (styrene sulfonate)) and **0.005 M TBABF₄** was prepared in de-ionized water. In this batch an aqueous solution was used in order to avoid the issues presented in Appendix A.5. The NaPSS molecules act as dopant materials as well as surfactant to increase the solubility of the monomers. Centrifuge mixing and degassing was used to evenly mix the solution.

Due to the high impedance of the Pt electrodes, it was relatively difficult to deposit PEDOT with potentiostatic deposition since a DC voltage only allows a very small current to be delivered to the interface. In addition to the impedance, the concentration of monomers in this deposition was lower than the deposition with organic solvent, which could also lower the deposition rate. Therefore cyclic voltammetry deposition was considered to replace the potentiostatic method. In cyclic voltammetry, the voltage sweep allows current to flow simultaneously through the faradaic and capacitive double layer mechanisms. Thus, more charge can be delivered in the same amount of time and given voltage level. This mechanism can be explained with the following formula;

$$I = C_{dl} \cdot \frac{dV}{dt} + I_{rx} \quad (5)$$

In the above formula, the total current (I) delivered to the interface is a sum of the capacitive current and faradaic current (I_{rx}). The capacitive current itself is determined by the value of the double-layer capacitance (C_{dl}) and the scan rate ($\frac{dV}{dt}$). Therefore, increasing the scan rate will increase the total current as well as the deposition rate proportionally.

In order to perform cyclic voltammetry deposition, the voltage sweep must pass the oxidation potentials of the monomer. In case of an aqueous solution, the oxidation potentials of EDOT monomers is often estimated as 0.8 V (vs. SCE). Therefore, in this experiment a CV deposition sequence was tested with a potentials range from 0.2 to 1.3 V (vs. Ag/AgCl) with scan rate of 500 mV/s. The switching voltage value of 1.3 V is chosen to compare the deposition result with the previous potentiostatic deposition. The deposition was limited by the amount of delivered charge, which was 3 μ C. The progression of the current responses over time and the delivered charge, are shown in the Fig.4.11.

During the first deposition, it can be observed that the deposition rate was not constant from both the current response and the charge delivery plots. It can be noticed that in the beginning of the deposition, the rate was significantly faster, as seen from the sudden increase in the amount of charge delivered, and started to slow down after few cycles. In fact, the magnitude of the current peaks was decaying over time, thus the charge delivery reached a linear pattern after few cycles. This sudden deposition at the beginning of the process can be an issue, since it most likely disrupt the orderly structure of the PEDOT film. With a high charge transfer rate, the polymerization also progresses proportionally fast, giving a very short amount of time for the monomers to orient themselves into an orderly structure [70]. Meanwhile, the decaying current in the later part of deposition was caused by the depletion of monomer concentration around the microelectrode surface. To investigate this, an EIS measurement was performed to determine the change of electrochemical characteristics of the microelectrode. Before performing the characterization, the deposition solution was drained, and the MEA was rinsed with DI water and then dried in vacuum. The result of EIS measurement is shown in Fig.4.12.

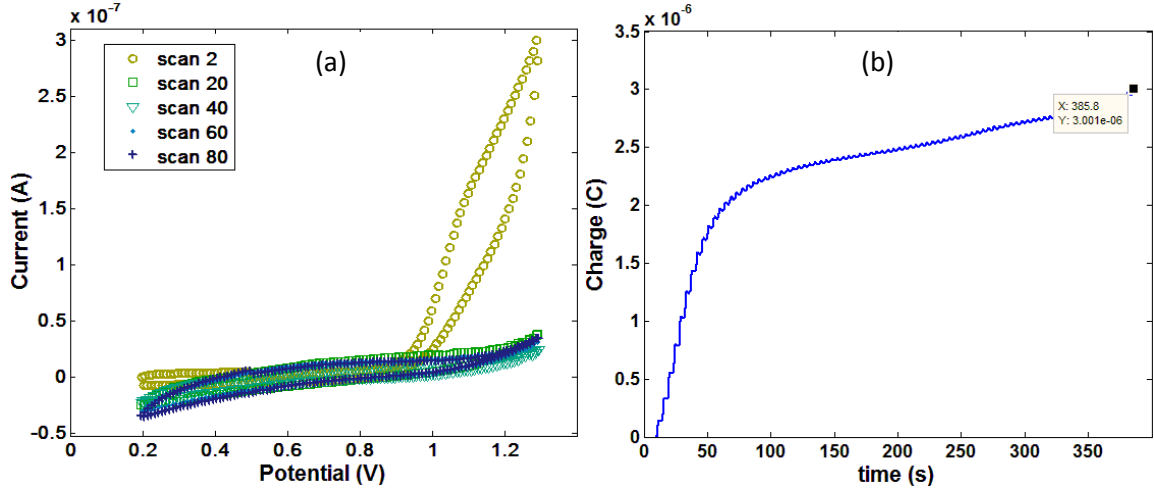


Figure 4.11. The I-V plots of the deposition over different scan cycles (a), and the amount of charge delivered over time (b).

In the plot, it can be observed that the deposited PEDOT film does not change the characteristics of the microelectrode significantly. The measured impedance at 1 KHz is 721 k Ω : 16.2 % lower than the impedance before the deposition. The phase plot also does not show any significant shift, after the deposition. This less pronounced characteristic change, proved the idea that the fast deposition rate caused disruption in the polymer film structure order. It has been known that the conductivity of PEDOT film is strongly affected by the ability of the PEDOT to form a layer by layer structures that allows ‘charge hopping’ between adjacent chains [70], [76]. The fast deposition rate reduces the time available for the monomers and oligomers to align themselves into this ordered structure, thus creating chaotic chains or even defect between layers [70].

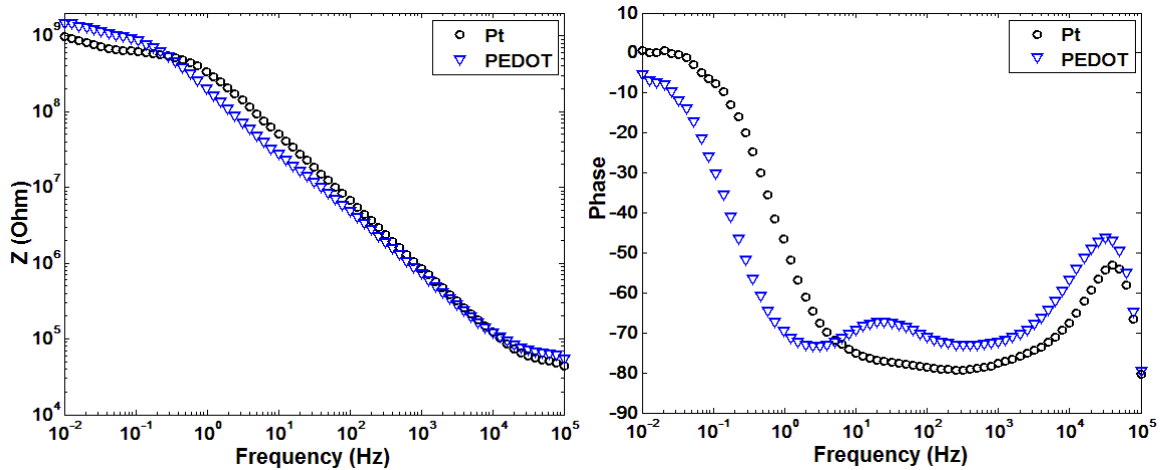


Figure 4.12. The Bode plots from EIS measurements of the deposited PEDOT compared to Pt coating prior to deposition.

In order to improve this deposition result, the correct approach is slowing down the deposition rate in the early phase of the deposition. In order to do this, the voltage range needs to be reduced. In principle, the larger the potential deviates from the oxidation potential, towards a more positive value: the larger faradaic current I_{rx} will flow on the electrode [38], [61].

The deposition program was then improved by reducing the switching voltage to 1.0 V and keeping the same scan rate and the amount of charge being delivered. The lower switching voltage was kept at 0.2 V since it did not contribute much to the deposition rate. The progression and the charge delivery of the second deposition are shown in the Fig.4.13. Since the voltage range was shorter, the number of cycles needed to deliver the same amount of charge was increased to 101 cycles but the total deposition time was slightly reduced.

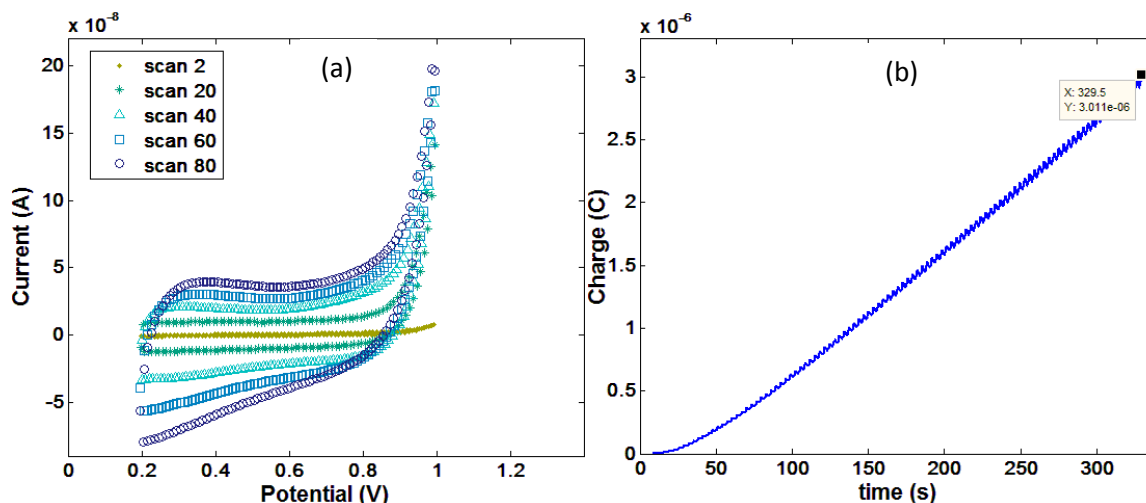


Figure 4.13. The I-V plots of the second deposition over different scan cycles (a), and the amount of charge delivered over time (b).

From the I-V plots, it can be observed that instead of decaying, the current response in this deposition sequence was “growing”. The sudden deposition at the beginning of the process disappeared completely in this case. The growing trend of the current response in this deposition was caused by the reduction of the impedance over time due to PEDOT being deposited on the electrode surface. It can also be observed that the charge delivery was relatively constant over the course of the deposition. An EIS measurement was then performed to characterize the deposition result. The EIS measurements are shown in the Fig.4.14.

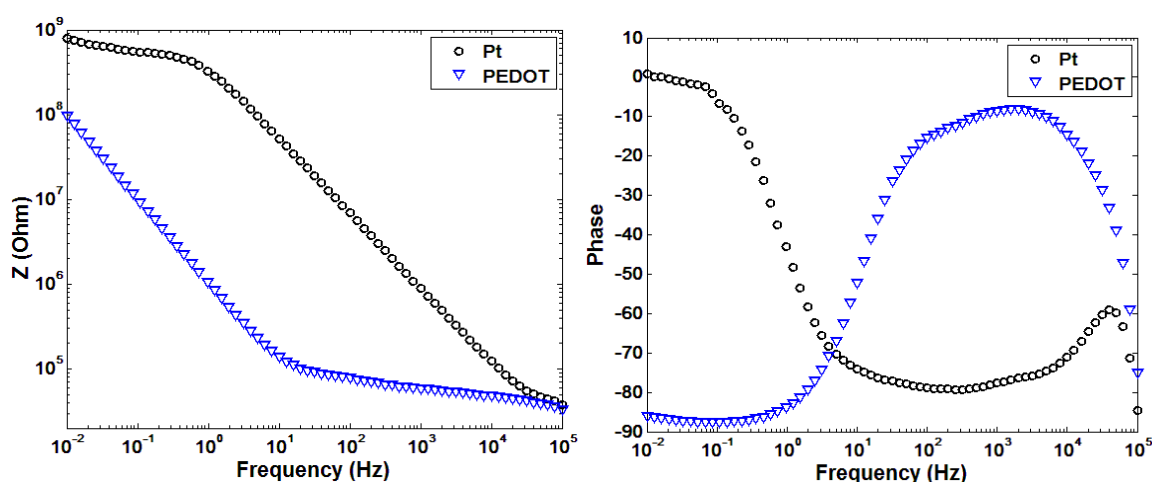


Figure 4.14. The Bode plot of EIS measurement from the second PEDOT deposition.

From this result, a significant change was observed in both the Impedance and the phase characteristics. The measured impedance at 1 kHz is now 59 k Ω which correspond to a 93.39 % of impedance reduction. The phase was also completely changed into a more ohmic behavior for middle range frequencies. These results further confirm the highly ordered, layer-by-layer growth in the second deposition [70], [96].

To confirm the validity of this result, another deposition was performed with the identical parameters on a different electrode. The progression of the response current and the charge delivery are plotted in the Fig.4.15.

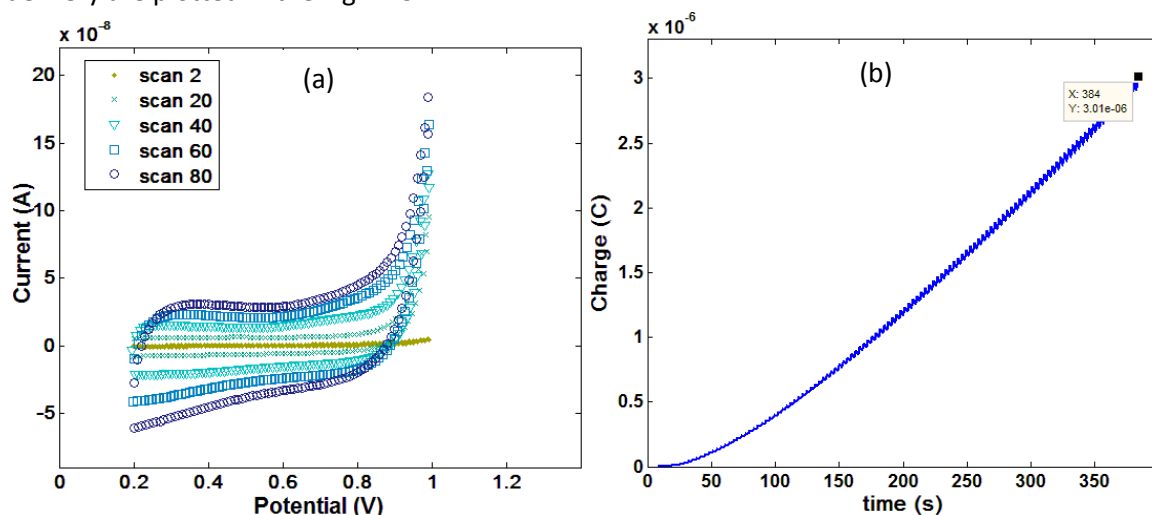


Figure 4.15. The I-V plots of the third deposition over different scan cycles (a), and the amount of charge delivered over time (b).

The number of cycles on this deposition was 118 cycles. The slight variation of the number of cycles might be due to the small difference of the impedance between the two Pt-coated electrodes. From both I-V plot and the charge delivery plot, it can be concluded that the deposition was progressing the same way as the second deposition scenario. To confirm this, another EIS measurement was performed, as shown in Fig.4.16.

From the EIS measurement, the impedance at 1 kHz was 55.6 k Ω , 94% lower than the electrode before the deposition. The phase measurement also exhibits an almost identical characteristic as the previous result. This confirms the reproducibility of this deposition program as well as the improvement of the electrochemical impedance. Further characterization and analysis of the electrochemical characteristics of the deposition results will be given in Chapter 5.

In order to assess the thickness of the deposited PEDOT, the correct amount of charge delivered during deposition needs to be quantified. Since the total deposition charge is used to determine and control the film thickness, having an accurate charge measurement is a critical issue. In the above experiments, the apparent total charge delivered during the deposition acquired from the scan result, included also the contribution of the voltage sweep below oxidation voltage (0.8 V), which in reality does not contribute to the film deposition. In addition to this, the reverse sweep also produces a negative current, which significantly reduces the apparent total charge delivered on each scan (see Fig.4.17). In reality, the negative current during the reverse sweep is only a measure of charge being discharged by the PEDOT film due to the reversal of polarity. This discharge current does not contribute to the total film deposited nor the reduction of the film thickness.

Therefore, to get an accurate charge measurements, both of these components must be taken into consideration.

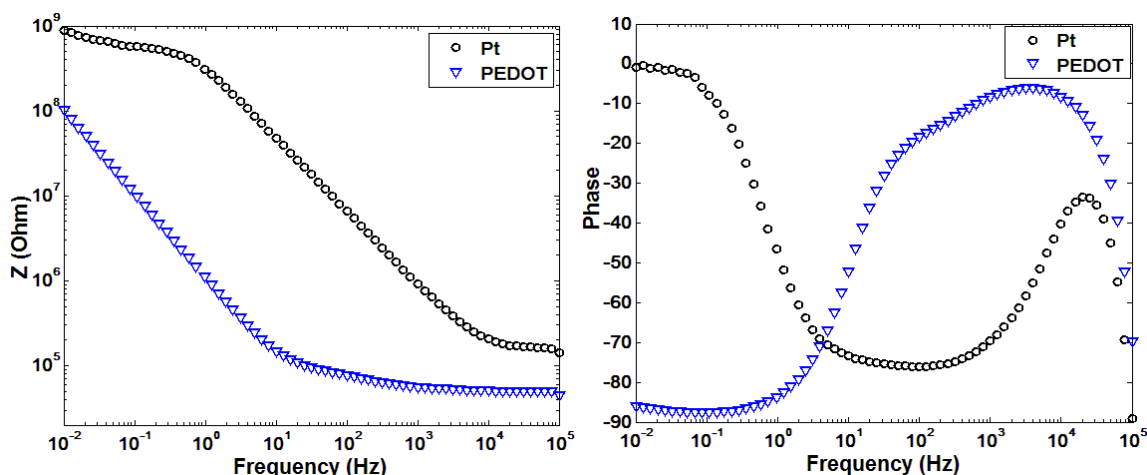


Figure 4.16. The Bode plot of EIS measurement from the third PEDOT deposition.

This problem was solved by neglecting the current below 0.8 V and as well as the negative currents. The remaining currents data are then integrated numerically in respect to the time, to get the approximate total charge. The new charge values are listed in the Tab.4-2.

The thickness are calculated with Equation 4, using the corrected charge value. Since, the concentration of TBABF₄ in the solution was negligible compared to the concentration of NaPSS, the calculation was done by assuming that the PEDOT film is doped with PSS only. Thus, the value of doping level (ratio of monomer unit/dopant in the polymer) in the calculation was 0.261, which refers to the doping level of PSS in the previous investigation done by Kayinamura et.al. [70]

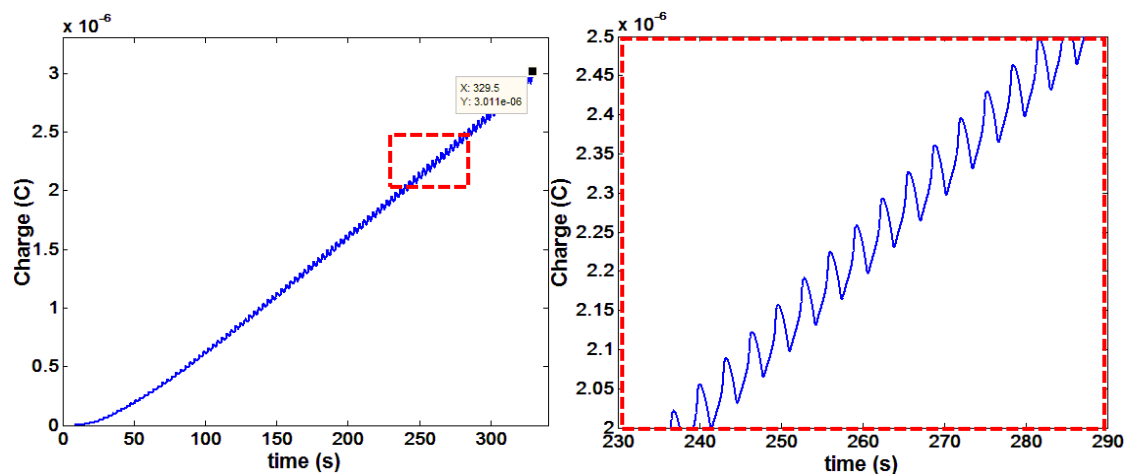


Figure 4.17. The plot of charge delivery from the second deposition shows the reduction of charge during deposition.

In the observation with optical microscope and SEM, there were not any visible side-deposition at all the three deposition process, as shown in the Fig.4.18. This demonstrated the adhesion improvement between polyimide layers and the validity of the measured impedance. These results confirm the feasibility of the PEDOT deposition on the MEA for organ-on-chip applications.

TABLE 4-2. The data of charge measurement and correction from each deposition.

Deposition	Voltage range	Measured Charge (C)	Corrected Charge (C)	Ratio	Thickness (μm)
1	0.2 – 1.3 V	3.00E-06	4.08E-06	1.36	3.98
2	0.2 – 1 V	3.01E-06	4.16E-06	1.38	4.06
3	0.2 – 1 V	3.01E-06	4.32E-06	1.44	4.22

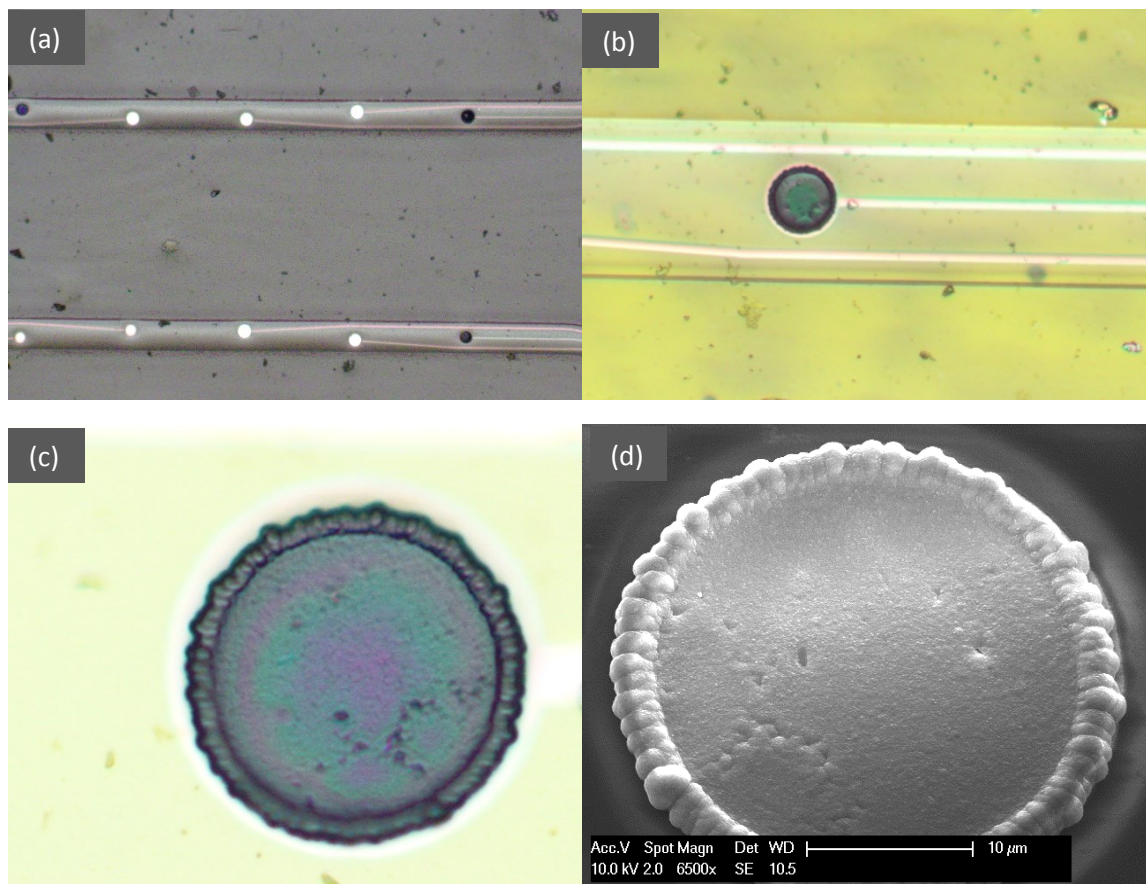


Figure 4.18. The results of PEDOT deposition on the Cytostretch MEA with the revised fabrication, showing no side-deposition (a,b). The result of the first deposition program, as seen under optical microscope (c), and SEM (d).

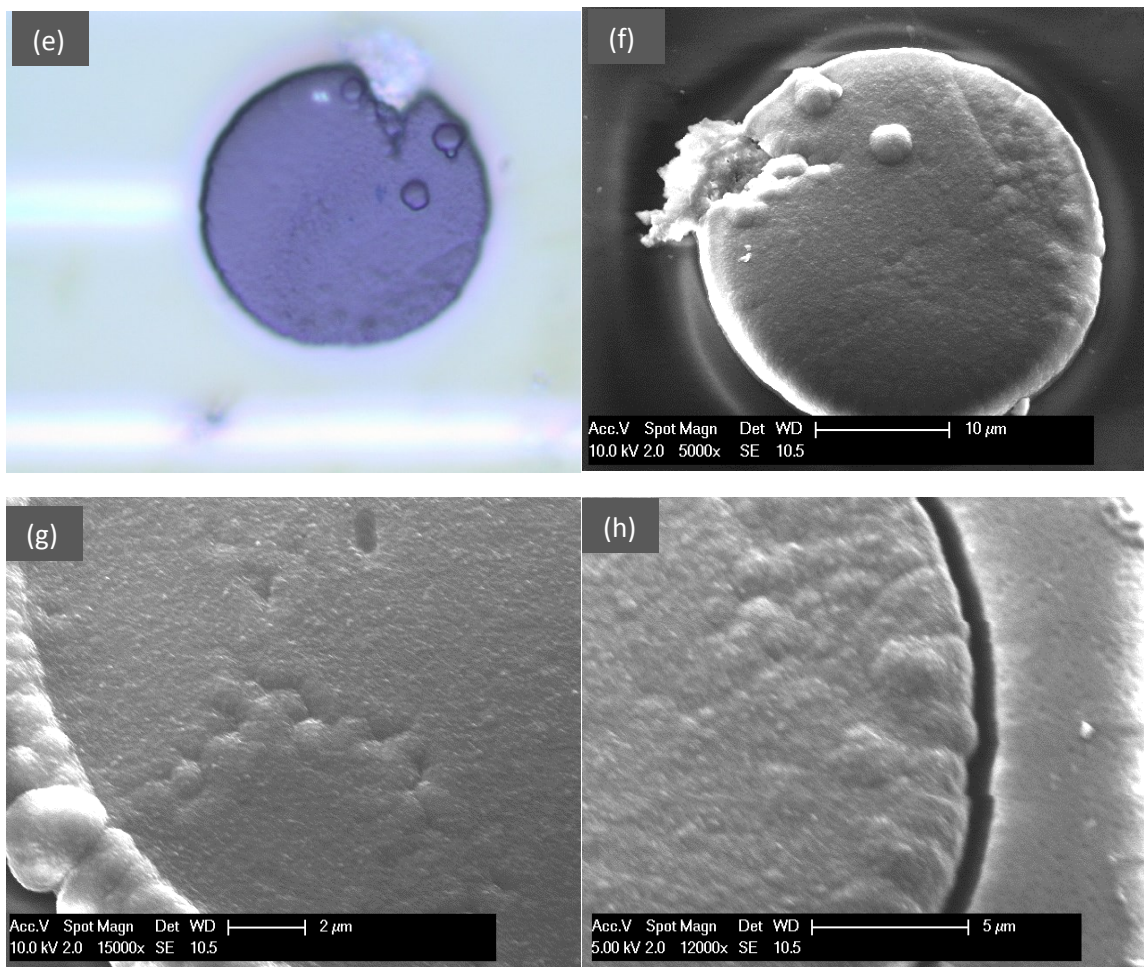


Figure 4.18. (cont.) The result of the second deposition program, as seen under optical microscope (e), and SEM (f). The rough surface of the PEDOT coating (g,h).

Chapter. 5 Final Characterization & Analysis

This chapter reports a detailed characterization of Cytostretch device fabricated before and after PEDOT deposition. Every measurement included in this chapter was performed after the optimization of the Cytostretch fabrication presented in Chapter 4. The electrochemical characterization consisted of EIS and CV measurements. In Section 5.1 the results of EIS measurements and the fitted circuit model are discussed. The results of CV measurement are presented in Section 5.2. Raman spectroscopy was also performed to confirm that the deposited material is indeed PEDOT polymer (Section 5.3).

5. 1 Electrochemical Impedance Spectroscopy

The comparison of EIS measurement results from TiN, Pt and PEDOT electrodes are shown in Fig.5.1. The results shown are the average of 5 measurement results. Each measurement was performed on a device fabricated after the revised fabrication presented in Section 4.3.

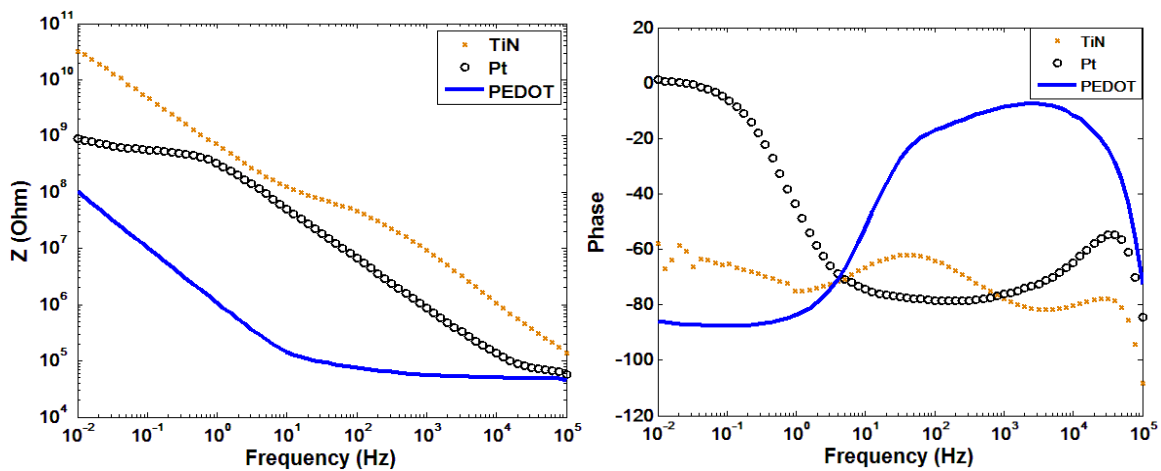


Figure 5.1. The Bode plot of EIS measurement results from all three type of microelectrode in this project.

PEDOT electrodes provided an outstanding improvement of the electrochemical impedance compared to Pt and TiN electrodes. As already mentioned in Section 4.4.2, the PEDOT coating provides a 94% improvement compared to Pt electrodes. Compared to TiN electrodes, which exhibits 9.32 M Ω impedance at 1 KHz, PEDOT coating reduced the impedance by as much as 99.4%. Moreover, Pt electrodes showed a lower impedance than TiN because of their higher faradaic activity [123]. From the phase plot it can be seen that the faradaic activity of the Pt coating are more concentrated on the low frequency range. This shows that the faradaic reactions on the Pt surface are relatively slow [34], [42]. Therefore, in the medium and higher frequency range the capacitive charge conduction is more predominant.

In case of PEDOT film, the faradaic activities of the materials are attributed to the faradaic doping/undoping reactions, which allow ions to react in a faster rate [77], [124]. at low frequencies, the charge transfer is promoted by the diffusion of ions inward and outward of the porous polymeric film. Moreover, the PEDOT coating was significantly thick, thus a large amount of mobile ions can be driven during charge transfer process. This mechanism results in a behavior resembling a capacitive component at low frequencies [42]. In the higher frequency range, the diffusion mechanism can not keep up with the faster charge conduction rate, following the potential oscillation, leaving the faradaic reaction as the main charge transfer mechanism.

In order to characterize even further the PEDOT electrodes, the impedance spectrum was fitted with a modified Randle's circuit. The average of 2 different EIS measurements from the second deposition program were used for this purpose. The resulting circuit model is shown in the Fig.5.2.

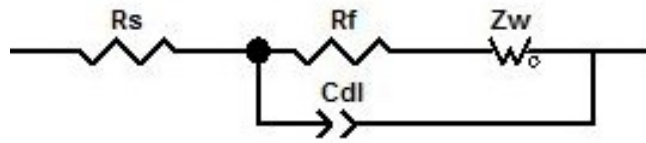


Figure 5.2. The circuit model of the PEDOT coated MEA, fitted from the measurement result.

TABLE 5-1. The parameter values of the circuit model of the PEDOT coated microelectrode.

Component	Value		Error %
Rs	15766	Ω	51.91
Rf	33322	Ω	24.75
Zw-R	103160	Ω	0.95
Zw-τ	0.014668		1.09
Zw-α	0.49		0.07
Cdl-C	2.223×10^{-10}		32.37
Cdl-α	0.93		11.69

This model is a modified Randle's circuit with a Warburg impedance added to account for ions diffusion and with a constant phase element to represent the double layer capacitance on the PEDOT film. This model also agrees with the result previously proposed by Cui and Martin [66] and Bobacka et al. [124]. This circuit model was fitted in the frequency range between 0.5 Hz and 10 kHz to avoid the noise in the lower frequency range. In this model, R_s is the total resistance of the interconnection line, contact pad, PCB, and the solution resistance combined. R_f is the resistance of the faradaic charge transfer. The parameter $Zw-\tau$ is the diffusional time constant, defined as L^2/D , with L and D described in the Section 2.2.3. The rest of the parameters of the Warburg impedance and the constant phase element are also described in Section 2.2.3.

The result of the fitting was plotted in comparison to the measurement result, in the Fig.5.3. From the Nyquist and Bode plot, it can be seen that the circuit model produces a similar characteristic in the observed frequency range.

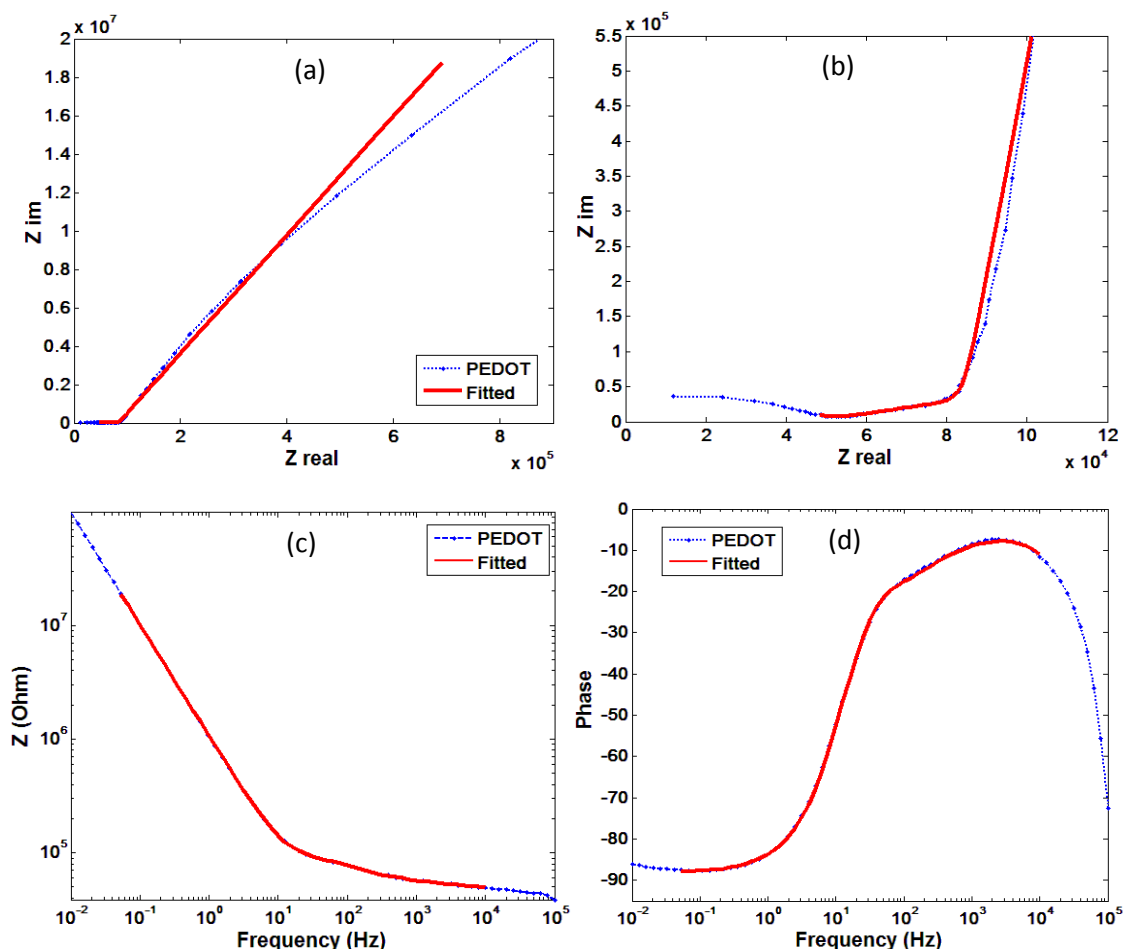


Figure 5.3. The comparison of the measurement and fitting result, as shown in the Nyquist plot (a) and the more detailed plot in the high frequency region (b), and the Bode plot (c,d).

5. 2 Cyclic Voltammetry

Cyclic voltammetry measurement on this project was used to collect additional information regarding the faradaic reactions at the electrode-electrolyte interface. Furthermore, the CDC value for each microelectrode type was derived from this measurement in order to qualitatively evaluate the microelectrode surface area. In order to obtain this information, a scan rate of 500 mV/s was used in every CV scan. This value was chosen in such a way that the CV measurements could detect both capacitive and faradaic phenomena on the electrode. Theoretically, the higher the scan rate the larger the capacitive current flows on the electrode [38]. However, most faradaic reactions at the electrode surface are not able to follow the fast potential sweep. Therefore, with a faster scan rate, the oxidation and reduction peaks shift further away from each other, resulting in a bigger peak distance compared to the measurement with a slower scan rate (see also Fig.4.4 in Section 4.2.2). This may result in the disappearance of one or more faradaic peaks during the CV measurement, which could be detrimental to the analysis of the faradaic characteristics of the electrode material.

The voltage sweep were performed within the electrochemical window of water (between -0.6 to 0.8 V). All the CV measurements were also repeated for 5 cycles. The comparison of average of the CV results, from each the microelectrodes type, are shown in Fig.5.4.

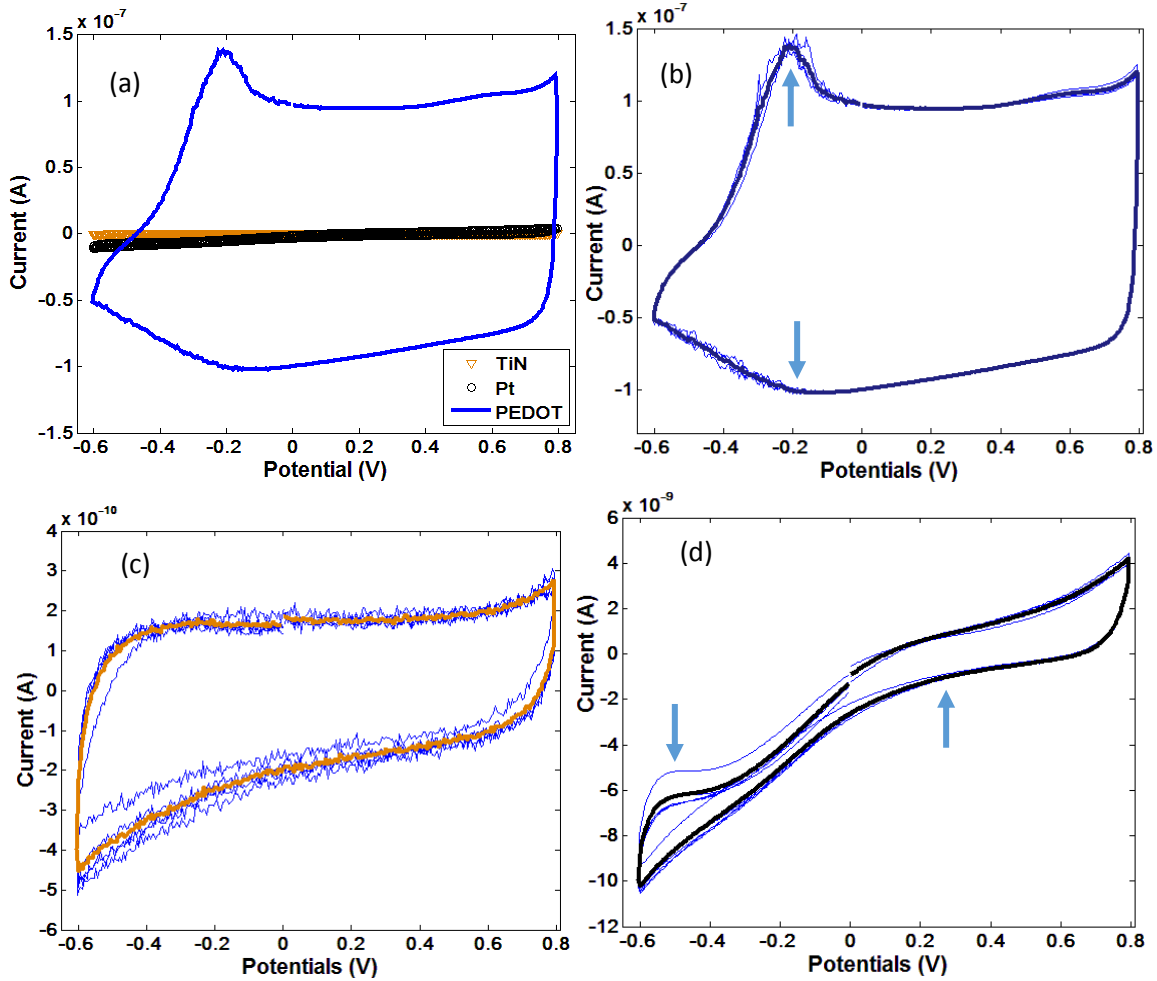


Figure 5.4. The CV results from three types of the microelectrodes combined in one graph (a). The results of CV scan of the PEDOT (b), TiN (c), and Pt (d) electrodes. Note that each graph has different maximum y-axis value. Blue arrows indicate the position of faradaic arcs and peaks.

The I-V plot of PEDOT coated microelectrode (Fig.5.4.b) is characterized by a pair of faradaic peaks (pointed with blue arrows) which corresponds to the change of oxidation state in the PEDOT polymer [75], [77]. The anodic peak at circa -0.19 V can be easily identified in the I-V plot, while the cathodic peak at circa -0.2 V is overshadowed by the capacitive current. The CV result of PEDOT coating also shows very large capacitive current, compared to TiN and Pt (Fig.5.4.a), both in the forward and the reverse scans, which is produced by the large double layer capacitance of the PEDOT coating. This proves that PEDOT provides better performance than TiN and Pt for MEA applications. For the TiN microelectrode, it is clearly seen that the plot lacks faradaic peaks, which is a characteristic of TiN microelectrode (Fig.5.4.c). Since TiN is an inert material, the charge is mainly conducted with capacitive double layer mechanisms. Therefore, the current responses in the plot are mainly showing the hysteresis coming from the charging and discharging of the TiN surface. For the Pt coated microelectrode, it can be observed that the current response is

characterized by several arcs (Fig.5.4.d). Although no faradaic peak is observed in this voltage range, the appearance of arc is only possible due to the faradaic reactions.

The values of CDC are calculated with Equation 1 in Section 2.2.2, separately for the cathodic (below 0 A) and anodic scans and listed in Tab.5-2.

TABLE 5-2. The CDC values of each microelectrode type.

Material	CDC _a	CDC _c
TiN	0.055 mC/cm ²	0.095 mC/cm ²
Platinum	0.364 mC/cm ²	0.532 mC/cm ²
PEDOT	30.88 mC/cm ²	33.45 mC/cm ²

The CDC values of PEDOT coated microelectrode are significantly higher than the other type of microelectrode in this research, proving once again the increase of the surface area of the microelectrode. This value is even higher than the value reported by King et al. [125]. This result confirms once again the superior electrochemical performance of PEDOT coated microelectrode, in comparison to the Pt coated and TiN microelectrode.

5. 3 Raman Spectroscopy

Raman spectroscopy was used to identify the material on the microelectrode surface and confirm the presence of PEDOT on top of the Cytostretch electrodes after the deposition step presented in Section 4.3.3. The results of the Raman spectroscopy measurements on the PEDOT coated microelectrode are shown in the Fig.5.5.

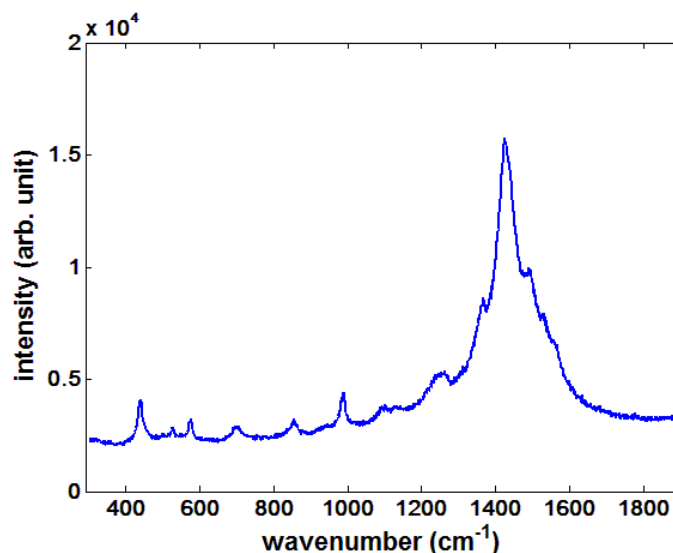


Figure 5.5. The results of Raman Spectroscopy of the PEDOT coated microelectrodes.

The Raman spectrum, shown in Figure 5.5 presents a similar trend with the results observed by Kayinamura et al. [70], also Łapkowski & Pron [126]. The maximum peak appears at 1436 cm⁻¹ that corresponds to the symmetric vibration of C_α=C_β bond in the oxidized polymer chain [70]. Several

peaks at circa 1249 cm^{-1} are also visible, which corresponds to the $\text{C}_\alpha - \text{C}_\alpha$ bond in the doped PEDOT polymer [126]. These results confirm the deposition results as PEDOT polymer film.

Chapter. 6 Conclusion

The TiN MEA embedded in the Cytostretch device exhibited a high electrochemical impedance due to their small surface area [12]. In this thesis, the possibility to improve the electrochemical performance of this MEA by coating the electrodes with PEDOT was investigated. The PEDOT layer was deposited with a microfabrication-compatible fabrication sequence, and resulted in a significant improvement of the electrochemical performance. In conclusion, the objectives of thesis research defined in Section 1.3 have been accomplished.

In order to coat the Cytostretch MEA with PEDOT, electrochemical deposition was chosen. To perform this procedure, the fabrication process of the Cytostretch was modified adding a Pt layer on the TiN electrodes. This coating acts as the adhesion layer between the PEDOT and the TiN. In order to increase the mechanical bonding of the Pt coating, a layer of Ti was added. The mask designs and the thicknesses of the added layer were optimized to prevent the failure of the Ti adhesion during the wet-etching processes included in the fabrication of the Cytostretch. In the end, the fabrication sequence presented in this thesis, resulted in a 100% yield of Pt coated MEA in the Cytostretch device.

Adhesion problems between the polyimide layers in the Cytostretch device were also addressed. This adhesion problem resulted in a leakage of the insulation, inducing a side-deposition of PEDOT. This problem was addressed by performing an oxygen plasma treatment on the Polyamide layers during the fabrication. This was proven to increase the hydrophilicity of Polyamide surface and ultimately increasing the adhesion between PI layers.

The electrochemical deposition process was performed with CV deposition techniques. In comparison to the potentiostatic deposition, this procedure allows the capacitive current to flow to the electrode and subsequently increases the polymerization rate. Two different CV deposition programs were performed, comparing the effect of the upper switching potentials during the CV scan. The first deposition program with voltage scan range of 0.2 – 1.3 V resulted in 16.2% reduction of impedance compared to prior the deposition. The second deposition program with a switching potential of 1 V, resulted in as much as 94% reduction of microelectrode impedance. These results were confirmed with multiple electrodes and multiple measurements.

Electrochemical characterization of the electrodes, including EIS and CV, was performed for each of microelectrode type (TiN, Pt and PEDOT). The average values of impedance at 1 kHz are 9.32 M Ω , 874 k Ω , and 57.3 k Ω for TiN, Pt, and PEDOT respectively. The CV measurements also showed clear differences among the microelectrode type. The average values of CDC are 0.055 mC/cm², and 0.095 mC/cm² for anodic and cathodic scans respectively. For the Pt coated microelectrode, the

CDC is significantly larger than TiN with a value of 0.364 mC/cm² for anodic and 0.532 mC/cm² for cathodic. This result was further improved by PEDOT coating to as much as 30.88 mC/cm² for anodic and 33.45 mC/cm² for cathodic. These results confirm the significant improvement of electrochemical performance provided by the PEDOT coating. The deposited PEDOT coating was also characterized with Raman Spectroscopy in order to verify the material characteristics of the PEDOT film.

6. 1 Recommendation and Future Work

The results in this thesis assessed the improvement of the electrochemical performance of the Cytostretch provided by PEDOT. A deeper investigation of the electrochemical properties, stability and biocompatibility must be performed to ensure the functionality of the PEDOT coated MEA for Organ-on-Chip application.

To optimize the deposition, various parameters can be adjusted to produce a low and stable deposition rate. One of the approach that could be employed is to lower the CV scan rate (v) to further reduce the deposition rate. Meanwhile, to compensate the time required for slow deposition, the voltage sweep range can be cut by shifting the lower switching voltage into a more positive value reducing in this way the deposition time. However this approach is rarely chosen and most of previous attempt of CV deposition of PEDOT used an even much broader voltage sweep range [23].

Deposition with acetonitrile was not fully investigated. However, previous works have proven that the use of ACN solvent can increase the stability of the resulting PEDOT film. In addition to the stability, the use of organic solvents can embed in the polymer various dopant material which otherwise would be insoluble. Therefore the use of ACN solvent should be further studied.

The addition of PEDOT coating into the Cytostretch MEA also opened up new possibilities of adding more functionality to the device. Various studies have focused on incorporating bioactive molecules on the PEDOT film, which could be used, among other things, to promote cell adherence to the MEA surface.

Finally, a series of characterization measurements needs to be performed in order to better understand the electrochemical characteristics of the PEDOT coating. Long-term measurements are also necessary to prove the stability of the coating, and preferably in various environment conditions. Pulse measurements can also be performed to characterize the voltage response of the MEA during current stimulation.

Appendix

A.1. Fabrication Result

In this section, the SEM results from each fabrication step are presented. The steps mentioned in this section refers to the fabrication step in the Section 3.1, Fig.3.1 (also shown below).

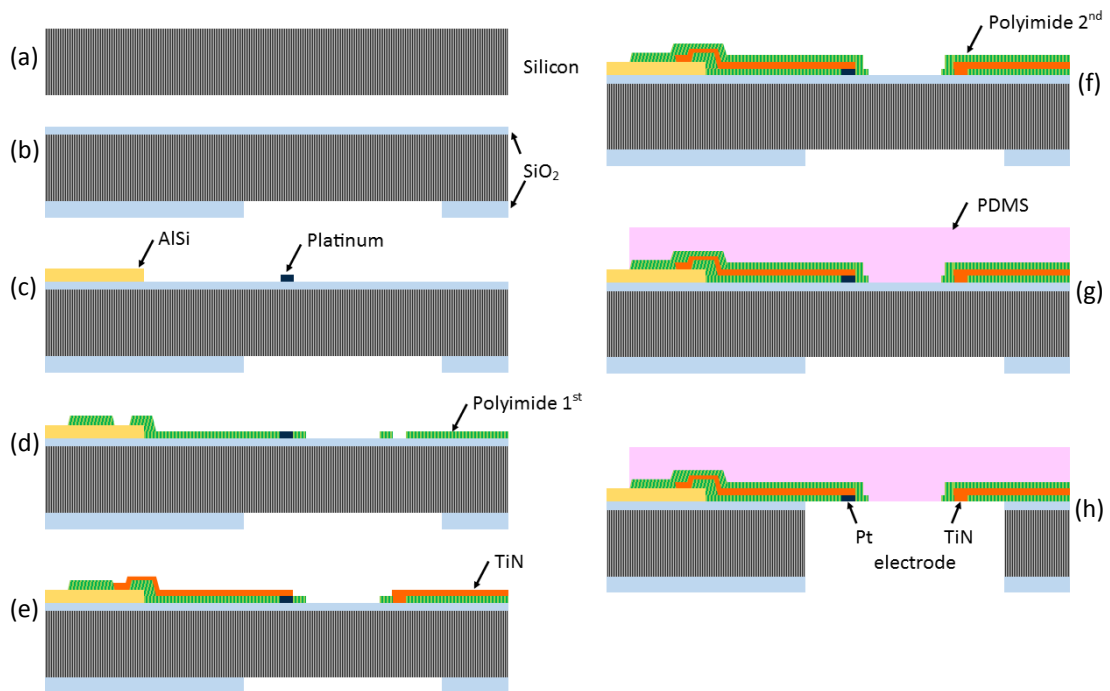


Figure 6.1. The schematic cross-section from each fabrication step of the Cytostretch device.

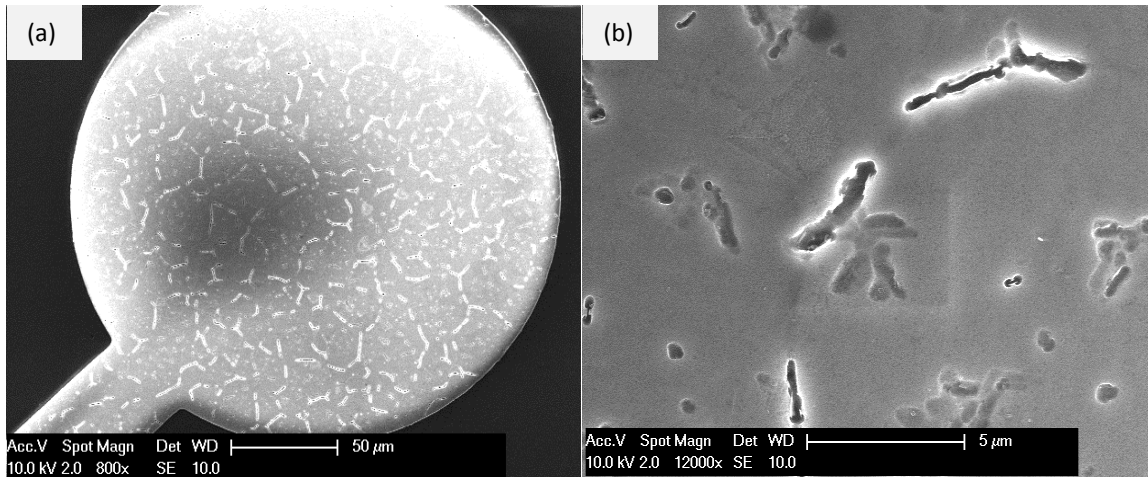


Figure A. 1. (a) The SEM image of the AlSi contact pad, after patterning in the step c. (b) A close-up image of the AlSi grainy structure, which was a result of the sputtering deposition.

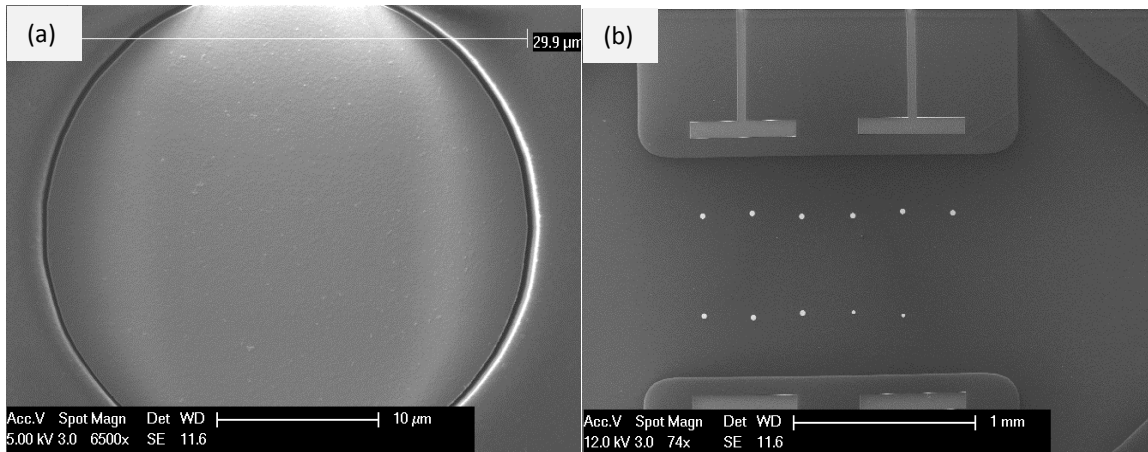


Figure A. 2. (a) The SEM image of Pt coating as seen from the wafer-front side, after the lift-off process in the step c. (b) Each dice has 12 microelectrodes, with 11 of them are Pt-coated.

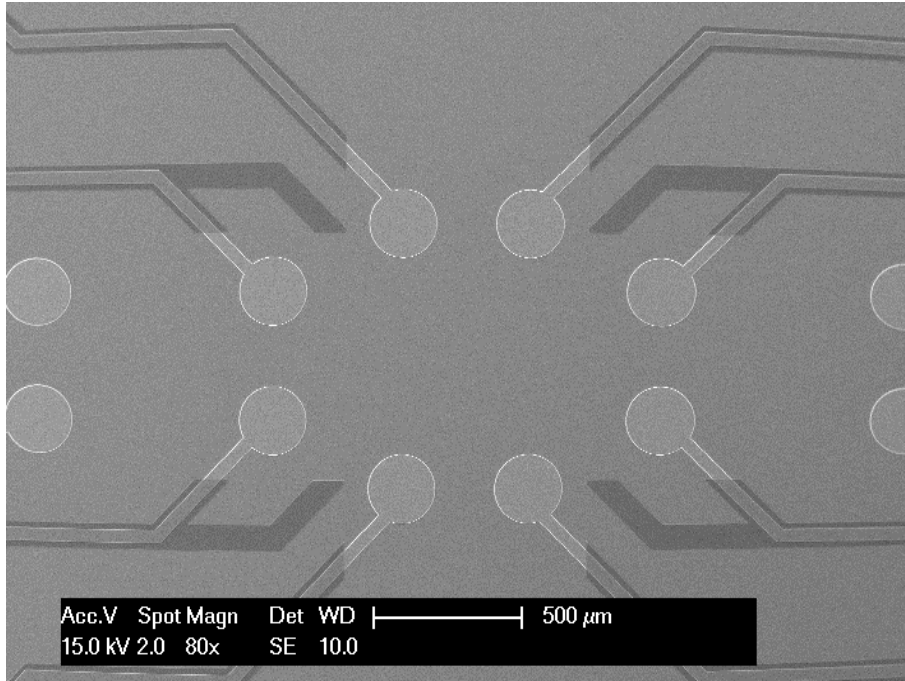


Figure A. 3. After the first polyimide deposition in step d, the extensions of the AlSi contact pads are covered, exposing only the connection sites to the wire-bonding and TiN.

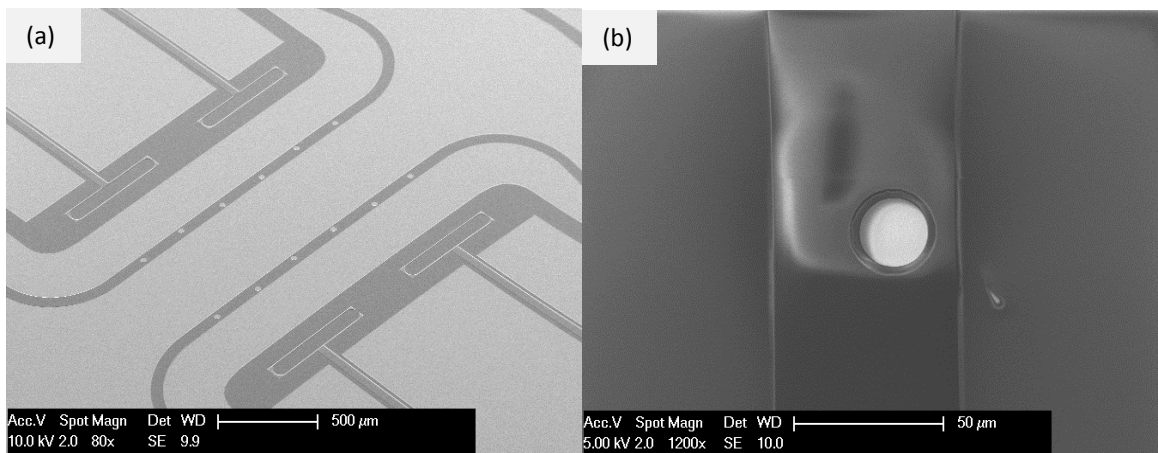


Figure A. 4. (a) The SEM image of the first PI film surrounding the Pt coating, as seen from the front side of the wafer. (b) A close-up image of the Pt coated surrounded by PI film.

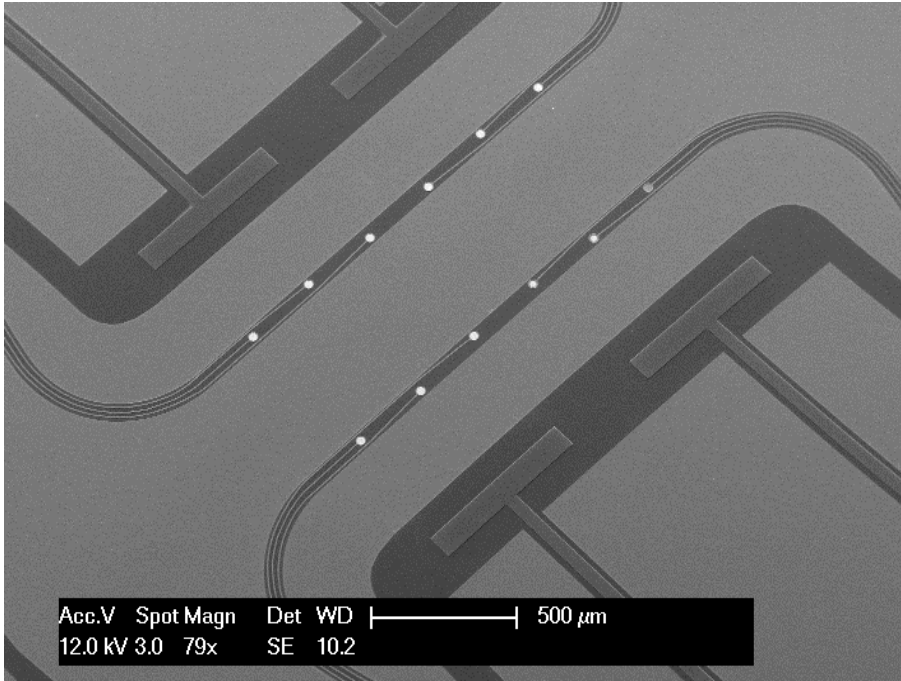


Figure A. 5. The results of the step e, showing the TiN interconnection lines connected to the microelectrodes.

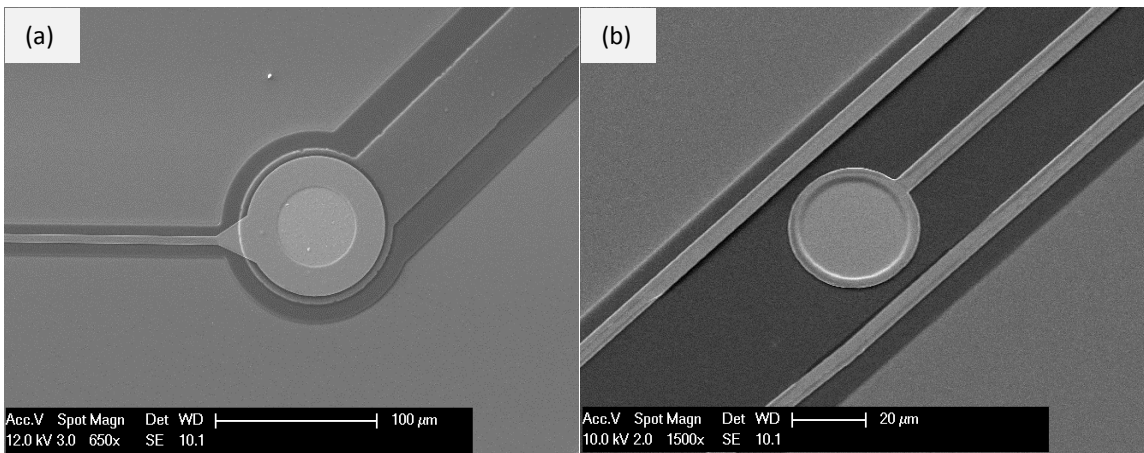


Figure A. 6. After step e, TiN lines are connected to the AlSi contact pad (a). The connection of TiN lines to the Pt (b).

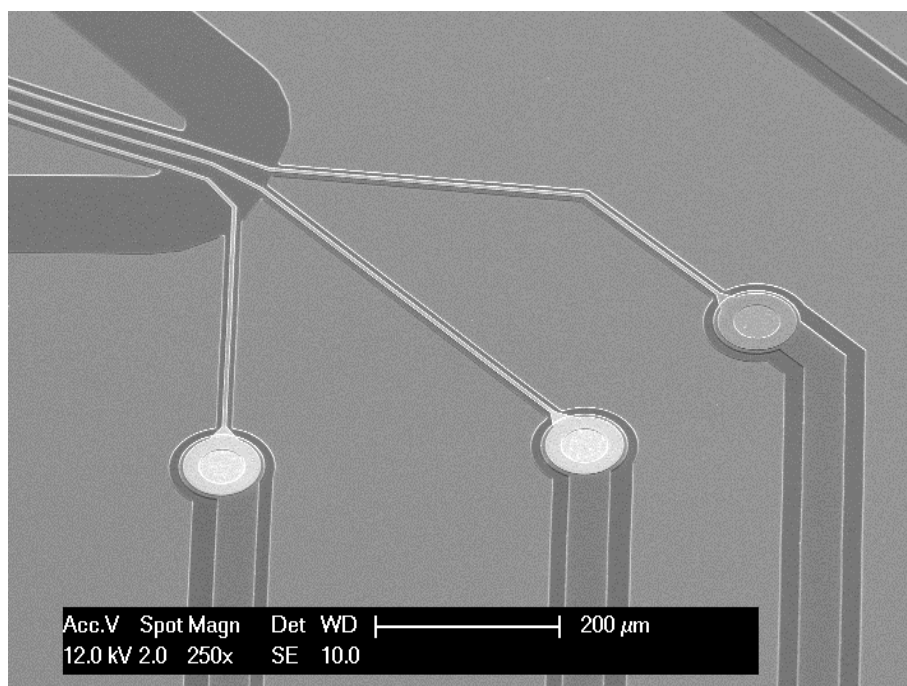


Figure A. 7. The connection sites between the TiN lines and AlSi contact pads.

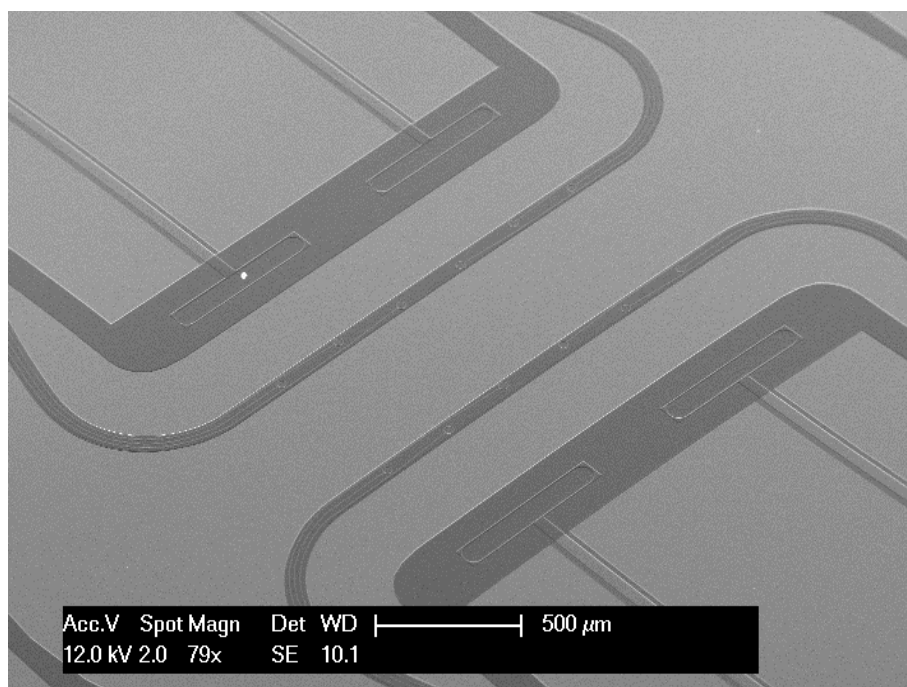


Figure A. 8. After the second PI layers in the step f, the TiN lines and MEA are completely covered with PI insulation.

Appendix

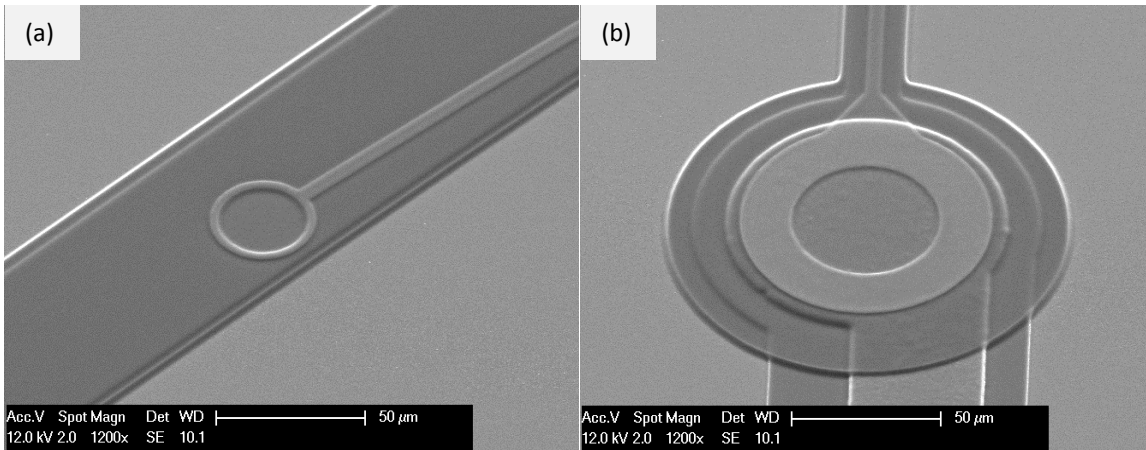


Figure A. 9. (a) The MEA and TiN lines are covered with PI insulation after step f. (b) The connection sites of the TiN and AlSi after step f.

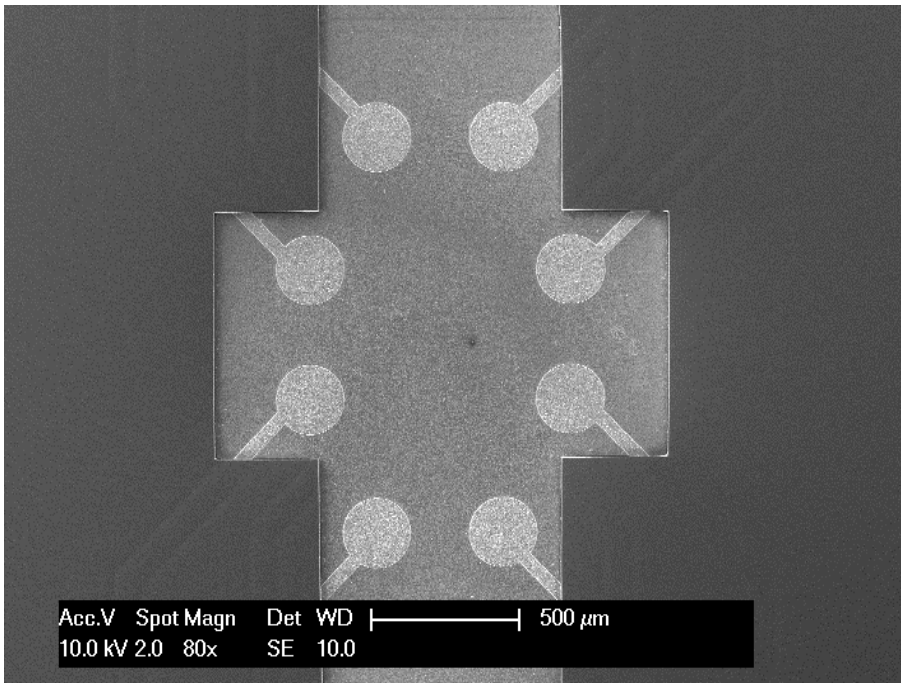


Figure A. 10. After the PDMS deposition, curing, and patterning in the step g, the device surface is covered with PDMS, and then the contact pads area is exposed.

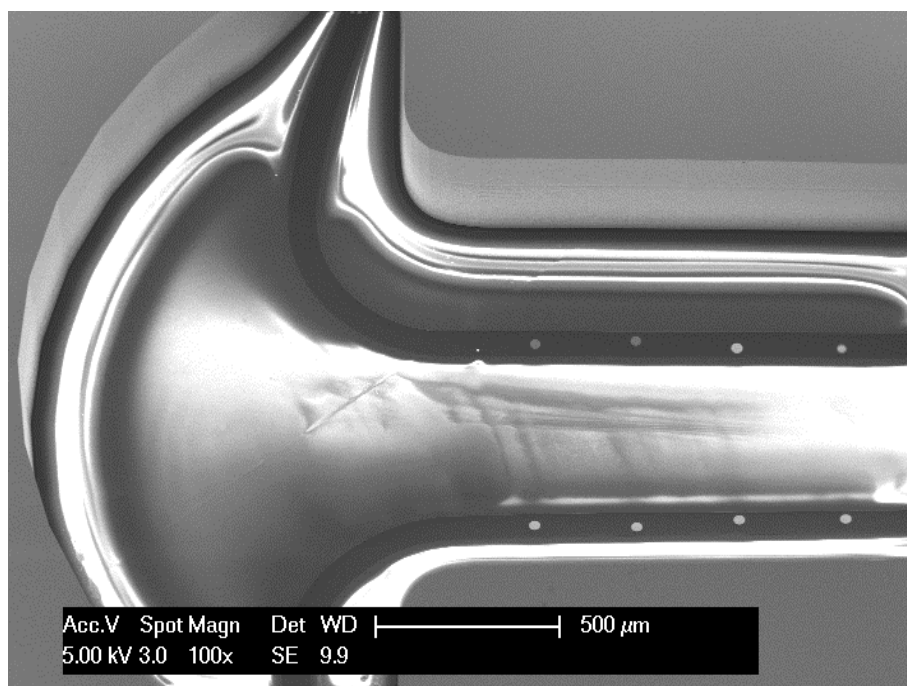


Figure A. 11. The finished result of the membrane releasing in the step h showing the MEA surface at the PDMS membrane, as seen from the wafer backside.

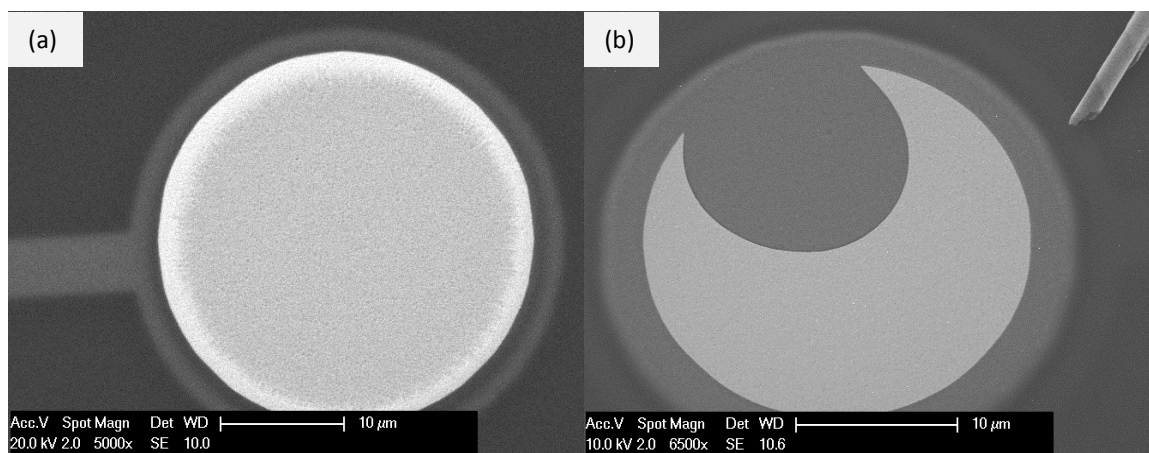


Figure A. 12. The resulting Pt coating surface, after step h (a). From the defected Pt coating (b), the surface quality of the microelectrode can be compared.

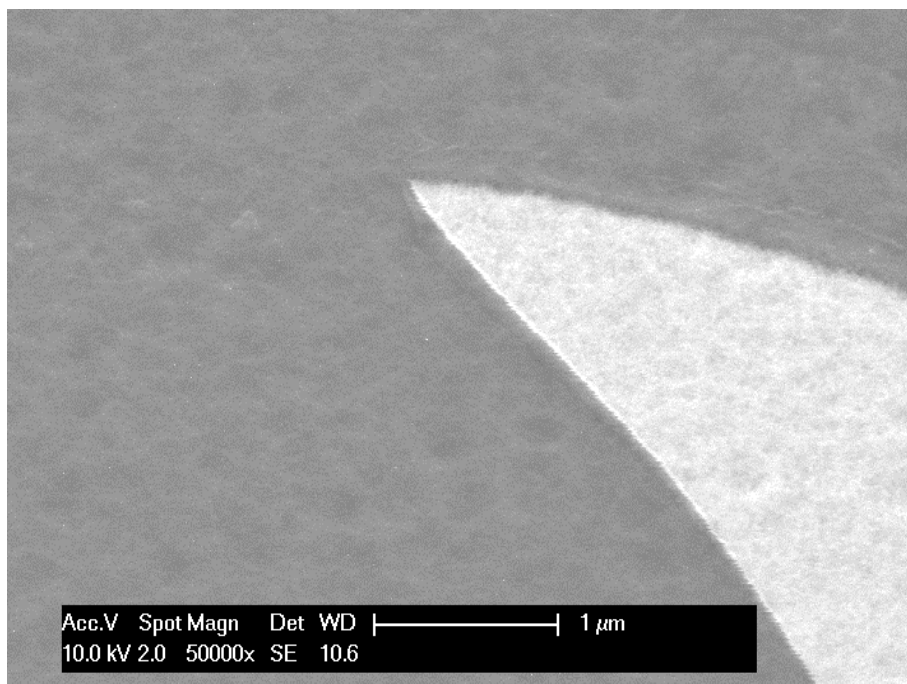


Figure A. 13. The relatively smooth surface of the TiN and Pt coating on the microelectrode.

A.2. Fabrication Flowchart

STARTING MATERIAL

Type:	n
Orientation:	<100>
Resistivity:	2-5 Ωcm
Thickness:	425 \pm 15 μm
Diameter:	100 mm

1. CLEANING: HNO₃ 99% and 69.5%

Clean	10 minutes in fuming nitric acid at ambient temperature. This will dissolve organic materials. Use wet bench "HNO ₃ 99% (Si)" and the carrier with the red dot.
Rinse	Rinse in the Quick Dump Rinser with the standard program until the resistivity is 5 M Ω .
Clean	10 minutes in concentrated nitric acid at 110 °C. This will dissolve metal particles. Use wet bench "HNO ₃ 69,5% 110C (Si)" and the carrier with the red dot.
Rinse	Rinse in the Quick Dump Rinser with the standard program until the resistivity is 5 M Ω .
Dry	Use the Semitool "rinser/dryer" with the standard program, and the white carrier with a red dot.

2. COATING

Use the coater station of the EVG120 system to coat the wafers with photoresist. The process consists of:

- a treatment with HMDS (hexamethyldisilazane) vapor, with nitrogen as a carrier gas
- spin coating of Shipley SPR3012 positive resist, dispensed by a pump
- a soft bake at 95 °C for 90 seconds
- an automatic edge bead removal with a solvent

Always check the relative humidity (48 \pm 2 %) in the room before coating, and follow the instructions for this equipment.

Use program "**Co - 3012 – zero layer**". No residue allowed on the back.

3. ALIGNMENT AND EXPOSURE

Processing will be performed on the ASML PAS5500/80 automatic wafer stepper.

Follow the operating instructions from the manual when using this machine.

Expose masks **COMURK** and **FWAM** with wafer with job "**ZEFWAM**" with the correct exposure energy: 150mJ

This results in alignment markers for the stepper and contact aligner for wafers.

4. DEVELOPING

Use the developer station of the EVG120 system to develop the wafers. The process consists of:

- a post-exposure bake at 115 °C for 90 seconds
- developing with Shipley MF322 with a single puddle process
- a hard bake at 100 °C for 90 seconds Always follow the instructions for this equipment.

Use program "**Dev - SP**".

5. INSPECTION: Linewidth and overlay

Visually inspect the wafers through a microscope, and check the line width. No resist residues are allowed in the exposed areas.

6. WAFER NUMBERING

Number the wafers writing number on resist with diamond pen.

7. PLASMA ETCHING: Alignment markers (URK's) in Silicon

Use the Trikon Omega 201 plasma etcher.

Follow the operating instructions from the manual when using this machine.

It is not allowed to change the process conditions and times from the etch recipe!

Use sequence **URK_NPD** (with a platen temperature of **20 °C**) to etch 120 nm deep ASM URK's into the Si.

8. LAYER STRIPPING: Photoresist

Strip resist Use the Tepla Plasma 300 system to remove the photoresist in an oxygen plasma.

Follow the instructions specified for the Tepla stripper, and use the quartz carrier.

Use **program 1**: 1000 watts power and automatic endpoint detection + 2 min. overetching.

9. CLEANING: HNO3 99% and 69.5%

Clean 10 minutes in fuming nitric acid at ambient temperature. This will dissolve organic materials.

Use wet bench "HNO3 99% (Si)" and the carrier with the red dot.

Rinse Rinse in the Quick Dump Rinser with the standard program until the resistivity is 5 MΩ.

Clean 10 minutes in concentrated nitric acid at 110 °C. This will dissolve metal particles.

Use wet bench "HNO3 69,5% 110C (Si)" and the carrier with the red dot.

Rinse Rinse in the Quick Dump Rinser with the standard program until the resistivity is 5 MΩ.

Dry Use the Semitool "rinser/dryer" with the standard program, and the white carrier with a red dot.

10. COATING

Use the coater station of the EVG120 system to coat the wafers with photoresist. The process consists of:

- a treatment with HMDS (hexamethyldisilazane) vapor, with nitrogen as a carrier gas
- spin coating of Shipley SPR3012 positive resist, dispensed by a pump
- a soft bake at 95 °C for 90 seconds
- an automatic edge bead removal with a solvent

Always check the relative humidity ($48 \pm 2\%$) in the room before coating, and follow the instructions for this equipment.

Use program "**Co - 3012 – 1.4um**". No residue allowed on the back.

11. ALIGNMENT AND EXPOSURE (BACK)

Processing will be performed on the ASML PAS5500/80 automatic wafer stepper.

Follow the operating instructions from the manual when using this machine.

Expose wafer with job "**FTBAFWAM**" with the correct exposure energy: 150mJ

This results in alignment markers for the stepper and contact aligner for wafers.

12. DEVELOPING (BACK)

Use the developer station of the EVG120 system to develop the wafers. The process consists of:

- a post-exposure bake at 115 °C for 90 seconds
- developing with Shipley MF322 with a single puddle process
- a hard bake at 100 °C for 90 seconds Always follow the instructions for this equipment.

Use program "**Dev - SP**".

13. INSPECTION: Linewidth and overlay

Visually inspect the wafers through a microscope, and check the line width. No resist residues are allowed in the exposed areas.

14. PLASMA ETCHING: Alignment markers (URK's) in Silicon

Use the Trikon Omega 201 plasma etcher.

Appendix

Follow the operating instructions from the manual when using this machine.
It is not allowed to change the process conditions and times from the etch recipe!

Use sequence **URK_NPD** (with a platen temperature of **20 °C**) to etch 120 nm deep ASM URK's into the Si.

15. LAYER STRIPPING: Photoresist

Strip resist Use the Tepla Plasma 300 system to remove the photoresist in an oxygen plasma.
Follow the instructions specified for the Tepla stripper, and use the quartz carrier.
Use **program 1**: 1000 watts power and automatic endpoint detection + 2 min. overetching.

16. CLEANING: HNO3 99% and 69.5%

Clean	10 minutes in fuming nitric acid at ambient temperature. This will dissolve organic materials. Use wet bench "HNO3 99% (Si)" and the carrier with the red dot.
Rinse	Rinse in the Quick Dump Rinser with the standard program until the resistivity is 5 MΩ.
Clean	10 minutes in concentrated nitric acid at 110 °C. This will dissolve metal particles. Use wet bench "HNO3 69,5% 110C (Si)" and the carrier with the red dot.
Rinse	Rinse in the Quick Dump Rinser with the standard program until the resistivity is 5 MΩ.
Dry	Use the Semitool "rinser/dryer" with the standard program, and the white carrier with a red dot.

17. PECVD DEPOSITION: 1000 nm Silicon oxide

Use the Novellus Concept One PECVD reactor.
Follow the operating instructions from the manual when using this machine.
Use macro **OXIDE program: xxxstdSiO2** to deposit a 1000 nm thick SiO₂ layer.
Change time to get the right thickness. (ca. 16 s / station)

Note: The deposition time is subject to minor changes, in order to obtain the correct film thickness, check the logbook close to Novellus.

18. MEASUREMENT: Silicon oxide thickness

Use the Leitz MPV-SP measurement system for layer thickness measurements. Follow the operating instructions from the manual when using this equipment.

Program:	Th_SiO2_onSi ; >50nm
Front side Oxide thickness:	on a process wafer
Expected thickness:	1000 nm

19. METALLIZATION 1: Barrier layer 100 nm Ti (RT or 350 °C)

Use the TRIKON SIGMA 204 sputter coater for the deposition of a Ti metal layer on the wafers.
Deposition must be done at RT or 350 °C with an Ar flow of 100 sccm.
Follow the operating instructions from the manual when using this machine.
Use recipe **Ti 100nm @350C** to obtain a 100 nm thick layer.
Visual inspection: the metal layer must look shiny.

20. PECVD DEPOSITION: 1000 nm Silicon oxide

Use the Novellus Concept One PECVD reactor.
Follow the operating instructions from the manual when using this machine.
Use macro **OXIDE program: xxxstdSiO2** to deposit a 1000 nm thick SiO₂ layer.
Change time to get the right thickness. (ca. 16 s / station)

Add test wafer to measure the thickness

21. MEASUREMENT: Silicon oxide thickness

Use the Leitz MPV-SP measurement system for layer thickness measurements.
Follow the operating instructions from the manual when using this equipment.

Program: Th_SiO2_onSi ; >50nm
Front side Oxide thickness: on a process wafer
Expected Thickness: 2000nm

22. PECVD DEPOSITION: 6000 nm Silicon oxide (BACK)

Use the Novellus Concept One PECVD reactor.
Follow the operating instructions from the manual when using this machine.
Use macro **OXIDE program: xxxstdSiO2** to deposit a 6000 nm thick SiO2 layer.
Change time to get the right thickness. (ca. 90 s / station)

23. MEASUREMENT: Silicon oxide thickness

Use the Leitz MPV-SP measurement system for layer thickness measurements.
Follow the operating instructions from the manual when using this equipment.

Program: Th_SiO2_onSi ; >50nm
Back side Oxide thickness: on a process wafer
Expected Thickness: 6000nm

24. COATING (BACK)

Use the coater station of the EVG120 system to coat the wafers with photoresist. The process consists of:

- a treatment with HMDS (hexamethyldisilazane) vapor, with nitrogen as a carrier gas
- spin coating of Shipley SPR3027 positive resist, dispensed by a pump
- a soft bake at 95 °C for 90 seconds
- an automatic edge bead removal with a solvent

Always check the relative humidity ($48 \pm 2 \%$) in the room before coating, and follow the instructions for this equipment.

Use program "**Co –3027 4µm - no EBR**". There will be no edge bead removal. Check backside. No residue are allowed

25. ALIGNMENT AND EXPOSURE (BACK)

Processing will be performed on the ASML PAS5500/80 automatic wafer stepper. Follow the operating instructions from the manual when using this machine.

Expose masks _____ with wafer with the correct exposure energy: 500mJ

26. DEVELOPING (BACK)

Use the developer station of the EVG120 system to develop the wafers. The process consists of:

- a post-exposure bake at 115 °C for 90 seconds
 - developing with Shipley MF322 with a double puddle process
 - a hard bake at 100 °C for 90 seconds
- Always follow the instructions for this equipment.

Use program "**Dev – SP**".

27. INSPECTION: Linewidth and overlay

Visually inspect the wafers through a microscope: No resist residues are allowed in exposed part.

28. PLASMA ETCHING: Open 5000 nm PECVD SiO2 (BACK)

Use the Drytek Triode 384T plasma etcher.
Follow the operating instructions from the manual when using this machine.

Appendix

It is not allowed to change the process conditions from the etch recipe, except for the etch times!
Use recipe **STDOXIDE** to etch 5000nm oxide and land in the Oxide layer. (ca. 10 mins)

29. LAYER STRIPPING: Photoresist

Strip resist Use the Tepla Plasma 300 system to remove the photoresist in an oxygen plasma.
Follow the instructions specified for the Tepla stripper, and use the quartz carrier.
Use **program 1**: 1000 watts power and automatic endpoint detection + 2 min. overetching.

30. CLEANING: HNO3 99% (METAL)

Clean 10 minutes in fuming nitric acid at ambient temperature. This will dissolve organic materials.
Use wet bench "HNO3 99% (metal)" and the carrier with a red and yellow dot.
Rinse Rinse in the Quick Dump Rinser with the standard program until the resistivity is 5 MΩ.
Dry Use the Semitool "rinser/dryer" with the standard program, and the white carrier with a black dot.

31. METALLIZATION: 1500nm AlSi (with 1% Si) @ 350° C

Use the TRIKON SIGMA 204 sputter coater for the deposition of an aluminium metal layer on the wafers.
The target must exist of 99% Al and 1% Si, and deposition must be done at RT or 350 °C with an Ar flow of 100 sccm.
Follow the operating instructions from the manual when using this machine.

Use recipe **AlSi 1500nm_350C**.
Visual inspection: the metal layer must look shiny.

32. COATING

Use the coater station of the EVG120 system to coat the wafers with photoresist. The process consists of:

- a treatment with HMDS (hexamethyldisilazane) vapor, with nitrogen as a carrier gas
- spin coating of Shipley SPR3012 positive resist, dispensed by a pump
- a soft bake at 95 °C for 90 seconds
- an automatic edge bead removal with a solvent

Always check the relative humidity (48 ± 2 %) in the room before coating, and follow the instructions for this equipment.
Use program "**Co - 3012 – 1.4um**". No residue allowed on the back.

33. ALIGNMENT AND EXPOSURE

Processing will be performed on the ASML PAS5500/80 automatic wafer stepper.
Follow the operating instructions from the manual when using this machine.
Expose wafer with job "_____ " with the correct exposure energy: 150mJ

34. DEVELOPING

Use the developer station of the EVG120 system to develop the wafers. The process consists of:

- a post-exposure bake at 115 °C for 90 seconds
- developing with Shipley MF322 with a single puddle process
- a hard bake at 100 °C for 90 seconds Always follow the instructions for this equipment.

Use program "**Dev - SP**".

35. WET ETCHING AlSi : PES 35 °C

Etch Use dedicated wet bench PES at temperature 35° C.
The bath contains PES solution.
Time Until all AL is removed. Time TBD (around 9 mins)
QDR Rinse in the Quick Dump Rinser with the standard program.

Appendix

Etch	Use dedicated wet bench Poly-Si etch
Time	Until all Si residue is removed. Time TBD (around 30 s)
QDR	Rinse in the Quick Dump Rinser with the standard program.
Dry	Use the manual dryer.

36. LAYER STRIPPING: Photoresist

Strip	Use dedicated wet bench Acetone 40 °C
-------	---------------------------------------

37. CLEANING: HNO₃ 99% (METAL)

Clean	10 minutes in fuming nitric acid at ambient temperature. This will dissolve organic materials. Use wet bench "HNO ₃ 99% (metal)" and the carrier with a red and yellow dot.
Rinse	Rinse in the Quick Dump Rinser with the standard program until the resistivity is 5 MΩ.
Dry	Use the Semitool "rinser/dryer" with the standard program, and the white carrier with a black dot.

38. COATING

Use the coater station of the EVG120 system to coat the wafers with photoresist. The process consists of:

- a treatment with HMDS (hexamethyldisilazane) vapor, with nitrogen as a carrier gas
- spin coating of AZNlof2020 negative resist, dispensed by syringe
- a soft bake at 95 °C for 90 seconds
- no edge bead removal

Always check the relative humidity (48 ± 2 %) in the room before coating, and follow the instructions for this equipment.

Use program "Co_Nlof_3,5μm_no EBR ". No residue allowed on the back.

39. ALIGNMENT AND EXPOSURE

Processing will be performed on the ASML PAS5500/80 automatic wafer stepper.

Follow the operating instructions from the manual when using this machine.

Expose wafer with job " _____ " with the correct exposure energy: **50mJ**

40. CROSS LINK BAKE

Use the hot plate to manually bake the wafers, and follow the instructions specified for this equipment.

Bake the wafers for 60 seconds @ 115 °C or Use X-link bake on developer

41. DEVELOPMENT

Use the EVG 120 Coater/developer to develop the wafers, and follow the instructions specified for this equipment. The process consists of:

- development step using Shipley MF322developer (single puddle process)
- hard bake at 100°C for 1.5 min.

Always check the temperature of the hotplates first. Use development program: "Dev –Lift off".

42. DUV BAKE

Use the program Lift-Off

43. TEPLA: O₂ plasma cleaning

Plasma flash: Use the Tepla plasma system to remove the photoresist residue in an oxygen plasma. Follow the instructions specified for the Tepla stripper, and use the quartz carrier.

Use Program # 2, Flash

Remark: Tepla should be at room temperature before starting (21°C), abort program after it reaches 28°C.

44. MANUAL COATING PHOTORESIST (BACK)

Use manual coater system to coat the wafers with photoresist. The process consists of:

- Spin coat the Shipley SPR3027 positive resist by dispensing it with manual syringe
- Use the Non-vacuum edge-chuck
- Make sure the edge of the wafer is completely covered with resist.

Use program: . Change spinning time. Spinning time:

45. MANUAL BAKING STEP

Use the Memmert oven in tunnel 1 to perform an extra resist bake:

bake the wafers at 100 °C for 15-30min minutes

Note: Use a dedicated rack to bake the wafers

CR 10000 & SAL

46. EVAPORATION

CHA evaporator 20nm Ti, 100nm Pt, 3Å/sec, T<85°C 3Å/sec

Use the dedicated Satellite for Pt, Ta, Ti and Si.

Check if Pt molt is done properly. If Copper holder next to the Pt pocket is damaged stop processing and contact Wim Wien.

Note: Test need to be performed to determine minimum thickness and the adhesion of platinum layer.

47. LIFT OFF (SAL lab)

Lift-off procedure:

- * Heat up a beaker with DI – water to 80°C
- * Put the heated DI-water in the Ultra Sone Bath
- * Switch on Temperature switch to 80°C
- * Heat up a beaker with NMP to 70°C
- * Put the heated NMP in a rectangle beaker that fits in the top lid opening.
- * Put the lift-off wafer in a single wafer holder or carrier.
- * Put the holder/carrier in the NMP beaker.
- * Switch on the Ultra Sone bath, t=8 min.

(remove the lift-off residues from the wafer surface after each 2 minutes with a Q-tip)

REMARK: For safety reasons 70°C is the maximum working temperature of the NMP solvent. Flashover temperature is ± 85°C!

Remark: Check if there is no Pt at the edge of the wafer for at least 5 mm from the edge after lift-off. Remark made by the PAC.

Remark: After lift-off put the NMP with Pt into the container: "Halogen arme Organische afvalstoffen" with a remark on the label that it contains Pt.

48. RINSING AND DRYING

Rinse the wafer with DI-water in a beaker for 5 minutes.

Manual dry with N2.

49. CLEANING: HNO3 SAL

Cleaning Prepare a nitric acid bath. Use a special Pt container.
Use HNO3 at RT to remove the resist for 10 min. No resist residues are allowed.
Rinse in water Manual drying.

CR 100

50. MANUAL COATING PHOTORESIST

Use manual coater system to coat the wafers with photoresist. The process consists of:

Cover the inside of the coating station with aluminum foil

Spin coat the Shipley SPR3027 positive resist by dispensing it with manual syringe

Note: Use contaminated chuck.

51. MANUAL BAKING STEP

Use the Memmert oven in tunnel 1 to perform an extra resist bake:

bake the wafers at 110 °C for 10 minutes

Note: Use a dedicated rack to bake the wafers

52. WET ETCHING BHF METAL: Etch 1µm PECVD SiO₂ (BACK)

Use special container, wafer holder and rinse bath for this step

Etch Use dedicated wet bench BHF 1:7 at ambient temperature,
 The bath contains a buffered HF solution.

Time Until the etched openings are hydrophobic. Time TBD

Rinse Rinse in the water for 5 minutes.

Dry Use the manual dryer.

53. RESIST LAYER STRIPPING: ACETONE SAL

Use special beaker, wafer holder and rinse bath for this step

Strip resist Use acetone at RT to remove the resist for 2 min.
 No resist residues are allowed. Rinse in water
 Manual drying.

54. CLEANING: HNO₃ SAL

Change the HNO₃ to prevent cross contamination

Cleaning Prepare a nitric acid bath.
 Use HNO₃ at RT to remove the resist for 10 min.
 No resist residues are allowed.
 Rinse in water
 Manual drying.

POLYIMIDE NOTE: SHOULD BE FINISHED IN A HALF DAY

55. MANUAL COATING

Use the Brewer Science manual coater system to coat the wafers with Polyimide LTC 9305.

The process consists of:

- Use the membrane chuck for non-contaminated wafers
- spin coating of Fujifilm LTC9305 negative polyimide, dispensed by a manual syringe

Use program "no 30: 60sec at 6000RPM". (recipe needs to be checked)

56. MANUAL BAKING STEP

Use the hotplate of manual coater system to soft bake the wafers with Polyimide LTC 9305.

The process consists of:

Bake 120 s @ 100C

57. INSPECTION AND CLEANING

Visually inspect the back side of the wafers and clean with acetone.
Also clean the edge of the wafer with a Q-tip with HTRD2 developer.
No polyimide residues are allowed.

58. ALIGNMENT AND EXPOSURE

Processing will be performed on the ASML PAS5500/80 automatic wafer stepper.
Follow the operating instructions from the manual when using this machine.

Use the transport wafer for clean wafers:

Develop the transport wafer also in HTRD2

Expose mask Polyimide 1 (box 437), with litho job Diesize_20mm/g20a-1, layer ID = 1 and E=120mJ.

59. POST EXPOSURE DELAY (PED) OR POST EXPOSURE BAKE (PEB)

PEB: 60s @ 50C

60. DEVELOPING MANUAL

Use the developer red room. Use special glassware for polyimide

- Developing with HTRD2, time 1m15s.
- A hard bake at 100°C for 90 seconds

Always follow the instructions for this equipment.

MEMS LAB

61. FINAL CURE

In vacuum and under low N2 flow.

Use dedicated Al carrier plate for clean wafers under the process wafer.

Standard Cure 60 min @ 350 °C

END POLYIMIDE

CR 100

62. METALLIZATION: RF etch + Ti 10nm + TiN 200nm @ 25

Use the TRIKON SIGMA 204 sputter coater for the deposition of a TiN metal layer with Ti adhesion layer on the wafers.

The deposition must be done at 25 °C with an Ar flow of 100 sccm. Follow the operating instructions from the manual when using this machine.

Use recipe Ti 10_TiN 200_25C.

Note a TiN in between needs to be done between the process wafers.

Visual inspection: the metal layer must look shiny.

63. COATING

Use the coater station of the EVG120 system to coat the wafers with photoresist. The process consists of:

- a treatment with HMDS (hexamethyldisilazane) vapor, with nitrogen as a carrier gas
- spin coating of Shipley SPR3012 positive resist, dispensed by a pump
- a soft bake at 95 °C for 90 seconds
- an automatic edge bead removal with a solvent

Always check the relative humidity (48 ± 2 %) in the room before coating, and follow the instructions for this equipment.

Appendix

Use program "**Co - 3012 – 1.4um**". No residue allowed on the back.

64. ALIGNMENT AND EXPOSURE

Processing will be performed on the ASML PAS5500/80 automatic wafer stepper.

Follow the operating instructions from the manual when using this machine.

Expose **mask INT** (box 437), with litho job Diesize_20mm/g20a-1, layer ID = 1 and E=150mJ.

65. DEVELOPING

Use the developer station of the EVG120 system to develop the wafers. The process consists of:

- a post-exposure bake at 115 °C for 90 seconds
- developing with Shipley MF322 with a double puddle process
- a hard bake at 100 °C for 90 seconds Always follow the instructions for this equipment.

Use program "**Dev – SP**".

66. INSPECTION: Linewidth and overlay

Visually inspect the wafers through a microscope: No resist residues are allowed in exposed part.

67. PLASMA ETCHING: TiN 100 nm (sputtered at 25 °C)

Use the Trikon Omega 201 plasma etcher.

Follow the operating instructions from the manual when using this machine.

It is not allowed to change the process conditions and times from the etch recipe!

Use sequence **TiN_NSL Special recipe** (with a platen temperature of 25 °C) to etch the TiN layer with endpoint detection.

Landing on Polyimide

68. LAYER STRIPPING: Photoresist

Strip resist Use the Tepla Plasma 300 system to remove the photoresist in an oxygen plasma.

Follow the instructions specified for the Tepla stripper, and use the quartz carrier.

Use **program 2** flash.

POLYIMIDE NOTE: SHOULD BE FINISHED IN A HALF DAY

69. MANUAL COATING

Use the Brewer Science manual coater system to coat the wafers with Polyimide LTC 9305.

The process consists of:

- Use the membrane chuck for non-contaminated wafers
- spin coating of Fujifilm LTC9305 negative polyimide, dispensed by a manual syringe

Use program "no 30: 60sec at 6000RPM". (recipe needs to be checked)

70. MANUAL BAKING STEP

Use the hotplate of manual coater system to soft bake the wafers with Polyimide LTC 9305.

The process consists of:

Bake 120 s @ 100C

71. INSPECTION AND CLEANING

Visually inspect the back side of the wafers and clean with acetone.

Also clean the edge of the wafer with a Q-tip with HTRD2 developer.

No polyimide residues are allowed.

72. ALIGNMENT AND EXPOSURE

Processing will be performed on the ASML PAS5500/80 automatic wafer stepper.

Follow the operating instructions from the manual when using this machine.

Use the transport wafer for clean wafers:

Develop the transport wafer also in HTRD2

Expose mask Polyimide 2 (box 437), with litho job Diesize_20mm/g20a-1, layer ID = 1 and E=100mJ.

73. POST EXPOSURE DELAY (PED) OR POST EXPOSURE BAKE (PEB)

PEB: 60s @ 50C

74. DEVELOPING MANUAL

Use the developer red room. Use special glassware for polyimide

- Developing with HTRD2, time 1m15s.
- A hard bake at 100°C for 90 seconds

Always follow the instructions for this equipment.

MEMS LAB

75. FINAL CURE

In vacuum and under low N2 flow.

Use dedicated Al carrier plate for clean wafers under the process wafer.

Standard Cure 60 min @ 350 °C

END POLYIMIDE

CR 100

76. MANUAL COATING PHOTORESIST (BACK)

Use manual coater system to coat the wafers with photoresist. The process consists of:

- Spin coat the Shipley SPR3027 positive resist by dispensing it with manual syringe
- Use the Non-vacuum edge-chuck
- Make sure the edge of the wafer is completely covered with resist.

Use program: . Change spinning time. Spinning time:

START PDMS IN POLYMER LAB

77. PREPARING PDMS

Use the weighing scale to mix PDMS curing agent (by pipette) and elastomer (by pouring) in a ratio of 1:10 in a plastic disposable cup. Depending on the number of wafers to be processed these amounts could vary but the ratio between the elastomer and curing agent must be keep on 1:10. (Normally 5-6 g of elastomer per wafer need to be used)

Stir thoroughly with disposable pipette.

78. PDMS MIXING AND DEGASING

Use the Thinky Speedmixer for mixing and degasing the PDMS elastomer and curing agent.

Weigh the total mass of the sample holder with the PDMS and adjust the mass in the Speedmixer.

Appendix

Make sure that the cup holder is properly located in the machine.
Select **program 01**, check the parameters for each step and then start the process.

79. MANUAL COATING PDMS

Use manual coater system to coat the wafers with PDMS. The process consists of:

- Cover the inside of the coating station with aluminum foil
- Spin coat the PDMS by dispensing it with manual syringe

Use program: **PDMS6000**. Change spinning time. Spinning time: 90seconds.

80. PDMS BAKE

Use the Memmert oven in tunnel 1 to perform an extra resist bake:
bake the wafers at 90 °C for 30 minutes Note: Use a dedicated rack to bake the wafers

END PDMS IN POLYMER LAB

81. MANUAL REMOVING RESIST ON BACKSIDE

Use the Spray coater system to remove the resist with acetone. The process consists of:

Use the membrane chuck for non-contaminated wafers

Spray the acetone on the wafer during spinning.

Use program: (need to be checked)

82. INSPECTION PDMS RESIDUES

Visually inspect the wafers through a microscope, and check if the wafers are clean. No resist or PDMS residues are allowed.

83. METALLIZATION: 250nm Al pure @ RT or 250nm Al/Si @ RT

Use the TRIKON SIGMA 204 sputter coater for the deposition of an aluminium metal layer on the wafers.
The target must exist of 99% Al and 1% Si And Ti, and deposition must be done at RT with an Ar flow of 100 sccm. Follow the operating instructions from the manual when using this machine.

Use recipe **Al 250nm_RT**.

Note: Before running the recipe it is **mandatory** for this process first of all to make a Leak-Up rate test of the PDMS layer in order to avoid any damage in the machine.

Whether this test is skip or the results of the test are not satisfactory the processing of the wafers in this machine is not allowed.

Visual inspection: The metal layer is not very shiny.

84. COATING

Use the coater station of the EVG120 system to coat the wafers with photoresist. The process consists of:

- a treatment with HMDS (hexamethyldisilazane) vapor, with nitrogen as a carrier gas
- spin coating of AZNlof2020 negative resist, dispensed by syringe
- a soft bake at 95 °C for 90 seconds
- no edge bead removal

Always check the relative humidity (48 ± 2 %) in the room before coating, and follow the instructions for this equipment.

Use program "**Co_Nlof_3,5µm_no EBR**". No residue allowed on the back.

85. ALIGNMENT AND EXPOSURE

Appendix

Processing will be performed on the ASML PAS5500/80 automatic wafer stepper.
Follow the operating instructions from the manual when using this machine.
Expose wafer with job "_____" (backside alignment) with the correct exposure energy: **100mJ**

86. DEVELOPMENT

Use the EVG 120 Coater/developer to develop the wafers, and follow the instructions specified for this equipment. The process consists of:

- development step using Shipley MF322 developer (single puddle process)
- hard bake at 100°C for 1.5 min.

Always check the temperature of the hotplates first. Use development program: "**Dev –Lift off**".

87. PLASMA ETCHING: AlSi 250 nm

Use the Trikon Omega 201 plasma etcher.

Follow the operating instructions from the manual when using this machine.

It is not allowed to change the process conditions and times from the etch recipe!

Use the sequence with a platen temperature of 25 °C) to etch the AlSi layer with endpoint detection.
Landing on PDMS

88. PLASMA ETCHING: PDMS 1000 nm

Use the Trikon Omega 201 plasma etcher.

Follow the operating instructions from the manual when using this machine.

It is not allowed to change the process conditions and times from the etch recipe!

Use sequence **PDMS_4** (with a platen temperature of 25 °C) to etch the PDMS layer without endpoint detection.
Landing on oxide

89. PLASMA ETCHING SILICON (BACK)

Use the Rapier Omega i2L plasma etcher. It is not allowed to change the process conditions from the etch recipe. Change only number of cycles.

Follow the operating instructions from the manual when using this machine.

It is not allowed to change the process conditions and times from the etch recipe! (Cross-contamination is avoided with Ti barrier layer.)

LANDING on SiO₂

Use the sequence with a platen temperature of 20 °C to etch the Si layer and stop on SiO₂. Ca. 500 cycles.
Etching program includes end-point detection.

90. MANUAL COATING PHOTORESIST

Use manual coater system to coat the wafers with photoresist. The process consists of:

- Spin coat the Shipley SPR3027 positive resist by dispensing it with manual syringe
- Use the Non-vacuum edge-chuck
- Make sure the edge of the wafer is completely covered with resist.

Use program: . Change spinning time. Spinning time:

91. MANUAL BAKING STEP

Use the Memmert oven in tunnel 1 to perform an extra resist bake:

bake the wafers at 100 °C for 15-30min minutes

Note: Use a dedicated rack to bake the wafers

SAL

92. WET ETCHING BHF (PDMS): Etch 1μm PECVD SiO₂ + 100nm Ti + Etch 1μm PECVD SiO₂

Etch Use dedicated wet bench BHF 1:7 at ambient temperature, and the carrier with the 2 blue dots.
 The bath contains a buffered HF solution.
 Change the BHF solution to prevent cross-contamination
Time Until all oxide is removed. Time TBD (around 30 minutes)
Rinse Rinse in the water for 5 minutes.
Dry Use the manual dryer.

93. RESIST LAYER STRIPPING: ACETONE SAL

Use special beaker, wafer holder and rinse bath for this step

Strip resist Use acetone at RT to remove the resist for 2 min.
 No resist residues are allowed. Rinse in water
 Manual drying.

94. WET ETCHING PES: 250 nm Al

Etch Use dedicated wet bench PES.
 The bath contains PES solution.
Time Until all Al is removed. Time TBD (around 5 mins)
Rinse Rinse in the water for 5 minutes.
Dry Use the manual dryer.

A.3. Polyimide to PDMS adhesion

The adhesion between PI and PDMS was investigated by performing a series of immersion test. In this experiment, a test device was fabricated with the following fabrication sequence; The device is fabricated on a 4" double-sided polished n-type silicon wafers with a thickness of 525 μm . PECVD SiO_2 is deposited with a thickness of 2 μm on the front side and 5 μm on the back side. The SiO_2 on the backside is patterned to serve as a hard mask latter in the process. Photo-sensitive polyimide (Fujifilm LTC 9305) is then spin-coated on the front side and patterned with lithography. After the development, the PI is cured in a low pressure N_2 flow, at 350°C for 1 hour. The PI film is utilized for electrode isolation in the original device, but in this experiment, electrodes are not embedded to simplify the fabrication. At this step, some samples of the test device are treated with sputter-etch, and the rest of the sample without sputter-etch, are used as control. The sputter etch treatment was performed with 300 Watt RF power, for 15 seconds at 25 °C. The stretchable membrane is made from PDMS with 10:1 elastomer to curing agent ratio, covering the already cured PI film. The mix of PDMS elastomer and curing agent is then spin-coated on the front side to get the intended thickness of 4 μm and cured in 90° C, for 1 hour. After the curing process, polyimide film is securely covered in the PDMS membrane. The final structure of the sample device is shown in Fig.A.14 top.

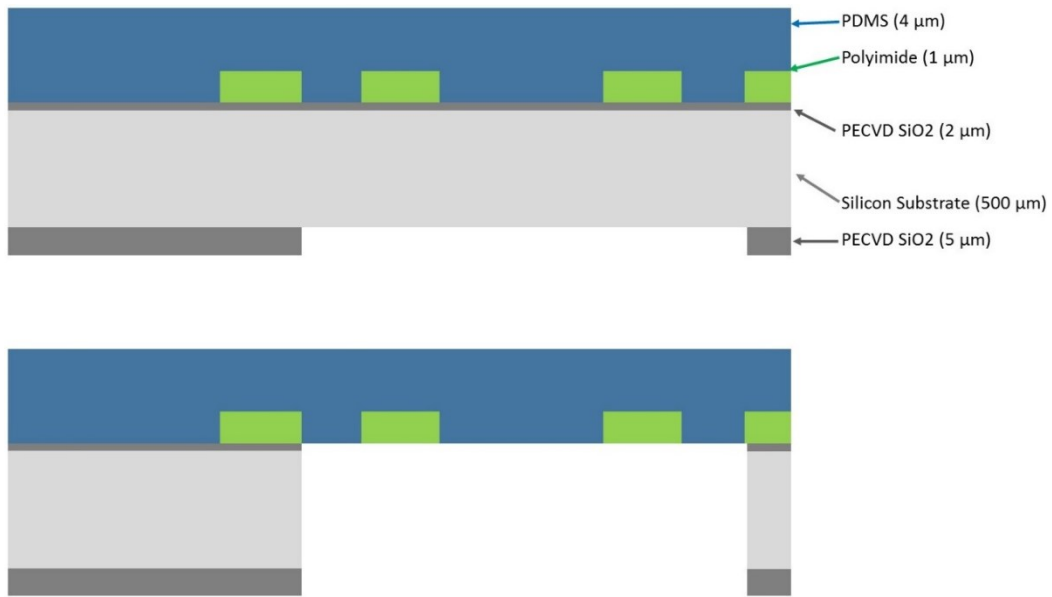


Figure A. 14. The cross section of the test device before (top) and after (bottom) the membrane releasing.

The final step of the fabrication is releasing the membrane, by etching through the silicon with DRIE from the back side. Utilizing the SiO_2 layer on the back as hard-etch mask, the silicon substrate is etched until the 2 μm SiO_2 layer on the front side is reached. At the end of this process, the holes in the silicon are completely open leaving only the SiO_2 layer covering the surface of the membrane. This SiO_2 layer is subsequently wet etched to expose the membrane with the PI structures, such as shown in Fig.A.14 (bottom). From this hole, solvent can be introduced to the polyimide and PDMS to test the adhesion between the two polymer layers.

Appendix

In this experiment, we were expecting to see detachment of the polyimide layer from the PDMS after being exposed to a solvent. Therefore, photographs of the sample were made before and after the solvent exposure. The step-by-step procedure of the experiment is listed below.

1. Observation under microscope, to get an image of the starting condition from each sample
2. Testing the sample with immersion in different solvent and different condition, @ 5 mins
 - a. Acetone Room Temperature (RT; 21° C)
 - b. Acetone 40° C
 - c. N-Methyl Pyrrolidone (NMP) RT
 - d. NMP 70° C
 - e. TMAOH (Tetramethylammonium Hydroxide) RT

** Note that each sample is placed front-side down so that solvent will come in contact directly with polyimide film and the PDMS membrane.*

3. After 5 minutes in the solvent, each sample is rinsed in the deionized water (RT) for 5 minutes to remove the solvent.
4. Observation under microscope to get image of the samples after immersion test.
5. Additional testing was done in acetone at 40° C up to 10 minutes for sample without sputter-etch treatment, and 20 minutes for sample with sputter etch treatment to see the adhesion after extended immersion.

The results of immersion test are listed in Tab.A-1. From the final result of this experiment, it was concluded that sputter etch treatment significantly improves the adhesion between polyimide film and PDMS layer during immersion in solvents.

TABLE A- 1. The result of immersion test of the test device in several organic solvents.

Solvent (sample)	5 min	10 min	15 min	20 min	1 x 20 min
(Untreated)					
Acetone RT	x	-	-	-	-
Acetone 40	v	x	-	-	-
NMP RT	v	-	-	-	-
NMP 70	x	-	-	-	-
TMAOH RT	v	-	-	-	-
(treated)					
Acetone RT	v	-	-	-	-
Acetone 40	v	v	v	v	v
NMP RT	v	-	-	-	-
NMP 70	v	-	-	-	-
TMAOH RT	v	-	-	-	-

'x' : delamination, 'v' : no delamination, '-' : not tested

5,10,15,20 mins : immersion for a period of 5 minutes, 2 x 5, 3 x 5, and 4 x 5 minutes

1 x 20 mins : immersion for an entire 20 minutes.

A.4. Non-Aqueous Reference Electrode

In order to prepare a reference system for the non-aqueous electrochemical process, there are two options that can be used. The first option is to use a Pt wire as *pseudo-reference* electrode. Since Pt was also used as the coating for the MEA, there should not be any potential difference between the Pt wire and the Pt coated MEA. The other option is to use the Ag/AgCl electrodes with a *salt bridge* (shown in the Fig.A.15). Both options are feasible in the scope of this project. Therefore, we investigated the performance of each reference system by performing cyclic voltammetry on a solution of **0.005 M Ferrocene** ($\text{Fc}|\text{Fc}^+$) with a supporting electrolyte of **0.1 M TBABF₄** in **Acetonitrile** (ACN) solvent, which also corresponds to the same concentration of the supporting electrolyte in the deposition (Section 4.2). Ferrocene is a common redox couple used as internal reference in organic electrochemical process [127]–[129]. The Ag/AgCl that is used in this experiment is a refillable miniaturized Ag/AgCl ($\varnothing = 2.2 \text{ mm}$), manufactured by eDAQ. The salt bridge is built from a PET tube, plugged with cotton in the sensing end and filled with an aqueous solution of **1 M NaCl**, and **1 M KCl**.

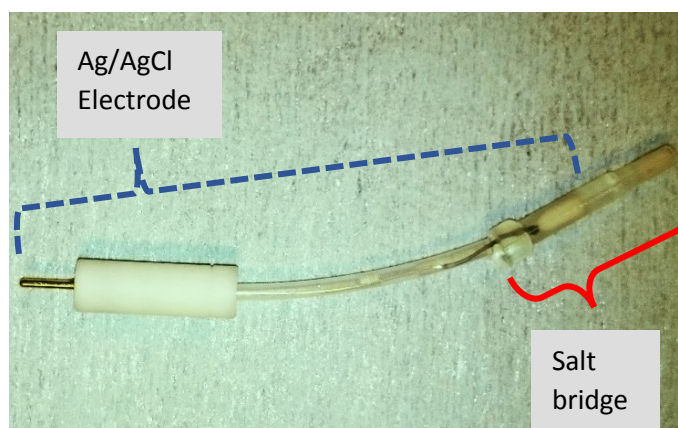


Figure A. 15. The construction of Ag/AgCl reference electrode with a salt bridge.

The results of the cyclic voltammetry measurement are shown in the Fig.A.16. The results of the CV measurement with the Pt pseudo-reference system are listed in the Tab.A-2 and the results of the measurement with Ag/AgCl + Salt Bridge are listed in the Tab.A-3.

From the calibration data, it can be concluded that the pseudo-reference electrode has a very low voltage consistency. This can be observed from the change of the formal redox potentials of ferrocene over time. In Tab.A-2, in addition to the scan rates variation, the scan results are listed in a chronological order from the first to the last row. It can be observed that the values of the formal potential of ferrocene shift to a more negative value over time, which implies the potential of pseudo-reference is increasing. This variation can also be observed in the I-V plot (Fig.A.16 (a)). In the plot, the average formal redox potential (shown as a dash line) is not located exactly in the middle of the distance between the oxidation and reduction peaks.

Normally, a stable reference gives a stable formal potential value over the different scan rates, and measurement period. The distance between the peaks may show a variation over different scan rates, but the formal potential value stays relatively constant. Meanwhile, for the Ag/AgCl with salt-bridge, the formal redox potential varies within a range of $\pm 4.2 \text{ mV}$, and does not show an

increasing or decreasing trend. This shows that the half-cell potential of the reference electrode is constant throughout the calibration measurement. Therefore, the Ag/AgCl with salt bridge can be used for the deposition experiment with non-aqueous solvent.

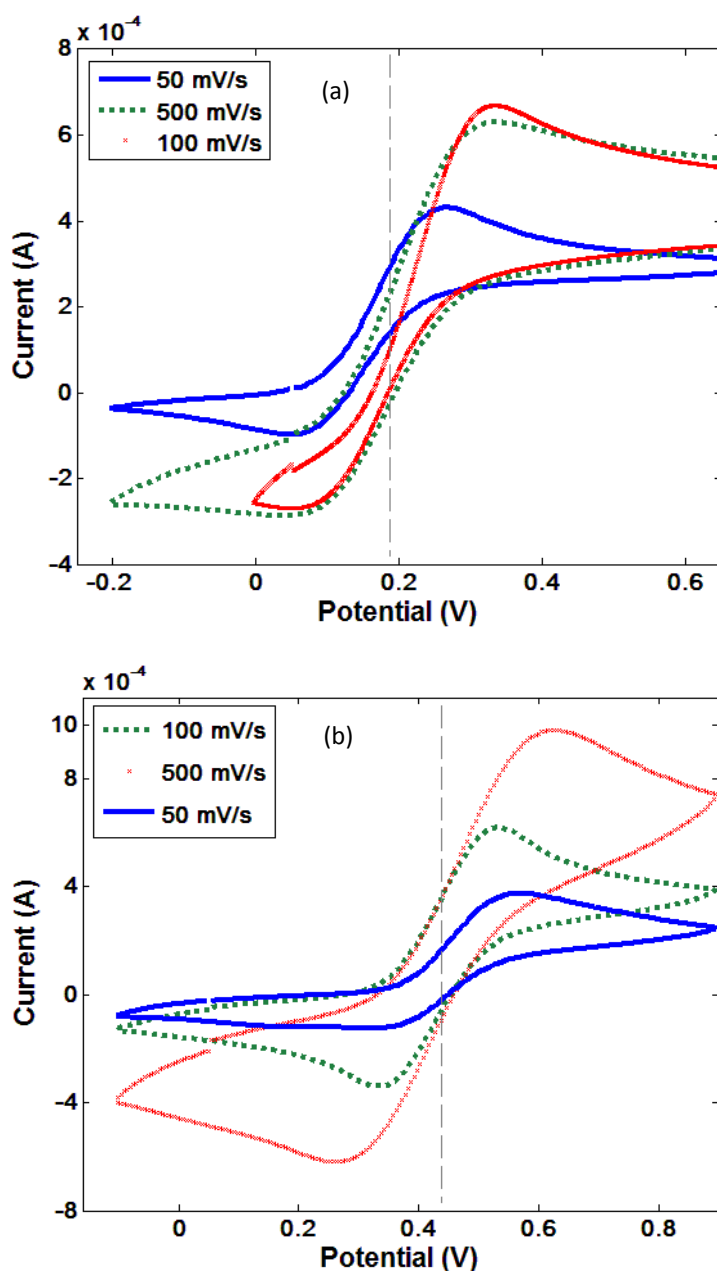


Figure A. 16. The I-V plots from the CV measurements of the Pt pseudo-reference (a), and Ag/AgCl with + bridge (b) in a solution of Ferrocene:TBABF₄:ACN, for various scan rates. The dash lines show the average formal redox potential of Ferrocene, measured in this experiment.

The large variation of the pseudo-reference potentials measured in this experiment, most likely is due to the polarization of the surface of the Pt-wire. Ideally, a reference electrode should be an NPE type electrode to avoid voltage variation due to the polarization of the double layer capacitance [130]. In case of the Ag/AgCl electrode with salt bridge, the voltage variation is small

Appendix

which indicates the low polarization of the electrode. The voltage variation that arises in this case might only due to the junction potential between different solvents.

TABLE A- 2. The calibration results of Pt wire pseudo-reference electrode in a solution of Ferrocene + TBABF₄ in ACN.

ν (mV/s)	E_o (mV)	E_r (mV)	E_{ro} (mV)	ΔE	E_{hc} (mV)
100	405.1	115.9	260.5	289.2	363.5
	334.3	49.8	192.1	284.5	431.9
500	340.6	39.1	189.8	301.5	434.2
	338.6	36.2	187.4	302.4	436.6
	336.6	37.2	186.9	299.4	437.1
50	274.9	55.4	165.2	219.4	458.8
	266.0	47.6	156.8	218.5	467.2
	258.3	65.3	161.8	193.0	462.2
Average =				187.5 \pm 30.5	436.4 \pm 30.5

TABLE A- 3. The calibration results of Ag/AgCl + Salt Bridge electrode in a solution of Ferrocene + TBABF₄ in ACN.

ν (mV/s)	E_o (mV)	E_r (mV)	E_{ro} (mV)	ΔE	E_{hc} (mV)
100	530.1	336.8	433.5	193.2	190.5
	533.0	333.1	433.1	199.8	190.9
	546.3	326.2	436.3	220.0	187.7
500	622.7	260.6	441.6	362.1	182.3
	641.9	244.9	443.4	397.1	180.6
	649.9	222.8	436.4	427.0	187.6
50	533.9	331.0	432.5	202.9	191.5
	568.4	316.9	442.6	251.5	181.4
Average =				437.4 \pm 4.2	186.6 \pm 4.2

To further verify the functionality of the salt bridge, an aqueous calibration was also done. The calibration method and the solution used in the measurement are similar to the method explained in Section 4.1. The results of the calibration measurement are shown in Fig.A.17 and Tab.A-4.

From the results of the aqueous calibration, it can be observed that the Ag/AgCl electrode with a salt bridge exhibits an even more stable half-cell potential compared to the results of the non-aqueous measurement. This is an indication that the junction potential is indeed affecting the variability of this reference system. However, this also proved that the salt bridge construction is functioning properly. Moreover, the variation of the half-cell potential in the non-aqueous media is insignificantly small (± 4.2 mV). In conclusion, these results confirms the possibility to use the reference system of Ag/AgCl with a salt bridge in the experiment with both aqueous and non-aqueous media.

Appendix

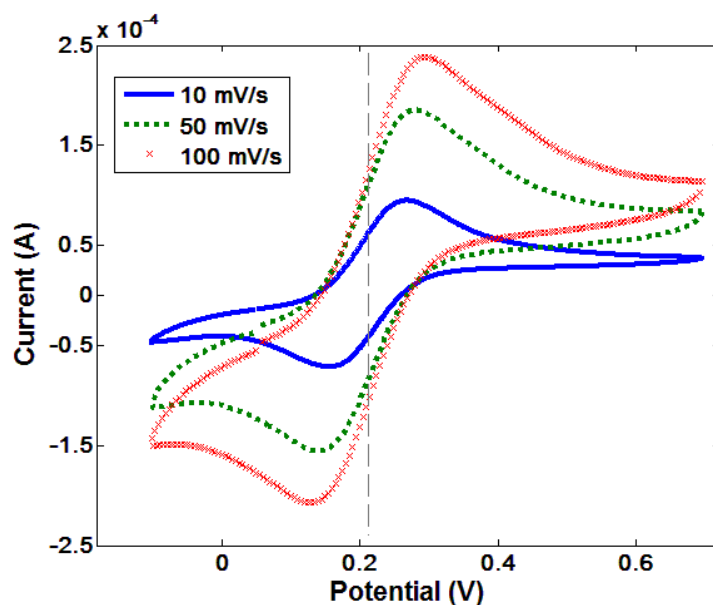


Figure A. 17. The I-V plot from the CV measurement of Ferrocyanide + KCl solution with Ag/AgCl + salt bridge reference system, with various scan rates. Vertical dash line shows the average of formal redox potentials of Ferrocyanide, measured in this experiment.

TABLE A- 4. The calibration results of Ag/AgCl + Salt Bridge electrode in an aqueous solution of Ferrocyanide + KCl.

ν (mV/s)	E_o (mV)	E_r (mV)	E_{ro} (mV)	ΔE	E_{hc} (mV)
50	284.7	140.5	212.5	144.3	226.7
	280.1	139.9	210.0	140.2	229.2
	278.8	141.6	210.2	137.2	229.0
100	299.0	129.5	214.3	169.5	225.0
	296.0	126.8	211.4	169.2	227.8
	294.8	126.8	210.8	168.0	228.4
10	266.8	155.4	211.1	111.4	228.1
	268.6	154.3	211.5	114.3	227.8
	269.1	154.1	211.6	115.0	227.6
Average =			211.5 ± 1.22		227.7 ± 1.22

A.5. Non-Aqueous PEDOT Deposition

To deposit PEDOT coating on the new batch of Pt coated microelectrode, the same sequence of deposition was performed with the salt-bridge reference electrode. The solution composition was identical to the solution in the test deposition. However, there was a problem during the LSV scan where the current on the working electrode suddenly reduced to a very low level, as shown in the Fig.A.18.

This phenomenon was consistently appearing on every microelectrode exposed to the solution mixture. Changing the solution into a freshly-mixed solution also did not solve this issue. Potentiostatic deposition was also tested without giving any result. The measured current during potentiostatic deposition only showed the noise measured on the working electrode, with a negligible transient current being observed in the beginning of the potential step.

This problem was reproducible on each microelectrode. Furthermore, all microelectrodes that were exposed to this solution were rendered unusable. Rinsing with DI water and vacuum drying did not recover the functionality of the microelectrode.

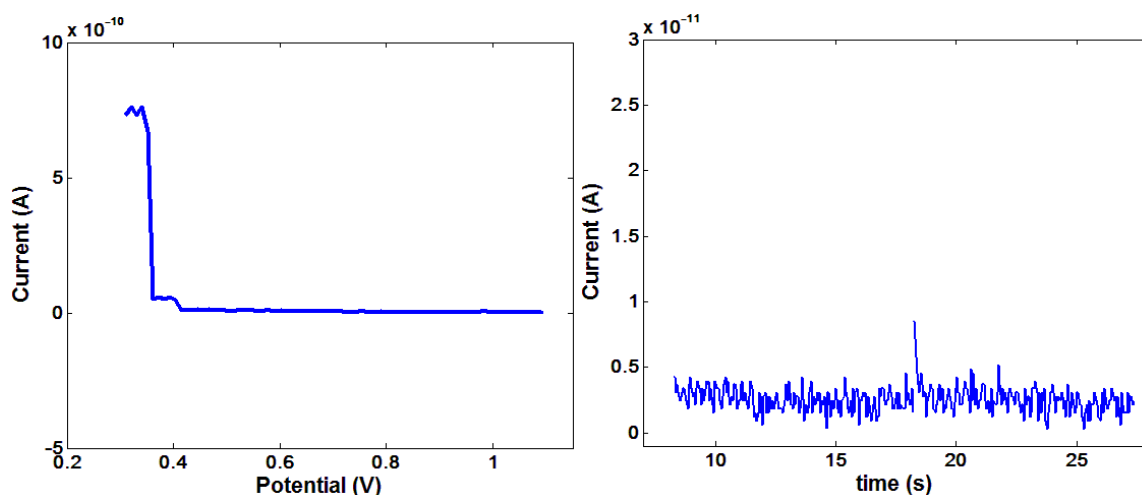


Figure A. 18. The I-V plot of LSV scan to determine the PEDOT:BF₄ deposition voltage on the new batch of MEA (a), and the result of current measurement during the potentiostatic deposition (b).

In the Fig.A.19, the results of cyclic voltammetry measurements before and after Acetonitrile exposure are shown. From the measurement results it can be observed that after the exposure to the solution, the microelectrode is not functioning at all.

In general, acetonitrile solvent will not reduce the functionality of platinum electrode due to the stability of both ACN and Pt over a broad range of potentials. Therefore, it is difficult to identify the exact origin of this issue. Beside the change of electrochemical characteristics, there was not any physical change observed on the microelectrode surface following this phenomenon. Due to the limited time, this problem was not further addressed. In order to avoid this problem, the PEDOT deposition in aqueous solution was tested.

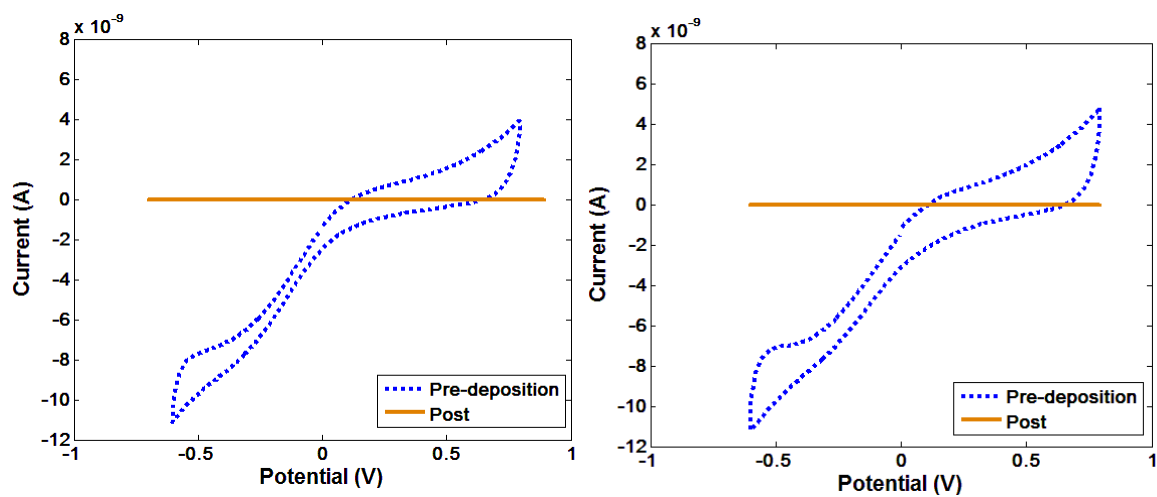


Figure A. 19. The results of CV scan from two different microelectrodes, comparing the current response prior and after the deposition.

A.6. Poster and Journal Paper

The preliminary results of this research have been published as a poster in the ICT OPEN conference 2017, and MEMS journal.

Platinum and Titanium-Nitride Microelectrodes Array on Flexible Substrate for Organ-on-Chip Application

Affan Kaysa Waafi¹, Nikolas Gaio¹, Ronald Dekker^{1,2}

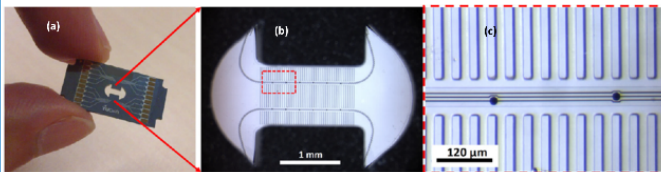
¹ Delft University of Technology, Mekelweg 4, 2628 CD Delft

² Philips Research Eindhoven, High Tech Campus 4, 5656 AE Eindhoven
The Netherlands

INTRODUCTION

Cytostretch is an Organ on Chip (OOC) device developed by TU Delft in collaboration with Phillips [1]. This platform can be adapted for various organ models, since it can be equipped with several modules such as flexible membranes, micro-grooves, and micro-electrode arrays (MEA) [1]. The stretchable membrane of the Cytostretch can be inflated in order to apply strain to the cell culture and mimic the pulsatile condition of a beating heart. Micro-grooves in the membrane promotes cell alignment. The electrodes in the membrane can be used to electrically stimulate or monitor the cell culture.

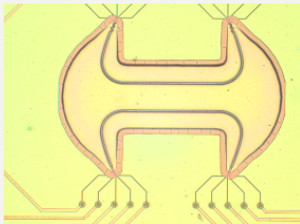
To detect the field potential of cardiomyocytes on top of the membrane, Cytostretch is equipped with a set of Titanium Nitride (TiN) electrodes. In the previous version of the device [1] an external platinum wire was used as reference electrode during measurement. In this work we present a novel fabrication process to coat few TiN electrodes with platinum in order to include a reference electrode directly on the membrane of Cytostretch.



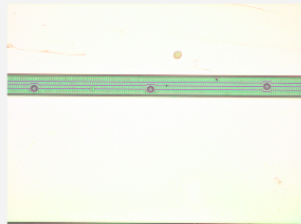
Overview of Cytostretch device with transparent flexible membrane covering the "dog bone" shaped hole (a). Flexible membrane of the cytostretch (b). Microgrooves, electrodes and wiring line on the membrane seen under optical microscope (c) (Reprinted from [1]).

RESULTS & CONCLUSION

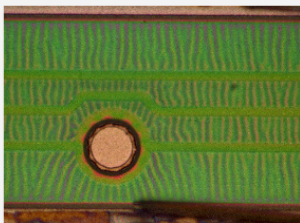
The process presented above was performed, proving that cytostretch device can be equipped with platinum reference electrode. In the next phase of the project, the electrochemical characterization of the platinum electrodes will be performed in order to study the electrical contact between the platinum and the TiN layers.



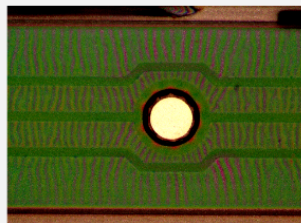
Overview of Cytostretch device with PDMS membrane covering the "dog bone" hole. Two lines of Polyimide with interconnection line and Platinum coated Micro-Electrode are embedded in the membrane



Structure of Micro-electrodes and Interconnection lines isolated with polyimide

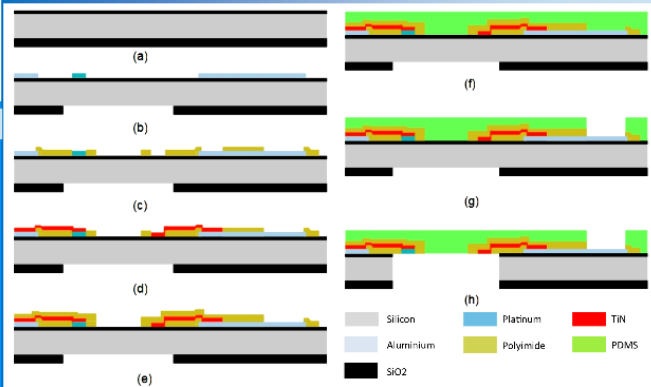


Surface of TiN micro-electrode as seen from the membrane surface (backside of wafer)

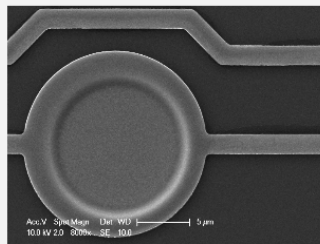


Surface of platinum micro-electrode as seen from the membrane surface (backside of wafer)

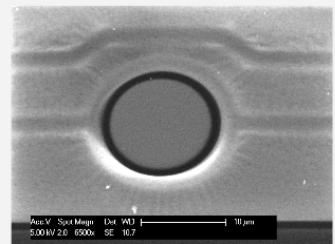
DEVICE FABRICATION



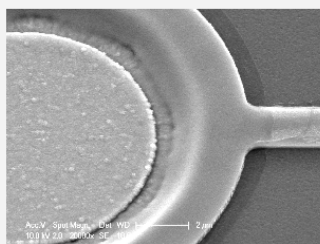
- Substrate is a 4" double-sided polished silicon wafer. Silicon Oxide (SiO_2) is deposited: 2 μm on the front and 6 μm on the back.
- SiO_2 in the back is patterned for hard mask. Aluminum (Al) deposition and patterning in the front side to build the electrical contact pads. Platinum is also deposited and patterned in the front side.
- The first layer of polyimide is deposited and patterned for isolation layer.
- Deposition of TiN for interconnection line, on top of polyimide, extending from Al contact to the microelectrode sites.
- Deposition and patterning of second layer of polyimide to make a sandwich structure which works as isolation layer.
- PDMS deposition to form the flexible membrane covering the entire structures (Polyimide, TiN, etc).
- Contact pads are then opened by patterning the PDMS layer.
- Bulk silicon etching from the backside to release the membrane. The remaining SiO_2 is removed by wet etching in BHF (Buffered Hydrogen Fluoride) exposing the surface of micro-electrode on the membrane.



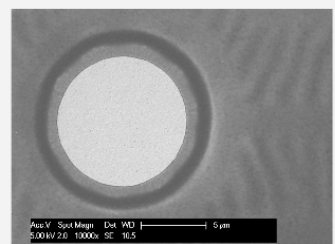
SEM image of TiN interconnection and micro-electrode before being covered with polyimide and PDMS, as seen from the front side of the wafer.



SEM image of TiN micro-electrode surface after membrane releasing, as seen from the backside of the wafer.



SEM image of connection between TiN and platinum micro-electrode before being covered with polyimide and PDMS, as seen from the front side of the wafer.



SEM image of platinum micro-electrode surface after membrane releasing, as seen from the backside of the wafer.

Reference

- [1] S. K. Pakazad, A. Savov, A. van de Stolpe, and R. Dekker, "A novel stretchable micro-electrode array (SMEA) design for directional stretching of cells," *J. Micromechanics Microengineering*, vol. 24, no. 3, p. 34003, 2014.

A MULTIWELL PLATE ORGAN-ON-CHIP (OOC) DEVICE FOR IN-VITRO CELL CULTURE STIMULATION AND MONITORING

N. Gaio¹, A. Waafi¹, M.L.H. Vlaming², E. Boschman³, P. Dijkstra⁴, P. Nacken², S.R. Braam², C. Boucsein⁵, P.M. Sarro¹, and R. Dekker^{1,6}

¹Laboratory of Electronic components, Technology & Materials (ECTM), EKL, Delft University of Technology, THE NETHERLANDS

²Ncardia, Biopartner building 3, Galileiweg 8, 2333 BD Leiden, THE NETHERLANDS

³Boschman Technologies/APC, Stenograaf 3, 6921 EX Duiven, THE NETHERLANDS

⁴Philips Innovation Center, 5656 AE Eindhoven, THE NETHERLANDS

⁵Multichannel System, Aspenhastrasse 21, 72770 Reutlingen, BW, GERMANY

⁶Philips Research, 5656 AE Eindhoven, THE NETHERLANDS

ABSTRACT

This work presents the first multi-well plate that allows for simultaneous mechanical stimulation and electrical monitoring of multiple *in-vitro* cell cultures in parallel. Each well of the plate is equipped with an Organ-on-Chip (OOC) device consisting of a stretchable micro-electrode array (MEA). For the first time, a film assisted molding (FAM) process was employed to embed an OOC into a multi well plate format packaging. The functionality of the MEA in the device was assessed with electrochemical impedance spectroscopy. Moreover, the biocompatibility of the plate was demonstrated with cardiomyocytes derived from human induced pluripotent stem cells (iPSC) cultured in the wells.

INTRODUCTION

Pharmaceutical companies are currently relying on cell-based assays and animal models in their preclinical tests in order to predict drug responses in humans. However, these models do not always fully capture the human physiology and pathology, and are thus not sufficiently predictive [1]. Organ on Chips (OOC) are much more sophisticated *in-vitro* models that aim at improving the prediction capability of cell-based assays [1,2].

OOCs combine micro-fabricated chips and cell cultures. The dynamic environment provided by the chip mimics the physiological conditions in a functional unit of a human organ. The chip could facilitate growth, proliferation, differentiation and maturation of the cells, which may then better recapitulate *in-vivo* human responses [3].

However, the fabrication and assembling methods employed are very often time consuming and heavily dependent on manual assembly [2,3], which conflicts with the need of high throughput screening. Moreover, it is becoming more and more clear that the integration of sensors will be a crucial feature to monitor and acquire quantitative and qualitative data from the cell cultures [2,3]. Last but not least, OOCs are often not user-friendly and are not compatible with standard biological work-flows [4].

Cytostretch is a modular platform for OOC applications [5] previously applied as a Heart-on-Chip model by Pakazad et al. [6]. Unlike the OOCs previously developed, the Cytostretch chip is based on conventional cleanroom-compatible micro-fabrication processes, thus

avoiding the labor-intensive fabrication steps often required in other OOC models. The Cytostretch key feature lies in the mechanical stimulation of the cell cultures [4] by means of a stretchable membrane. Moreover, due to the silicon based fabrication process, it can be easily equipped with a micro-electrode array (MEA) to record the electrical activity of the cells [5].

However, the initial concept still needed several manual handling steps. In fact, to culture, stimulate and monitor a cell monolayer, the Cytostretch needed to be manually loaded and unloaded in a system composed of a printed circuit board (PCB), multiple screws and a plastic well [6]. The assembly of the system drastically reduced the ease-of-use and might affect the reproducibility of the results. Last but not least, the previously used system was not compatible with a multi-well plate format and thus only useful for low throughput experiments.

Here we propose the integration of multiple Cytostretch chips on a novel multi-well plate (Fig. 1). The multi-well plate is in fact realized using film assisted molding (FAM) [8], a straightforward and monolithic packaging technique, which allows the formation of wells directly and automatically on top of the chip and the PCB. The resulting device allows for simultaneous mechanical stimulation and electrical monitoring of the cells. The multi-well plate was designed in order to be compatible with conventional readout equipment [9].

In order to mount four chips on a single plate, the Cytostretch chips were re-designed to a new format. The electrochemical performance of the MEA embedded in the new chip was characterized in order to assess its functionality. Moreover, in order to prove the biocompatibility of the chip, a preliminary biological assessment was performed by culturing human iPSC-

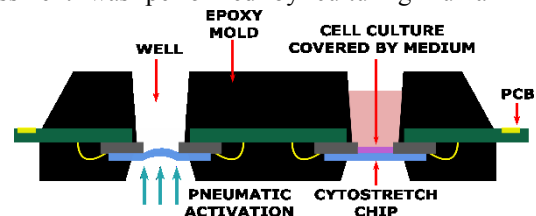


Figure 6.2: Cross section of the plate composed of Cytostretch chips glued and wirebonded on a Printed Circuit Board (PCB) and covered with molded wells. The stretchable membranes on the Cytostretch chips can be actuated by applying a pneumatic pressure to the backside of the plate.

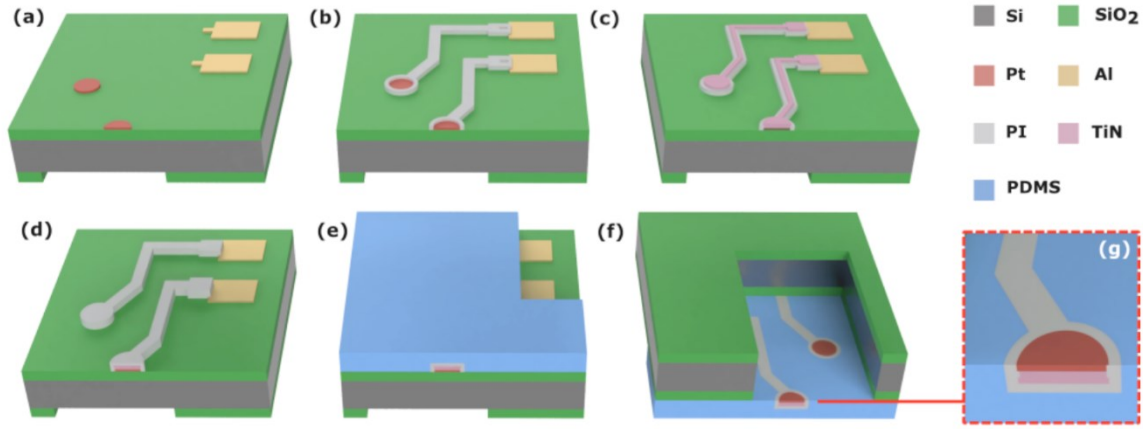


Figure 2: Process flow for the fabrication of the Cytostretch chips on Silicon (Si) wafer: (a) contact pads and Platinum (Pt) electrodes are fabricated on top of a 2 μm Silicon Oxide (SiO_2) layer. A 5 μm -thick SiO_2 layer is deposited and patterned on the back of the wafer. (b) A 1 μm layer of Polyimide (PI) is deposited and patterned. (c) The 200 nm thick Titanium Nitride (TiN) metal lines are fabricated. (d) The second layer of PI is deposited and patterned to isolate the metal lines. (e) A Polydimethylsiloxane (PDMS) layer is deposited and patterned to access the contact pads. (f,g) The PDMS membrane is released by etching the Si under the PDMS layer making the electrodes accessible.

derived cardiomyocytes (Pluricyte® Cardiomyocytes) in the wells and monitoring them for seven days.

MULTI-WELL PLATE FABRICATION

Chip Manufacturing

The Cytostretch chips are fabricated on 4 inch silicon wafers. The process starts with the deposition of 2 and 6 μm of silicon oxide (SiO_2) by plasma-enhanced chemical vapor deposition (PECVD) on the front and back of the wafer, respectively. The SiO_2 layer on the back is patterned by dry-etching to define the membrane area. The process continues by sputtering a 1.5 μm -thick aluminum (Al) layer on the frontside of the wafer. The Al is then patterned by dry-etching to define the contact pads. Then, a 100 nm-thick platinum layer is evaporated on the wafer and patterned by lift off to form the electrodes of the MEA (Fig. 2a). Next, the metal lines extending from the contact pads to the Pt electrodes are fabricated. For this, an 800 nm-thick photosensitive polyimide (Fujifilm LT9305) layer is deposited by spin coating and patterned (Fig. 2b). Subsequently, a layer of 200 nm of TiN is sputtered on the frontside of the wafer, and patterned by dry etching (Fig. 2c). A second layer of 800 nm-thick polyimide is deposited and patterned to provide electrical insulation to the metal lines (Fig. 2d). Subsequently, a 10- μm -thick PDMS layer is deposited by spin coating on the frontside of the wafer at 6000 rpm for 60 s, and cured for 30 min at 90 $^{\circ}\text{C}$. The contact pads are then open by patterning the PDMS layer by means of reactive ion etching using an Al layer as hard mask (Fig. 2e). Finally, the membrane is released by removing the Si and the SiO_2 layers underneath the membrane using deep reactive ion etching (DRIE) and buffered hydrofluoric acid (BHF), respectively (Fig. 2f,g).

Packaging

The packaging procedure starts by dicing the 4 inch wafer with an automatic dicing saw to obtain 100 Cytostretch chips. Four chips are mounted on a PCB with a fully-automatic pick-and-place system. The PCB is designed to fit into a MultiChannel System *in-*

vitro recording system (MEA2100-System). The Al contact pads on the chip are subsequently wire-bonded to the PCB.

Finally, the PCB and the chips are encapsulated with an epoxy compound by means of Film-Assisted Molding (FAM), using a Boschman Unistar Innovate 2-FF system. FAM is a proprietary technology of Boschman Technologies [8] that guarantees a molding process without

FILM-ASSISTED MOLDING

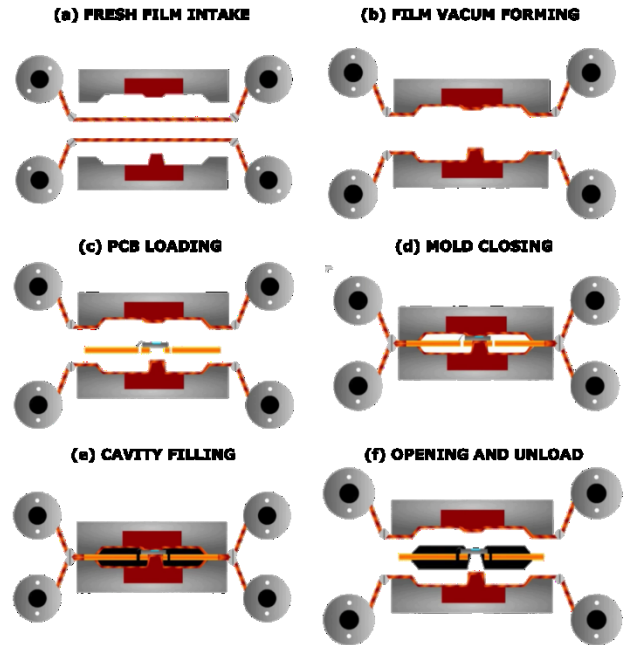


Figure 3: Process flow for the Film-Assisted Molding of the plate: (a) two Teflon films are rolled inside the mold, (b) the films are sucked into the inner surface of the mold, (c) the PCB is loaded inside the mold, (d) the mold is closed, (e) the liquefied epoxy material is injected in the mold and cured and (f) the mold is opened and the plate can be unloaded.

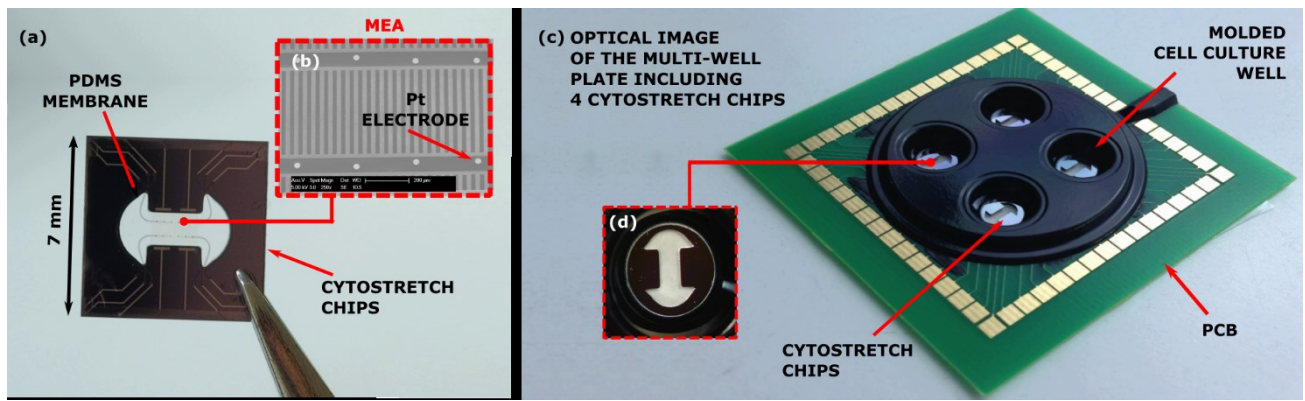


Figure 4: (a) Optical image of one Cytostretch chips including the MEA embedded in a stretchable PDMS membrane. The chip includes 12 circular electrodes (diameter: 30 μm , pitch 100 μm). (b) SEM image of Pt MEA. (c) Optical image of the multi-well plate consisting of four Cytostretch chips mounted on a PCB and encased by the molded wells (d) Optical image of the bottom of a well consisting of one of the chip.

physical contact between the mold-tool and the epoxy. This is achieved by two Teflon foils (Fig. 3a) that are sucked to the inner surfaces of the mold (Fig. 3b). The PCB is then inserted in the tool (Fig. 3c,d) and the epoxy material liquefied by heat and pressure is then forced into closed mold cavities and held there until the epoxy is solidified (Fig. 3e). A Sumitomo G700 serie epoxy material was used with a process temperature of 175°C and an end-cure pressure of 45 bar. The in-mold cure time used for this application was 80 sec.

The mold was customized in order to create the open-wells on top of the four chips, where the cells will be seeded and to protect the wirebonds from the humid environment of a cell culture incubator. After opening the mold, the encapsulated products are unloaded (Fig. 3g). Next, the vacuum is removed, and the foils are transported and renewed so that a new cycle can start without the need for a manual cleaning step.

CHARACTERIZATION

Electrochemical Characterization

The electrochemical performance of the MEA embedded in the Cytostretch was characterized by performing electrochemical impedance spectroscopy (EIS) on the Pt electrodes embedded in the membrane before mounting the chip on the plate. A measurement set-up similar to the one presented in [9] was used. The PDMS membrane on the Cytostretch chip was covered by Phosphate-Buffered Saline (PBS). A Silver/Silver chloride (Ag/AgCl) electrode and a Pt strip were used as reference and counter electrode, respectively.

EIS tests were performed with an Autohom Metrolab galvanostat/potentiostat (PGSTAT302N) with FRA32M Module. The amplitude of potential variations between working and reference electrode was equal to 50 mV and the stimulation frequency was swept between 0.01 and 10 kHz. The output current was monitored during the measurements to detect potential non-linearity caused by high-amplitude stimulations.

Cell culture

A preliminary biological assessment of the novel plate was performed by culturing human iPSC-derived Cardiomyocytes (Pluricyte® Cardiomyocytes, Ncardia, Belgium) in the wells (100.000 cells/cm²) and monitoring

them for seven days. Cell culture was performed according to manufacturer's protocol under standardized cell culture conditions (37°C, 5%CO₂, ~100% relative humidity).

Cell and monolayer appearance was monitored with light microscopy and beating of the cardiomyocytes was further assessed using a calcium sensitive dye (FLIPR Calcium 6 Assay Kit, Molecular Devices).

RESULTS

Figure 4 shows an optical image of the silicon chip (Fig. 4a) and a SEM image of the stretchable microelectrodes (Fig. 4b). The final plate after FAM is shown in Figure 4c. The FAM molding did result in a clean chip surface without epoxy residues on the chip-surface (Fig. 4d). Both sides of the chip where clamped with high precision without inducing too much stress on the chip that remained intact during the FAM. Standard transfer molding process conditions for the epoxy molding compound were used to mold the chips to assure a perfect adhesion between the epoxy mold and the chip.

In Figure 5 the Bode plot of the impedance spectra of one of the Pt electrodes is shown. At 1 kHz the average

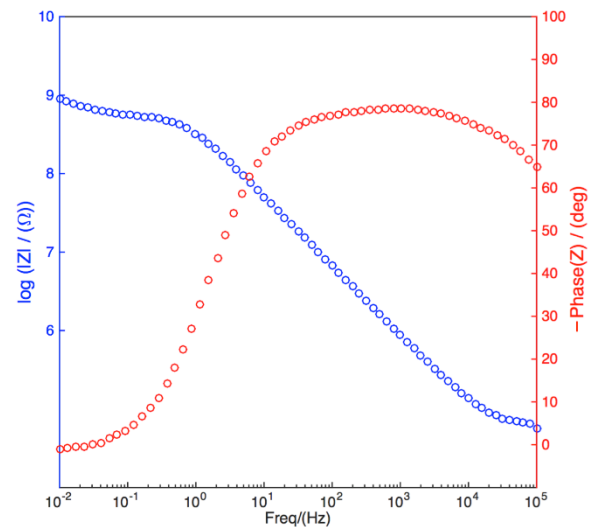


Figure 5: (a) Average bode plot of impedance spectra of five Pt electrodes (705 μm^2 geometric surface area). The average electrode impedance (1 kHz) is 870 k Ω .

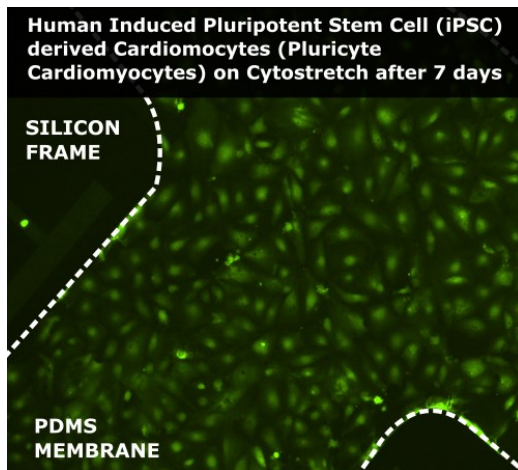


Figure 6: Microscopic image of hiPSC-derived cardiomyocytes cultured on the stretchable membrane for 7 days. Cells were stained with Calcium 6 dye (Molecular Devices). The Cardiomyocytes continue to appear normal and viable under fluorescent imaging even after seven days.

impedance calculated over five Pt microelectrodes is 870 k Ω . The impedance trend and the recorded value is comparable to the one previously presented by Pakazad et al. [6].

The biological results achieved after applying the mentioned protocol shows cardiomyocytes which appeared overall normal and viable under fluorescent imaging (Fig. 6) up to seven days of culturing. However, no spontaneous beating of the cells was observed throughout the study. The reason for this has to be further investigated. During the cell culture, no leakage was observed, indicating adequate adhesion at the interface molded epoxy material, which forms the the wells, and the Cytostretch chips.

CONCLUSIONS

A novel multi-well plate that can be used to simultaneously mechanically stimulate, and electrically monitor *in-vitro* cell cultures was designed, fabricated and characterized. The plate includes an optimized version of the previously presented Cytostretch, mounted on a PCB. The wells and the insulation of the wirebonding were directly molded on top of the PCBs using a fully automatic film assisted molding technology. This is the first time that such a packaging technique is employed for an OOC device, and this work demonstrates that FAM can be a valuable option for directly molding a cell culture environment on top of OOC devices, creating a multi-well plate platform. The dimensions of the PCB and the mold can be easily re-defined in order to fit more Cytostretch in one plate, which will eventually be fabricated with a high-throughput format.

The new version of the Cytostretch chip was electrochemically characterized and the presented results showed an impedance in line with previously presented results.

This novel plate provides monolithic and robust biocompatible packaging for the Cytostretch. This was tested by culturing human iPSC-derived cardiomyocytes (Pluricyte® Cardiomyocytes) in the molded wells. Unlike most of the previously presented OOCs, the cells are seeded

in open-wells by simply using a pipette. The plate has proven to provide easy cell culturing, sampling and inspection. The presented results show that the plate is biocompatible even though further investigations are needed to determine the cause of the absence of spontaneous beating of the cardiomyocytes.

The combination of high quality microfabrication and standard assembly and conventional packaging techniques are an important step forwards toward high-throughput Organ-on-Chip applications.

ACKNOWLEDGEMENTS

The authors would like to thank the Institute for human Organ and Disease Model Technologies (hDMT). Moreover, the authors gratefully acknowledge the technical support and advice of the staff at the Else Kooi Laboratory (EKL). This work was performed in the framework of the ECSEL JU InForMed Project (grant no. 2014-2-662155).

REFERENCES

- [1] A.D. van der Meer and A. van den Berg, "Organs-on-chips: breaking the in vitro impasse." *Integrative Biology* 4.5, 2012, pp. 461-470.
- [2] N. Beißner, T. Lorenz, and S. Reichl, "Organ on chip." *Microsystems for Pharmatechnology*. Springer International Publishing, pp. 299-339, 2016.
- [3] A. van de Stolpe, and J. den Toonder, "Workshop meeting report Organs-on-Chips: human disease models." *Lab on a chip* 13.18, pp. 3449-3470, 2013.
- [4] A. Junaid, A. Mashaghi, T. Hankemeier, and P. Vulto, "An End-User Perspective on Organ-on-a-Chip: Assays and Usability Aspects." *Current Opinion in Biomedical Engineering*, 2017.
- [5] N. Gaio, B. van Meer, W. Quirós Solano, L. Bergers, A. van de Stolpe, C. Mummery, P. M. Sarro, and R. Dekker, "Cytostretch, an organ-on-chip platform." *Micromachines* 7, no. 7, 120, 2016.
- [6] S.K. Pakazad, A. Savov, A. Van de Stolpe, and R. Dekker, "A novel stretchable micro-electrode array (SMEA) design for directional stretching of cells.", *Journal of Micromechanics and Microengineering* 24, no. 3, 2014, 034003.
- [7] S.K. Pakazad, "Stretchable Micro-Electrode Arrays for Electrophysiology." PhD diss., 2015.
- [8] L. Wang, A. Bos, T. van Weelden, and F. Boschman, "The next generation advanced MEMS& sensor packaging.", *Electronic Packaging Technology & High Density Packaging (ICEPT-HDP)*, 11th International Conference on, pp. 55-60, 2010.
- [9] N. Gaio, C. Silvestri, B. van Meer, S. Vollebregt, C. L. Mummery, and R. Dekker, "Fabrication and characterization of an Upside-down Carbon Nanotube (CNT) Microelectrode array (MEA)." *IEEE Sens. J.*, 1-1, 2016.

CONTACT

*N. Gaio, tel: +31 (0) 15 2786294; n.gaio@tudelft.nl

References

- [1] E. W. Esch, A. Bahinski, and D. Huh, "Organs-on-chips at the frontiers of drug discovery," *Nat. Rev. Drug Discov.*, vol. 14, no. 4, pp. 248–260, Apr. 2015.
- [2] G. Wang *et al.*, "Modeling the mitochondrial cardiomyopathy of Barth syndrome with induced pluripotent stem cell and heart-on-chip technologies," *Nat. Med.*, vol. 20, no. 6, pp. 616–623, Jun. 2014.
- [3] S. S. C. Hung, S. Khan, C. Y. Lo, A. W. Hewitt, and R. C. B. Wong, "Drug discovery using induced pluripotent stem cell models of neurodegenerative and ocular diseases," *Pharmacol. Ther.*
- [4] F. Zheng, F. Fu, Y. Cheng, C. Wang, Y. Zhao, and Z. Gu, "Organ-on-a-Chip Systems: Microengineering to Biomimic Living Systems," *Small*, vol. 12, no. 17, pp. 2253–2282, May 2016.
- [5] B. Jiang, W. Zheng, W. Zhang, and X. Jiang, "Organs on microfluidic chips: A mini review," *Sci. China Chem.*, vol. 57, no. 3, pp. 356–364, Mar. 2014.
- [6] A. R. Perestrelo, A. C. P. Águas, A. Rainer, and G. Forte, "Microfluidic Organ/Body-on-a-Chip Devices at the Convergence of Biology and Microengineering," *Sensors*, vol. 15, no. 12, pp. 31142–31170, Dec. 2015.
- [7] D. Huh, B. D. Matthews, A. Mammoto, M. Montoya-Zavala, H. Y. Hsin, and D. E. Ingber, "Reconstituting Organ-Level Lung Functions on a Chip," *Science*, vol. 328, no. 5986, pp. 1662–1668, Jun. 2010.
- [8] M. B. Esch, A. S. T. Smith, J.-M. Prot, C. Oleaga, J. J. Hickman, and M. L. Shuler, "How multi-organ microdevices can help foster drug development," *Adv. Drug Deliv. Rev.*, vol. 69–70, pp. 158–169, Apr. 2014.
- [9] I. Maschmeyer *et al.*, "A four-organ-chip for interconnected long-term co-culture of human intestine, liver, skin and kidney equivalents," *Lab. Chip*, vol. 15, no. 12, pp. 2688–2699, Jun. 2015.
- [10] A. Skardal *et al.*, "Multi-tissue interactions in an integrated three-tissue organ-on-a-chip platform," *Sci. Rep.*, vol. 7, no. 1, p. 8837, Aug. 2017.
- [11] N. Gaio *et al.*, "Cytostretch, an Organ-on-Chip Platform," *Micromachines*, vol. 7, no. 7, p. 120, Jul. 2016.
- [12] S. K. Pakazad, A. Savov, A. van de Stolpe, and R. Dekker, "A novel stretchable micro-electrode array (SMEA) design for directional stretching of cells," *J. Micromechanics Microengineering*, vol. 24, no. 3, p. 034003, 2014.
- [13] J. D. Weiland, D. J. Anderson, and M. S. Humayun, "In vitro electrical properties for iridium oxide versus titanium nitride stimulating electrodes," *IEEE Trans. Biomed. Eng.*, vol. 49, no. 12, pp. 1574–1579, Dec. 2002.
- [14] M. Janders, U. Egert, M. Stelzle, and W. Nisch, "Novel thin film titanium nitride micro-electrodes with excellent charge transfer capability for cell stimulation and sensing applications," in *Proceedings of 18th Annual International Conference of the IEEE Engineering in Medicine and Biology Society*, 1996, vol. 1, pp. 245–247 vol.1.
- [15] D. M. Zhou and R. J. Greenberg, "Electrochemical characterization of titanium nitride microelectrode arrays for charge-injection applications," in *Proceedings of the 25th Annual International Conference of the IEEE Engineering in Medicine and Biology Society (IEEE Cat. No.03CH37439)*, 2003, vol. 2, p. 1964–1967 Vol.2.

References

- [16] N. Gaio, C. Silvestri, B. van Meer, S. Vollebregt, C. L. Mummery, and R. Dekker, "Fabrication and Characterization of an Upside-Down Carbon Nanotube Microelectrode Array," *IEEE Sens. J.*, vol. 16, no. 24, pp. 8685–8691, Dec. 2016.
- [17] X. T. Cui and D. D. Zhou, "Poly (3,4-Ethylenedioxythiophene) for Chronic Neural Stimulation," *IEEE Trans. Neural Syst. Rehabil. Eng.*, vol. 15, no. 4, pp. 502–508, Dec. 2007.
- [18] S. Venkatraman, J. Hendricks, S. Richardson-Burns, E. Jan, D. Martin, and J. M. Carmenta, "PEDOT coated microelectrode arrays for chronic neural recording and stimulation," in *2009 4th International IEEE/EMBS Conference on Neural Engineering*, 2009, pp. 383–386.
- [19] T. D. Y. Kozai *et al.*, "Chronic In Vivo Evaluation of PEDOT/CNT for Stable Neural Recordings," *IEEE Trans. Biomed. Eng.*, vol. 63, no. 1, pp. 111–119, Jan. 2016.
- [20] A. Schander, T. Teßmann, S. Stokov, H. Stemmann, A. K. Kreiter, and W. Lang, "In-vitro evaluation of the long-term stability of PEDOT:PSS coated microelectrodes for chronic recording and electrical stimulation of neurons," in *2016 38th Annual International Conference of the IEEE Engineering in Medicine and Biology Society (EMBC)*, 2016, pp. 6174–6177.
- [21] H. Charkhkar *et al.*, "Chronic intracortical neural recordings using microelectrode arrays coated with PEDOT-TFB," *Acta Biomater.*, vol. 32, pp. 57–67, Mar. 2016.
- [22] A. L. Hodgkin and B. Katz, "The effect of sodium ions on the electrical activity of the giant axon of the squid," *J. Physiol.*, vol. 108, no. 1, pp. 37–77, 1949.
- [23] A. L. Hodgkin, "The Ionic Basis of Electrical Activity in Nerve and Muscle," *Biol. Rev.*, vol. 26, no. 4, pp. 339–409, 1951.
- [24] D. R. Curtis, J. W. Phillis, and J. C. Watkins, "Chemical Excitation of Spinal Neurones," *Nature*, vol. 183, no. 4661, pp. 611–612, 1959.
- [25] D. R. Kenshalo, G. J. Giesler, R. B. Leonard, and W. D. Willis, "Responses of neurons in primate ventral posterior lateral nucleus to noxious stimuli," *J. Neurophysiol.*, vol. 43, no. 6, pp. 1594–1614, Jun. 1980.
- [26] A. Stett *et al.*, "Biological application of microelectrode arrays in drug discovery and basic research," *Anal. Bioanal. Chem.*, vol. 377, no. 3, pp. 486–495, Oct. 2003.
- [27] S. F. Cogan, "Neural Stimulation and Recording Electrodes," *Annu. Rev. Biomed. Eng.*, vol. 10, no. 1, pp. 275–309, 2008.
- [28] M. E. Spira and A. Hai, "Multi-electrode array technologies for neuroscience and cardiology," *Nat. Nanotechnol.*, vol. 8, no. 2, pp. 83–94, Feb. 2013.
- [29] R. Kim, S. Joo, H. Jung, N. Hong, and Y. Nam, "Recent trends in microelectrode array technology for in vitro neural interface platform," *Biomed. Eng. Lett.*, vol. 4, no. 2, pp. 129–141, Jun. 2014.
- [30] J. O. Bockris, M. A. V. Devanathan, and K. Müller, "On the Structure of Charged Interfaces," *Proc. R. Soc. Lond. Ser. Math. Phys. Sci.*, vol. 274, no. 1356, pp. 55–79, 1963.
- [31] J. O. Bockris and K.-T. Jeng, "Water structure at interfaces: the present situation," *Adv. Colloid Interface Sci.*, vol. 33, no. 1, pp. 1–54, Sep. 1990.
- [32] J. O. Bockris, A. K. N. Reddy, and M. Gamboa-Aldeco, Eds., "The Electrified Interface," in *Modern Electrochemistry 2A: Fundamentals of Electrode Processes*, Boston, MA: Springer US, 2000, pp. 771–1033.
- [33] Z. Stojek, "The Electrical Double Layer and Its Structure," in *Electroanalytical Methods*, F. Scholz, Ed. Berlin, Heidelberg: Springer Berlin Heidelberg, 2005, pp. 3–8.
- [34] S. Srinivasan, "Electrode/Electrolyte Interfaces: Structure and Kinetics of Charge Transfer," in *Fuel Cells*, Springer, Boston, MA, 2006, pp. 27–92.
- [35] J. O. Bockris and A. K. N. Reddy, Eds., "Electrochemistry," in *Modern Electrochemistry 1: Ionics*, Boston, MA: Springer US, 1998, pp. 1–34.
- [36] J. O. Bockris and A. K. N. Reddy, Eds., "Ion-Ion Interactions," in *Modern Electrochemistry 1: Ionics*, Boston, MA: Springer US, 1998, pp. 225–359.

References

- [37] J. O. Bockris and A. K. N. Reddy, Eds., "Ion Transport in Solutions," in *Modern Electrochemistry 1: Ionics*, Boston, MA: Springer US, 1998, pp. 361–599.
- [38] Allen J. Bard and Larry R. Faulkner, *Electrochemical Methods: Fundamentals and Applications, 2nd Edition*. New York: John Wiley and Sons, 2001.
- [39] N. Joye, A. Schmid, and Y. Leblebici, "Electrical modeling of the cell–electrode interface for recording neural activity from high-density microelectrode arrays," *Neurocomputing*, vol. 73, no. 1, pp. 250–259, Dec. 2009.
- [40] L. A. Geddes, "Historical evolution of circuit models for the electrode-electrolyte interface," *Ann. Biomed. Eng.*, vol. 25, no. 1, p. 1, Jan. 1997.
- [41] B. V. Tilak and B. E. Conway, "Overpotential decay behavior—I. Complex electrode reactions involving adsorption," *Electrochimica Acta*, vol. 21, no. 10, pp. 745–752, Oct. 1976.
- [42] S. R. Taylor and E. Gileadi, "Physical Interpretation of the Warburg Impedance," *Corrosion*, vol. 51, no. 09, Sep. 1995.
- [43] G. Barbero and I. Lelidis, "Analysis of Warburg's impedance and its equivalent electric circuits," *Phys. Chem. Chem. Phys.*, vol. 19, no. 36, pp. 24934–24944, Sep. 2017.
- [44] C.-H. Chen, D.-J. Yao, S.-H. Tseng, S.-W. Lu, C.-C. Chiao, and S.-R. Yeh, "Micro-multi-probe electrode array to measure neural signals," *Biosens. Bioelectron.*, vol. 24, no. 7, pp. 1911–1917, Mar. 2009.
- [45] J. O. Bockris and K. T. Jeng, "In-situ studies of adsorption of organic compounds on platinum electrodes," *J. Electroanal. Chem.*, vol. 330, no. 1, pp. 541–581, Jul. 1992.
- [46] J. O. Bockris, M. Gamboa-Aldeco, and M. Szklarczyk, "Ionic adsorption at the solid—solution interphase using three in situ methods," *J. Electroanal. Chem.*, vol. 339, no. 1, pp. 355–400, Nov. 1992.
- [47] A. Dekanski, J. Stevanović, R. Stevanović, B. Ž. Nikolić, and V. M. Jovanović, "Glassy carbon electrodes: I. Characterization and electrochemical activation," *Carbon*, vol. 39, no. 8, pp. 1195–1205, Jul. 2001.
- [48] N. P. Aryan, M. I. H. B. Asad, C. Brendler, S. Kibbel, G. Heusel, and A. Rothermel, "In vitro study of titanium nitride electrodes for neural stimulation," in *2011 Annual International Conference of the IEEE Engineering in Medicine and Biology Society*, 2011, pp. 2866–2869.
- [49] S. Patra, K. Barai, and N. Munichandraiah, "Scanning electron microscopy studies of PEDOT prepared by various electrochemical routes," *Synth. Met.*, vol. 158, no. 10, pp. 430–435, Jun. 2008.
- [50] R. A. Green, N. H. Lovell, G. G. Wallace, and L. A. Poole-Warren, "Conducting polymers for neural interfaces: Challenges in developing an effective long-term implant," *Biomaterials*, vol. 29, no. 24–25, pp. 3393–3399, Aug. 2008.
- [51] A. R. Harris, P. J. Molino, R. M. I. Kapsa, G. M. Clark, A. G. Paolini, and G. G. Wallace, "Correlation of the impedance and effective electrode area of doped PEDOT modified electrodes for brain–machine interfaces," *Analyst*, vol. 140, no. 9, pp. 3164–3174, Apr. 2015.
- [52] N. Chen *et al.*, "Neural interfaces engineered via micro- and nanostructured coatings," *Nano Today*, vol. 14, pp. 59–83, Jun. 2017.
- [53] X. Cui, J. F. Hetke, J. A. Wiler, D. J. Anderson, and D. C. Martin, "Electrochemical deposition and characterization of conducting polymer polypyrrole/PSS on multichannel neural probes," *Sens. Actuators Phys.*, vol. 93, no. 1, pp. 8–18, Aug. 2001.
- [54] E. Slavcheva, R. Vitushinsky, W. Mokwa, and U. Schnakenberg, "Sputtered Iridium Oxide Films as Charge Injection Material for Functional Electrostimulation," *J. Electrochem. Soc.*, vol. 151, no. 7, pp. E226–E237, Jul. 2004.
- [55] S. Negi, R. Bhandari, and F. Solzbacher, "A novel technique for increasing charge injection capacity of neural electrodes for efficacious and safe neural stimulation," in *2012 Annual International Conference of the IEEE Engineering in Medicine and Biology Society*, 2012, pp. 5142–5145.

References

- [56] E. Valderrama, P. Garrido, E. Cabruja, P. Heiduschka, A. Harsch, and W. Gopel, "Microfabrication And Characterisation Of Microelectrode Arrays For In Vivo Nerve Signal Recording," in *The 8th International Conference on Solid-State Sensors and Actuators, 1995 and Eurosensors IX.. Transducers '95*, 1995, vol. 1, pp. 63–66.
- [57] T. Wang, W. Yang, H. Huang, and C. Fu, "A novel fabrication method of flexible micro electrode array for neural recording," in *IEEE 20th International Conference on Micro Electro Mechanical Systems, 2007. MEMS, 2007*, pp. 295–300.
- [58] L. M. Borland and A. C. Michael, "An Introduction to Electrochemical Methods in Neuroscience," in *Electrochemical Methods for Neuroscience*, A. C. Michael and L. M. Borland, Eds. Boca Raton (FL): CRC Press/Taylor & Francis, 2007.
- [59] P. Spitzer *et al.*, "Reference Electrodes for Aqueous Solutions," in *Handbook of Reference Electrodes*, Springer, Berlin, Heidelberg, 2013, pp. 77–143.
- [60] C. M. A. Brett, "Standard Electrode Potentials and Application to Characterization of Corrosion Phenomena," in *Reference Module in Chemistry, Molecular Sciences and Chemical Engineering*, Elsevier, 2017.
- [61] Gary A. Mabbott, "An introduction to cyclic voltammetry," *J. Chem. Educ.*, vol. 60, no. 9, p. 697, Sep. 1983.
- [62] N. Peixoto, K. Jackson, R. Samiyi, and S. Minnikanti, "Charge Storage: Stability measures in implantable electrodes," in *2009 Annual International Conference of the IEEE Engineering in Medicine and Biology Society*, 2009, pp. 658–661.
- [63] T. L. Rose and L. S. Robblee, "Electrical stimulation with Pt electrodes. VIII. Electrochemically safe charge injection limits with 0.2 ms pulses (neuronal application)," *IEEE Trans. Biomed. Eng.*, vol. 37, no. 11, pp. 1118–1120, Nov. 1990.
- [64] M. F. Nichols, A. W. Halm, W. J. James, A. K. Sharma, and H. K. Yasuda, "Cyclic voltammetry for the study of polymer film adhesion to platinum neurological electrodes," *Biomaterials*, vol. 2, no. 3, pp. 161–165, Jul. 1981.
- [65] S. Meijs, M. Fjorback, C. Jensen, S. Sørensen, K. Rechendorff, and N. J. M. Rijkhoff, "Electrochemical properties of titanium nitride nerve stimulation electrodes: an in vitro and in vivo study," *Front. Neurosci.*, vol. 9, 2015.
- [66] X. Cui and D. C. Martin, "Electrochemical deposition and characterization of poly(3,4-ethylenedioxythiophene) on neural microelectrode arrays," *Sens. Actuators B Chem.*, vol. 89, no. 1–2, pp. 92–102, Mar. 2003.
- [67] H. Cesiulis, N. Tsytsaru, A. Ramanavicius, and G. Ragoisha, "The Study of Thin Films by Electrochemical Impedance Spectroscopy," in *Nanostructures and Thin Films for Multifunctional Applications*, Springer, Cham, 2016, pp. 3–42.
- [68] J. R. Macdonald, "Impedance spectroscopy," *Ann. Biomed. Eng.*, vol. 20, no. 3, pp. 289–305, May 1992.
- [69] S. Venkatraman *et al.*, "In Vitro and In Vivo Evaluation of PEDOT Microelectrodes for Neural Stimulation and Recording," *IEEE Trans. Neural Syst. Rehabil. Eng.*, vol. 19, no. 3, pp. 307–316, Jun. 2011.
- [70] Y. P. Kayinamura, M. Ovadia, D. Zavitz, and J. F. Robinson, "Investigation of near ohmic behavior for poly(3,4-ethylenedioxythiophene): a model consistent with systematic variations in polymerization conditions," *ACS Appl. Mater. Interfaces*, vol. 2, no. 9, pp. 2653–2662, Sep. 2010.
- [71] P. H. Bottelberghs and G. H. J. Broers, "Interfacial impedance behaviour of polished and paint platinum electrodes at Na₂WO₄-Na₂MoO₄ solid electrolytes," *J. Electroanal. Chem. Interfacial Electrochem.*, vol. 67, no. 2, pp. 155–167, Jan. 1976.
- [72] N. K. Guimard, N. Gomez, and C. E. Schmidt, "Conducting polymers in biomedical engineering," *Prog. Polym. Sci.*, vol. 32, no. 8–9, pp. 876–921, Aug. 2007.

References

- [73] R. Ravichandran, S. Sundarrajan, J. R. Venugopal, S. Mukherjee, and S. Ramakrishna, "Applications of conducting polymers and their issues in biomedical engineering," *J. R. Soc. Interface*, vol. 7, no. Suppl 5, pp. S559–S579, Oct. 2010.
- [74] N. Rozlosnik, "New directions in medical biosensors employing poly(3,4-ethylenedioxy thiophene) derivative-based electrodes," *Anal. Bioanal. Chem.*, vol. 395, no. 3, pp. 637–645, Oct. 2009.
- [75] J. L. Bredas and G. B. Street, "Polarons, bipolarons, and solitons in conducting polymers," *Acc. Chem. Res.*, vol. 18, no. 10, pp. 309–315, Oct. 1985.
- [76] A. J. Heeger, "Semiconducting and Metallic Polymers: The Fourth Generation of Polymeric Materials," *J. Phys. Chem. B*, vol. 105, no. 36, pp. 8475–8491, Sep. 2001.
- [77] H. J. Ahonen, J. Lukkari, and J. Kankare, "n- and p-Doped Poly(3,4-ethylenedioxythiophene): Two Electronically Conducting States of the Polymer," *Macromolecules*, vol. 33, no. 18, pp. 6787–6793, Sep. 2000.
- [78] M. Asplund *et al.*, "Toxicity evaluation of PEDOT/biomolecular composites intended for neural communication electrodes," *Biomed. Mater.*, vol. 4, no. 4, p. 045009, 2009.
- [79] G. Cellot *et al.*, "PEDOT:PSS Interfaces Support the Development of Neuronal Synaptic Networks with Reduced Neuroglia Response In vitro," *Front. Neurosci.*, vol. 9, Jan. 2016.
- [80] V. D. Bhatt, S. Teymouri, K. Melzer, A. Abdellah, Z. Guttenberg, and P. Lugli, "Biocompatibility Tests on Spray Coated Carbon Nanotube and PEDOT:PSS Thin Films," *IEEE Trans. Nanotechnol.*, vol. 15, no. 3, pp. 373–379, May 2016.
- [81] R. Kiebooms, A. Aleshin, K. Hutchison, and F. Wudl, "Thermal and Electromagnetic Behavior of Doped Poly(3,4-ethylenedioxythiophene) Films," *J. Phys. Chem. B*, vol. 101, no. 51, pp. 11037–11039, Dec. 1997.
- [82] R. Kiebooms, A. Aleshin, K. Hutchison, F. Wudl, and A. Heeger, "Doped poly(3,4-ethylenedioxythiophene) films: Thermal, electromagnetical and morphological analysis," *Synth. Met.*, vol. 101, no. 1, pp. 436–437, May 1999.
- [83] S. Kim, M. Cho, J. Nam, and Y. Lee, "Fabrication and Characterization of PEDOT/Au Films by Chemical Vapor Polymerization Using Au³⁺ Oxidant," *J. Nanosci. Nanotechnol.*, vol. 8, no. 9, pp. 4714–4717, Sep. 2008.
- [84] R. Brooke, D. Evans, M. Dienel, P. Hojati-Talemi, P. Murphy, and M. Fabretto, "Inkjet printing and vapor phase polymerization: patterned conductive PEDOT for electronic applications," *J. Mater. Chem. C*, vol. 1, no. 20, pp. 3353–3358, May 2013.
- [85] Z.-Q. Feng *et al.*, "Highly aligned poly(3,4-ethylene dioxythiophene) (PEDOT) nano- and microscale fibers and tubes," *Polymer*, vol. 54, no. 2, pp. 702–708, Jan. 2013.
- [86] S. E. Atanasov *et al.*, "Highly Conductive and Conformal Poly(3,4-ethylenedioxythiophene) (PEDOT) Thin Films via Oxidative Molecular Layer Deposition," *Chem. Mater.*, vol. 26, no. 11, pp. 3471–3478, Jun. 2014.
- [87] L. R. Stevens, D. G. Harman, K. J. Gilmore, M. in het Panhuis, and G. G. Wallace, "A Comparison of Chemical and Electrochemical Synthesis of PEDOT:Dextran Sulphate for Bio-Application," *MRS Online Proc. Libr. Arch.*, vol. 1717, Jan. 2015.
- [88] F. Zabihi, Y. Xie, S. Gao, and M. Eslamian, "Morphology, conductivity, and wetting characteristics of PEDOT:PSS thin films deposited by spin and spray coating," *Appl. Surf. Sci.*, vol. 338, pp. 163–177, May 2015.
- [89] B. R. Pistillo *et al.*, "One step deposition of PEDOT films by plasma radicals assisted polymerization via chemical vapour deposition," *J. Mater. Chem. C*, vol. 4, no. 24, pp. 5617–5625, Jun. 2016.
- [90] Y. Wen and J. Xu, "Scientific Importance of Water-Processable PEDOT–PSS and Preparation, Challenge and New Application in Sensors of Its Film Electrode: A Review," *J. Polym. Sci. Part Polym. Chem.*, vol. 55, no. 7, pp. 1121–1150, Apr. 2017.

References

- [91] M. Sessolo *et al.*, "Easy-to-Fabricate Conducting Polymer Microelectrode Arrays," *Adv. Mater.*, vol. 25, no. 15, pp. 2135–2139, Apr. 2013.
- [92] H. Randriamahazaka, V. Noël, and C. Chevrot, "Nucleation and growth of poly(3,4-ethylenedioxythiophene) in acetonitrile on platinum under potentiostatic conditions," *J. Electroanal. Chem.*, vol. 472, no. 2, pp. 103–111, Aug. 1999.
- [93] H. S. Mandal *et al.*, "Improving the performance of poly(3,4-ethylenedioxythiophene) for brain–machine interface applications," *Acta Biomater.*, vol. 10, no. 6, pp. 2446–2454, Jun. 2014.
- [94] M. R. Abidian, D.-H. Kim, and D. C. Martin, "Conducting-Polymer Nanotubes for Controlled Drug Release," *Adv. Mater.*, vol. 18, no. 4, pp. 405–409, Feb. 2006.
- [95] M. Sebaa, T. Y. Nguyen, S. Dhillon, S. Garcia, and H. Liu, "The effects of poly(3,4-ethylenedioxythiophene) coating on magnesium degradation and cytocompatibility with human embryonic stem cells for potential neural applications," *J. Biomed. Mater. Res. A*, vol. 103, no. 1, pp. 25–37, Jan. 2015.
- [96] F. Li and W. J. Albery, "A novel mechanism of electrochemical deposition of conducting polymers: two-dimensional layer-by-layer nucleation and growth observed for poly(thiophene-3-acetic acid)," *Electrochimica Acta*, vol. 37, no. 3, pp. 393–401, Mar. 1992.
- [97] L. Niu, C. Kvarnström, K. Fröberg, and A. Ivaska, "Electrochemically controlled surface morphology and crystallinity in poly(3,4-ethylenedioxythiophene) films," *Synth. Met.*, vol. 122, no. 2, pp. 425–429, Jun. 2001.
- [98] K. C. (nee Włodarczyk), J. Karczewski, and P. Jasiński, "Influence of electropolymerization conditions on the morphological and electrical properties of PEDOT film," *Electrochimica Acta*, vol. 176, pp. 156–161, Sep. 2015.
- [99] F.-B. Li and W. J. Albery, "Two-dimensional nucleation and layer-by-layer deposition of conducting polymers," *Adv. Mater.*, vol. 4, no. 10, pp. 673–675, Oct. 1992.
- [100] H. Yamato, M. Ohwa, and W. Wernet, "Stability of polypyrrole and poly(3,4-ethylenedioxythiophene) for biosensor application," *J. Electroanal. Chem.*, vol. 397, no. 1, pp. 163–170, Nov. 1995.
- [101] Y. H. Xiao, C. M. Li, M.-L. Toh, and R. Xue, "Adenosine 5'-triphosphate incorporated poly(3,4-ethylenedioxythiophene) modified electrode: a bioactive platform with electroactivity, stability and biocompatibility," *J. Appl. Electrochem.*, vol. 38, no. 12, pp. 1735–1741, Dec. 2008.
- [102] M. Suzuki, M. Nakayama, K. Tsuji, T. Adachi, and K. Shimono, "Electrochemical Polymerization of PEDOT/Biomolecule Composite Films on Microelectrodes for the Measurement of Extracellular Field Potential," *Electrochemistry*, vol. 84, no. 5, pp. 354–357, 2016.
- [103] X. Cui and D. C. Martin, "Fuzzy gold electrodes for lowering impedance and improving adhesion with electrodeposited conducting polymer films," *Sens. Actuators Phys.*, vol. 103, no. 3, pp. 384–394, Feb. 2003.
- [104] Y. P. Kaynamura, J. H. Roberts, and J. F. Robinson, "Near-Ohmic Behavior for Conducting Polymers: Extension Beyond PEDOT on Gold-Plated Platinum to Other Polymer-Counterion/Substrate Combinations," *ACS Appl. Mater. Interfaces*, vol. 4, no. 3, pp. 1601–1607, Mar. 2012.
- [105] X. Luo and X. T. Cui, "Electrochemical deposition of conducting polymer coatings on magnesium surfaces in ionic liquid," *Acta Biomater.*, vol. 7, no. 1, pp. 441–446, Jan. 2011.
- [106] Y. Furukawa, A. Shimada, K. Kato, H. Iwata, and K. Torimitsu, "Monitoring neural stem cell differentiation using PEDOT–PSS based MEA," *Biochim. Biophys. Acta BBA - Gen. Subj.*, vol. 1830, no. 9, pp. 4329–4333, Sep. 2013.
- [107] R. Gerwig *et al.*, "PEDOT–CNT Composite Microelectrodes for Recording and Electrostimulation Applications: Fabrication, Morphology, and Electrical Properties," *Front. Neuroengineering*, vol. 5, May 2012.

References

- [108] X. Crispin *et al.*, "Conductivity, morphology, interfacial chemistry, and stability of poly(3,4-ethylene dioxythiophene)–poly(styrene sulfonate): A photoelectron spectroscopy study," *J. Polym. Sci. Part B Polym. Phys.*, vol. 41, no. 21, pp. 2561–2583, Nov. 2003.
- [109] N. Sakmeche *et al.*, "Anionic micelles; a new aqueous medium for electropolymerization of poly(3,4-ethylenedioxythiophene) films on Pt electrodes," *Chem. Commun.*, no. 24, pp. 2723–2724, Jan. 1996.
- [110] N. Sakmeche, J.-J. Aaron, S. Aeiya, and P.-C. Lacaze, "Usefulness of aqueous anionic micellar media for electrodeposition of poly-(3,4-ethylenedioxythiophene) films on iron, mild steel and aluminium," *Electrochimica Acta*, vol. 45, no. 12, pp. 1921–1931, Feb. 2000.
- [111] H. S. Mandal, J. S. Kaste, D. G. McHail, J. F. Robinson, J. J. Pancrazio, and T. C. Dumas, "Improved Poly(3,4-Ethylenedioxythiophene) (PEDOT) for Neural Stimulation," *Neuromodulation Technol. Neural Interface*, vol. 18, no. 8, pp. 657–663, Dec. 2015.
- [112] P.-H. Aubert, L. Groenendaal, F. Louwet, L. Lutsen, D. Vanderzande, and G. Zotti, "In situ conductivity measurements on polyethylenedioxythiophene derivatives with different counter ions," *Synth. Met.*, vol. 126, no. 2, pp. 193–198, Feb. 2002.
- [113] L. Sui *et al.*, "In vitro and in vivo evaluation of poly(3,4-ethylenedioxythiophene)/poly(styrene sulfonate)/dopamine-coated electrodes for dopamine delivery," *J. Biomed. Mater. Res. A*, vol. 102, no. 6, pp. 1681–1696, Jun. 2014.
- [114] R. A. Green *et al.*, "Conducting polymer electrodes for visual prostheses," in *2010 Annual International Conference of the IEEE Engineering in Medicine and Biology*, 2010, pp. 6769–6772.
- [115] A. R. Harris, S. J. Morgan, J. Chen, R. M. I. Kapsa, G. G. Wallace, and A. G. Paolini, "Conducting polymer coated neural recording electrodes," *J. Neural Eng.*, vol. 10, no. 1, p. 016004, 2013.
- [116] K. A. Ludwig, J. D. Uram, J. Yang, D. C. Martin, and D. R. Kipke, "Chronic neural recordings using silicon microelectrode arrays electrochemically deposited with a poly(3,4-ethylenedioxythiophene) (PEDOT) film," *J. Neural Eng.*, vol. 3, no. 1, p. 59, 2006.
- [117] J. Che, Y. Xiao, X. Zhu, and X. Sun, "Electro-synthesized PEDOT/glutamate chemically modified electrode: a combination of electrical and biocompatible features," *Polym. Int.*, vol. 57, no. 5, pp. 750–755, May 2008.
- [118] S. Joshi, A. van Loon, A. Savov, and R. Dekker, "Adhesion Improvement of Polyimide/PDMS Interface by Polyimide Surface Modification," *MRS Adv.*, vol. 1, no. 1, pp. 33–38, Jan. 2016.
- [119] V. V. Pavlishchuk and A. W. Addison, "Conversion constants for redox potentials measured versus different reference electrodes in acetonitrile solutions at 25°C," *Inorganica Chim. Acta*, vol. 298, no. 1, pp. 97–102, Jan. 2000.
- [120] I. M. Kolthoff and W. J. Tomsicek, "The Oxidation Potential of the System Potassium Ferrocyanide–Potassium Ferricyanide at Various Ionic Strengths," *J. Phys. Chem.*, vol. 39, no. 7, pp. 945–954, Jan. 1934.
- [121] P. A. Rock, "The Standard Oxidation Potential of the Ferrocyanide-Ferricyanide Electrode at 25° and the Entropy of Ferrocyanide Ion," *J. Phys. Chem.*, vol. 70, no. 2, pp. 576–580, Feb. 1966.
- [122] Y. Nakamura, Y. Suzuki, and Y. Watanabe, "Effect of oxygen plasma etching on adhesion between polyimide films and metal," *Thin Solid Films*, vol. 290–291, no. Supplement C, pp. 367–369, Dec. 1996.
- [123] K. G. Shah, V. M. Tolosa, A. C. Tooker, S. H. Felix, and S. S. Pannu, "Improved chronic neural stimulation using high surface area platinum electrodes," in *2013 35th Annual International Conference of the IEEE Engineering in Medicine and Biology Society (EMBC)*, 2013, pp. 1546–1549.
- [124] J. Bobacka, A. Lewenstam, and A. Ivaska, "Electrochemical impedance spectroscopy of oxidized poly(3,4-ethylenedioxythiophene) film electrodes in aqueous solutions," *J. Electroanal. Chem.*, vol. 489, no. 1–2, pp. 17–27, Jul. 2000.

References

- [125] Z. A. King, C. M. Shaw, S. A. Spanninga, and D. C. Martin, "Structural, chemical and electrochemical characterization of poly(3,4-Ethylenedioxythiophene) (PEDOT) prepared with various counter-ions and heat treatments," *Polymer*, vol. 52, no. 5, pp. 1302–1308, Mar. 2011.
- [126] M. Łapkowski and A. Proń, "Electrochemical oxidation of poly(3,4-ethylenedioxythiophene) — 'in situ' conductivity and spectroscopic investigations," *Synth. Met.*, vol. 110, no. 1, pp. 79–83, Mar. 2000.
- [127] R. R. Gagne, C. A. Koval, and G. C. Lisensky, "Ferrocene as an internal standard for electrochemical measurements," *Inorg. Chem.*, vol. 19, no. 9, pp. 2854–2855, Sep. 1980.
- [128] D. Bao *et al.*, "Electrochemical Oxidation of Ferrocene: A Strong Dependence on the Concentration of the Supporting Electrolyte for Nonpolar Solvents," *J. Phys. Chem. A*, vol. 113, no. 7, pp. 1259–1267, Feb. 2009.
- [129] A. Lewandowski, L. Waligora, and M. Galinski, "Ferrocene as a Reference Redox Couple for Aprotic Ionic Liquids," *Electroanalysis*, vol. 21, no. 20, pp. 2221–2227, Oct. 2009.
- [130] G. Inzelt, "Pseudo-reference Electrodes," in *Handbook of Reference Electrodes*, Springer, Berlin, Heidelberg, 2013, pp. 331–332.